Bridging the gap between the mechanical and metabolic activity in cell-ECM interactions

Ana San Felix Garcia-Obregon

BSc, MSc

Submitted in fulfilment of the requirements for the Degree of Doctor of Philosophy

School of Engineering

College of Science and Engineering

University of Glasgow

April 2023

AUTHOR'S DECLARATION

"I declare this research is the result of my own work and has not been submitted for any other degree at the University of Glasgow or any other institution, with the exception of the mentioned references to the contribution of others ".

ACKNOWLEDGEMENTS

I finally made it to the most expected section and even now, with a whole thesis written, is going to be a difficult part. Especially because there are many people that I want to thank for, and the space is starting to be limited.

To start, I would like to thank the University of Glasgow and the EPRSC for funding the three and a half years of my PhD. Thanks to my supervisors Manuel and Matt, for giving me the opportunity of being here. In particular, thank you Manuel for all the guidance and support you gave me, mainly in the last couple of years when everything seemed to fall apart.

I would like to thank my family. My grandma for always believing in me and look me with that much love. A special thanks to my aunt Ana, for being there in every step of my PhD and be that interested in my work. Also, thanks for all your help during the writing period. Of course, my parents and my brother with them none of this would have been possible. To you Mum, for being my rock, for listening to me for good and for bad, for picking up the phone every time I needed and rescuing me all the time. Thank you Dad for making me who I am today. Thanks for sharing with me all your knowledge, in particular, in music. In the last three months, it has helped me to feel closer to you. Even though I am miles away, for what I am sorry. To you Iñaki, the last but not the least. Thanks for having that facility to make me laugh and cheer me up. You have become a wonderful person and I cannot be more proud.

My friends from Spain. Estefania, there is not much to say, you are my best friend. You are one of the few people that completely understand me and after all these years apart nothing has changed. I hope that distance does not last for longer. Thanks for always being there for me. Celia and Elena, the best gift of my years in uni. Thanks for our long WhatsApp conversations, talking about everything. Thanks for not leave apart when I do not reply in ages and always being there to take me back. Pablo, thank you so much for being my excuse to write all these long emails where I could escape, somehow, from my own mind. Alma and Isa, we might not talk that often, but you are the kind of people that you always know are there.

Thanks to my Glasgow family. To Eva for making sure that I had a break every weekend to go for dinner, brunch or any other plan that could help me to clean my mind. To Sofia for sharing all these years together. I hope we can meet again soon. To Virginia and Alfred, you are the best guys and I miss you every day. Thanks for taking good care of me and introducing me to my obsession with ceramics (especially Virginia). To Marco, thank you for all your help and support, and for checking up on me constantly to make sure I was reasonably okay. Sara, thanks for everything, you have been my supervisor but most of all my friend. Without you, this project wouldn't have been possible, for what I cannot be more thankful.

I want to thank the whole CeMi group. Especial mention to Eonan and Marta, thank you, guys, for coming and "bothering" me all the time in the office so I could have a break. Again, Eonan, for checking my grammar in all this section. To my small office group Mariana, Dora and Seb, I couldn't have had better colleagues of desk (even though Seb has been happy to replace me all the time). To Juan, I am so happy to have had the opportunity to meet you, thanks for having been such a good friend, still, I am not going to analyse TFM. Lola, Lydia, Nadia and Camilla you are amazing guys. Thanks to Álvaro for sharing all this hard time without mentioning the thesis too much but understanding the agony. After all, we survived. To Vini, thanks for solving all my doubts about orders, shipping, etc. Thank you Rui for treating me with those delicious chocolate almonds, you saved me for a breakdown more than one evening. Also, I want to thank the people I have met in the ARC. Marina, I cannot thank you enough for having been encouraging me to keep going and trying to make me see that this was not that horrible. Thank you for listening to me over and over again complaining about the writing and always be there with your best possible advice. Thanks to Greig, for coming to talk every now and then, and listing me explaining the more tedious analysis to see if it was possible to automatise it (of course, it wasn't).

A big thanks to all the people I met during this long journey and now they are a big part of my life. My Spanish community in Glasgow, in particular Tania and Jemima. Anni, for the long dinners of good food and wine. Ilaria and Dani, three months living together were not enough. Prateek for always being there with a big

smile. Thank you to all the people I met in Padova. Especially, May and Kalin my two food monsters I hope we can have *aperitivo* together again soon.

To all of you, thank you for your support during all these years. I hope I did not disappoint you.

ABSTRACT

Cells are in constant communication with their surroundings. This is possible by establishing focal adhesions (FAs) formed by the attachment of transmembrane proteins known as integrins, with proteins from the extracellular matrix (ECM) (e.g. fibronectin (FN) or collagen). The ECM is the natural scaffold of the cells within the tissues. It is a three-dimensional scaffold generated by molecules secreted by the cells themselves. The properties of the ECM vary among the different tissues, which influences different cellular behaviour and differentiation (1,2). For instance, bone presents a stiffer ECM than the brain, which has one of the softest matrices within the body (1). The ECM is the direct link of the cell with the environment and every piece of information gathered from the FAs plays an important role in cellular fate (1).

Mesenchymal stem cells (MSCs) are multipotent cells that have self-renewal capacity and can differentiate into different tissues such as bone, adipose tissue or cartilage (3). In the last decade, those cells have gained high importance in research, especially in regenerative medicine since they can be used *in vivo* and *in vitro* (4). The type of tissue they differentiate into depends on how they sense the matrix, among other things. It has been shown that on stiff surfaces they differentiate into harder tissues, such as bone, while on softer matrices they differentiate into a less rigid tissue as is the case of adipose tissue (1,5). Therefore, it is important to understand cell-ECM interactions and what intracellular changes occur upon these interactions.

Multiple studies have demonstrated the implications of matrix mechanical properties in cellular mechanical and metabolic activity (6,7). In general, cells on stiff matrices can form mature FAs where all the proteins involved are gathered to resist the ECM tension and attach (8). Cells form their actin-cytoskeleton and contract to generate high intracellular tension. This is necessary to exert forces through the FAs and compensate for that extrinsic tension (9). This increase in cellular contractility and tension triggers different pathways (e.g. YAP/TAZ) and leads to nuclear flattening, which favours the translocation of transcriptional factors into it such as YAP to the nucleus (10–12). Once in the nucleus YAP binds to the DNA and starts the expression of different proteins involved in cellular

mechanics and metabolism (13). All this implies high energy investment from the cell. The main source of energy is ATP, which is generated during cell respiration. Thereby, on stiff surfaces cellular respiration increases to supply that energy demand (13). On the contrary, on soft surfaces FAs maturation, cell contractility, nuclear flattering and YAP nuclear translocation decreases (11,12). Under these circumstances, cells do not consume as much energy as on stiff surfaces, hence cellular respiration decreases as it does ATP production and consumption.

We hypothesise that cells require mechanical and metabolic energy during ECM-cell interactions to generate forces and create an adaptive response. This work aims to bring together how cells behave from mechanical and metabolic perspectives during their attachment, proliferation, migration and differentiation, in relation to the matrix properties, in particular depending on matrix stiffness and degradability. This will provide a better understanding of how microenvironmental cues can be used to control cell fate, enhancing studies in multiple fields e.g. tissue regeneration or drug testing. In order to do this, cells were seeded on full-length FN-PEG and polyacrylamide (PAA) hydrogels of different stiffnesses. Traction Force Microscopy (TFM) was used to study cellular force generation on different surfaces and YAP nuclear translocation was followed by immunostaining. Cellular respiration rate, metabolites, and ATP generation were analysed to complete the cellular mechanobiological activity studied with TFM. Also, different metabolic pathways such as AMPK, NAD^+/NADH or ATP/ADP were studied using ratiometric sensors. Blebbistatin was incorporated to demonstrate the importance of cell contractility in cellular response. This study concludes that cellular mechanical and metabolic activity are not independent of one to another and they are influenced by the properties of the matrix. These finding contribute to get a better understanding of cellular behaviour and, hence, develop optimal scaffolds that can be used in tissue regeneration.

TABLE OF CONTENTS

LIST OF TABLES

LIST OF FIGURES

ABBREVIATIONS

2D	Two dimensional
2-DG	2-deoxy-glucose
3D	Three dimensional
Aam	Acrylamide
ACRL	Acrylate
AICAR	5-Aminoimidazole-4-carboxamide 1-ß-D-ribofuranoside, Acadesine, N1-(ß-D-Ribofuranosyl)-5-aminoimidazole-4-carboxamide
ALP	Alkaline phosphatase
APS	Ammonium persulfate
BSA	Bovine Serum Albumin
BisAAm	N,N'-Methylene-Bis-Acrylamide
CFU-F	Colony forming unit-fibroblasts
DD	Dehydroepiandrosterone/ Diamide
DHEA	Dehydroepiandrosterone
DIA	Diamide
ECM	Extracellular Matrix
ETC	Electron transport chain
FA	Focal adhesion
FBS	Foetal Bovine Serum
FCCP	Carbonyl cyanide – 4 (trifluoromethoxy) phenylhydrazone
FN	Fibronectin

FN-PEG	Full-length fibronectin PEG-ACRL hydrogel
GAGs	Glycosaminoglycans
GFs	Growth Factors
IAA	Iodoacetamide
L-Glu	L-Glutamine
LINC	Linker of Nucleoskeleton and Cytoskeleton
LM	Laminin
ML-7	1-(5-Iodonaphthalene-1-sulfonyl)-1H-hexahydro-1,4-diazepine hydrochloride
MSCs	Mesenchymal Stem Cells
OCN	Osteocalcine
OCR	Oxygen consumption rate
OXPHOS	Oxidative phosphorylation
PAA	Polyacrilamide
PBS	Phosphate buffered saline
PEG	Polyethylene glycol
PEG-(4)-ACRL	4-arm-PEG-Acrylate
PEG-(4)-MAL	4-arm-PEG-Maleimide
ROS	Reactive Oxigen Species
RT	Room temperature
RUNX-2	Runt-related transcription factor 2
SDS	Sodium dodecyl sulfate

SH-PEG-SH	PEG dithiol
SP	Sodium pyruvate solution
Sulfo-SANPAH	Sulfosuccinimidyl 6-(4′-azido-2′ nitrophenylamino)hexanoate
TAZ	PDZ-binding motif
TCA	Tricarboxylic acid cycle
TCEP	Tris(2-carboxyethyl)phosphine hydrochloride
TCP	Tissue culture plate
TEMED	N,N,N',N'-Tetramethylethylenediamine
UV	Ultraviolet
YM	Y27632 and ML7

CHAPTER 1 : INTRODUCTION

1.1. RELATIONSHIP BETWEEN EXTRACELLULAR MATRIX (ECM) AND CELLS

Cells are the basic unit that forms the tissues within the body. The three-dimensional scaffold where cells are embedded to support the integrity of the tissues is called the extracellular matrix (ECM). How this matrix and cells are organised establishes the different tissues in the organism. The properties of a particular tissue are given by the interactions between ECM-cell and cell-cell. When this communication is interrupted, the stability of the tissue is lost. In regenerative medicine is particularly important to understand how cells interact with their environment and what leads to losing the homeostasis of the tissue, in order to develop new ways to solve it.

1.1.1. Extracellular matrix

The ECM is the natural scaffold of the cells within the tissues. It is generated by cell-secreted molecules (Figure 1-1), present in all tissues and has an important role in cell proliferation, differentiation and migration (14). The main components of the ECM are proteoglycans, hyaluronic acid, soluble molecules (e.g. growth factors (GFs)) and proteins. There are four main proteins: collagen, the main structural element; elastin, responsible for ECM elasticity and stiffness together with collagen; and two adhesion proteins, fibronectin (FN) and laminin (LM) (2,15). Cells establish physical connections with the ECM by binding transmembrane proteins, known as integrins, with proteins in the ECM (e.g. FN and collagen). These interactions allow an exchange of information between the cells and the microenvironment. The information gathered by the cells will initiate a series of mechanical and metabolic cues to generate a response, which will be transmitted to the ECM (2,16)

For this project, two of the four main proteins in the ECM were selected: collagen and FN. Both of them contain cell adhesion binding domains and have been widely

studied in the literature (17,18) gaining great importance in regenerative medicine.

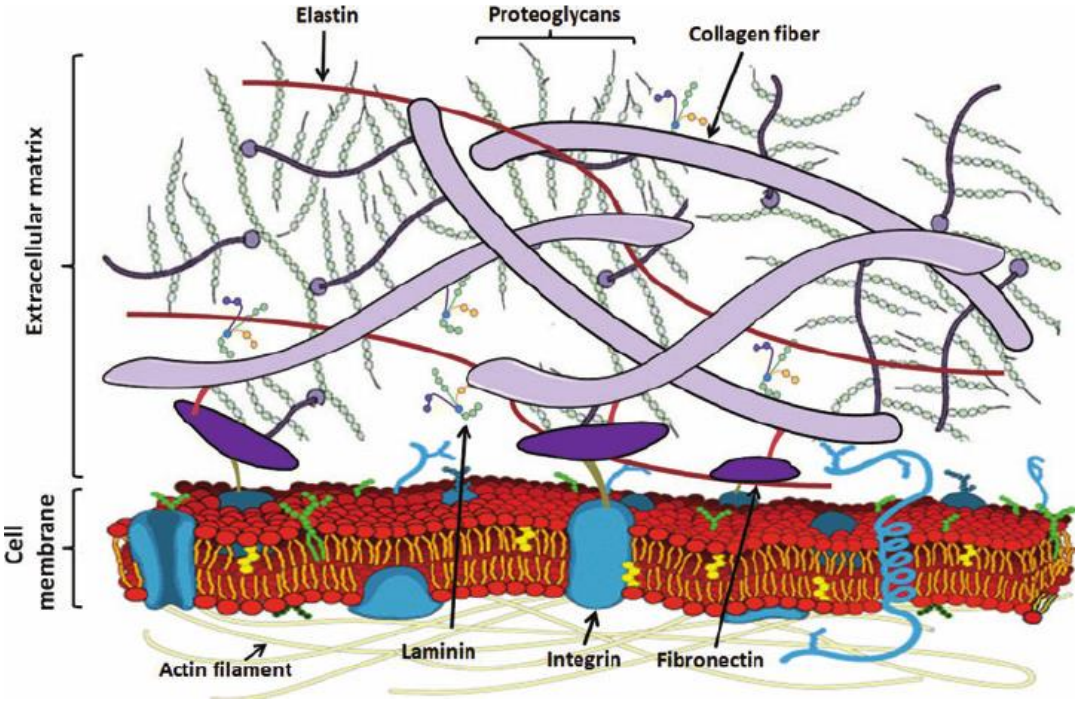

Figure 1-1. Extracellular matrix (ECM) structure and interactions cell-ECM (figure taken from (19)**.** *The ECM is formed by proteoglycans (glycosaminoglycans joined to specific protein core with exception of hyaluronic acid, a GAG without protein core linkage) and fibrous proteins. There are four main fibrous proteins: collagen, elastin, fibronectin and laminin. Integrins are transmembrane proteins formed by two subunits that attach to ECM proteins such as FN, being the connection of the ECM with the internal actin-cytoskeleton* (19)

Collagen

Collagen is discussed to be the most abundant protein in the ECM (20). It consists of a triple helix composed of three polypeptide chains, known as α-chains, twisted, which have one or more regions of a repeating amino acid motif glycine (Gly)-X-Y, where X and Y can be any amino acid (18,20). However, the most frequent combination is glycine, proline and hydroxyproline. This tripeptide sequence allows the establishment of interchain and intrachain hydrogen bonds, which, together with electrostatic interactions, stabilises the triple helix (20). Collagen can be assembled as a homotrimer, when the three chains are identical,

or as a heterotrimer when they are different. The different combinations lead to different types of collagens. So far, it has been identified 28 different types of collagens. For our study, the type of collagen that is of special interest is fibrillar collagen. This family of collagens is integrated by the types I, II, III, V, XI, XXIV and XXVII (18,20). The distribution of these collagens within the body is not uniform. Some tissues are richer in one type than another, which determines their properties. For instance, collagen type I can be found in bone, skin or tendons; while type II appears mainly in cartilage (18). These collagens are synthesised in the cell and released into the extracellular space as a precursor. Outside the cell, the amino and carboxy terminals of the procollagen are cut by specific enzymes. The resulting protein goes through a process of oxidative deamination of its peptidyl lysine residues by a lysyl oxidase, facilitating the crosslinking of individual collagen molecules to form a supramolecular assembly in the ECM (20). Fibrillar collagens have an important structural role, they confer mechanical strength and are involved in signalling functions by interacting with cellular receptors and other components of the ECM (18).

Even though collagen has an essential role in maintaining the structure of the ECM, it is also involved in cell adhesion. Cells can interact with collagen either directly by expressing integrins that bind to specific adhesion domains in the protein (21), or indirectly through glycoproteins in the ECM (e.g. Fibronectin) (22). There are four main groups of receptor-binding motifs in collagen: i) specific domains integrated in the triple helix that can only be recognised by integrins with a high affinity for them (21). One example is the GFOGER motif, recognised by the integrins $\alpha_1\beta_1$ and $\alpha_2\beta_1$ (21,23). ii) The second type of binding sites are well-conserved domains to which cells have evolutionally created receptors that can recognise and bind to them (e.g. glycine-proline-hydroxyproline (GPO)). iii) Collagen contains cell-adhesion domains that are only accessible to their cellular receptors after protein denaturation (21). iv) The last category are receptor binding sites in non-collagenous domains (e.g. NC1) (24,25).

Fibronectin

Fibronectin is a glycoprotein which exists as a dimer connected by two disulphide bonds near their C-termini (Figure 1-2). Each of these monomers is integrated by three repeating units: type I, which appears twelve times; two repeats of type II and fifteen to seventeen type III. The whole protein is encoded in one gene and depending on the RNA splicing it is possible to find different isoforms of FN. Two extra type III units can be generated from the splicing known as EIIIA and EIIIB. Type I and type II modules have two disulphide bonds that stabilise the protein conformation. The absence of disulphide bonds in type III facilitates protein to unfold under applied forces (17,26). In vertebrates, there are two types of fibronectin: plasma fibronectin and cellular fibronectin. Plasma fibronectin is a soluble protein which forms part of the blood and is produced by hepatocytes. EIIIA and EIIIB are not present in this type of FN. On the contrary, cellular FN does contain these two extra type III repetitions. Cellular FN is insoluble and is secreted by the cells to integrate the ECM (17).

FN binds to multiple other components of the ECM, such as collagen or fibrin, as well as to the cells (17). This association between FN and cells takes place through integrins, which are heterodimeric (α and ß subunits) transmembrane receptors that link the ECM with the cytoskeleton. This linkage could be direct when integrins bind to specific domains on FN; or indirect, when integrins interact with actin via cytoplasmic proteins (2). The FN sequence has binding domains to a wide range of biomolecules. One of the most studied ones is an integrin-binding sequence that consists of three amino acids: arginine glycine and aspartic acid (RGD). This peptide motif has become a paradigm in cell adhesion (27,28). Scaffolds are engineered to present these adhesion motifs (via either the use of full-length proteins, protein fragments or peptide sequences) to allow cell attachment, which is, in general, one of the first events that need to happen before other cell functions (29).

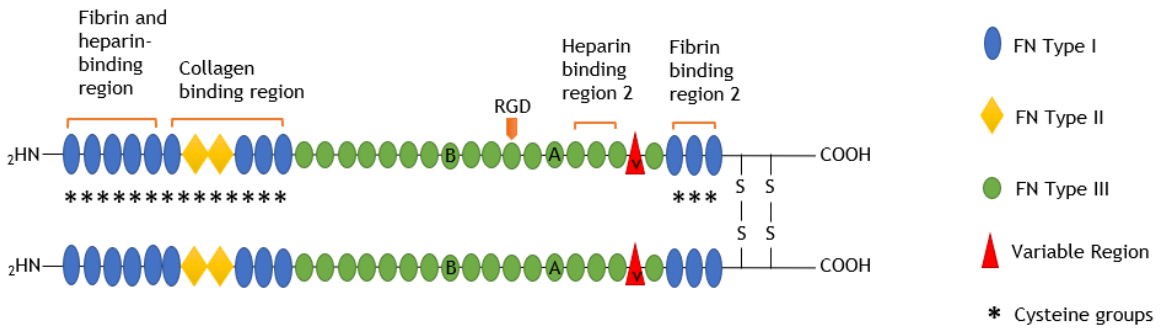

***Figure 1-2. Fibronectin structure**. FN is a dimer linked by two disulphide bonds near the C-terminal. Each monomer contains three types of repeating subunits: 12 type I repeats (in blue), two type II (in yellow) and 15-17 type III (in green). Brackets in orange indicate the binding regions to different molecules. The cysteine residues contained in the protein are marked with asterisks (*). FN can bind to multiple biological molecules (e.g. collagen, heparin, GFs or fibrin) and cells through their integrins (transmembrane proteins). There are multiple integrins domains within the fibronectin, but it is of special relevance RGD peptide.*

The ECM undergoes constant remodelling among tissues, being degraded and reassembled all the time by cells to maintain homeostasis, especially during development or in a stressful situation (e.g. wound healing or diseases) (2,14,15). This remodelling allows cells to migrate within the ECM. Any change in the ECM will be directly translocated to the cell, triggering distinct metabolic cascades in response. Therefore, the ECM plays an important role in tissue homeostasis and cell behaviour regulation (2,15).

1.1.2. Mesenchymal stem cells (MSCs)

Mesenchymal Stem Cells (MSCs) are stromal cells that have the capacity of self-renewal and differentiation into different cell types (multipotency) such as osteoblasts, adipocytes or chondrocytes (Figure 1-3). The capacity of self-renewal involves all the biological processes that maintain a pool of undifferentiated MSCs, which has great importance in tissue healing (30–32). They are found in many adult tissues from where they can be isolated, but the most common one is from bone marrow (3,33).

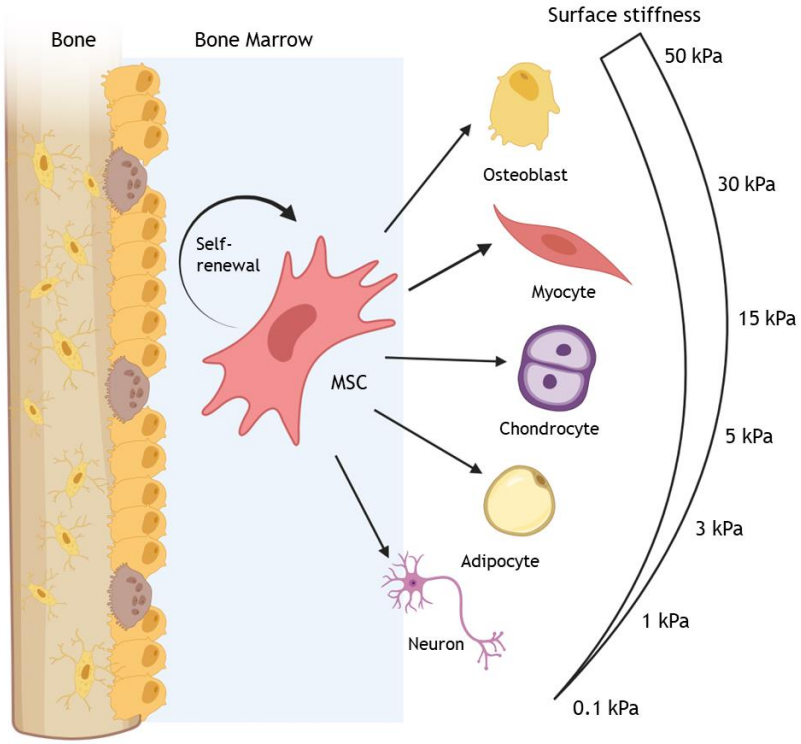

Figure 1-3 Mesenchymal stem cells (MSCs) differentiate into different tissues depending on substrate stiffness (Biorender made). *MSCs are stromal cells that can be isolated from bone marrow. They have multipotency being able to differentiate into osteoblasts on stiffnesses around 40 kPa or above, chondrocytes (3-5 kPa) or adipocytes (1-3 kPa). It has been demonstrated that MSCs can also differentiate into myocytes on stiffnesses around 15-25 kPa, or into neurons on really soft matrices* (5).

The characteristics of the niche will ultimately determine mesenchymal stem cell commitment and fate (1). The process through which cells sense mechanical signals in the environment and transform them into a biochemical intracellular response is called *mechanotransduction*. This is mediated by cell-ECM and cell-cell interactions, which are constituted mainly by integrins and cadherins, respectively, and regulate intracellular signalling pathways. Cells generate and transfer forces to the ECM and neighbour cells through these connections. Also, external forces applied by shear, compression or tension produce changes in the cell cytoskeleton which will transfer these forces from the membrane proteins to intracellular organs (34).

Since MSCs may be produced and cultured *ex vivo*, they have gained a lot of interest in regenerative medicine (4). Their use together with synthetic matrices (whose mechanical properties can be finely tuned) is very promising in regenerative medicine, to design new biomaterials with better control of stem cell fate. It has been shown that on soft surfaces, MSCs differentiate into soft tissues as can be adipose tissue, while stiffer surfaces direct cell differentiation more into bone (1,35). Also, it has been shown that actin-cytoskeleton and cell contractility are of great importance in MSCs differentiation (1). On stiffer surfaces, cells present an organised actin-cytoskeleton, being able to contract more leading to osteogenesis differentiation. Whereas on softer surfaces, the cell cytoskeleton is disorganised, which is related to low contractility and differentiation into softer tissues. Therefore, regardless of how rigid the surface is, if cell contractility is inhibited cells perceive it as soft, and as a result, other cell differentiation pathways are triggered (1).

1.1.3. Influence of stiffness and degradability in stem cell differentiation and migration

Prior to their attachment, cells probe the matrix to sense the rigidity. Then, focal adhesions (FAs) are assembled, which are multiprotein structures that bridge ECM proteins (e.g. fibronectin) and the cytoskeleton (36). It is through these links that cells exert forces, pull to deform the matrix and transmit these forces through the cytoskeleton to the nucleus (37).

FAs are formed by integrins and a series of adaptor proteins. These proteins can be divided into two groups: i) adaptors that directly link the actin cytoskeleton with integrins (e.g. talin, tensin), and ii) a second group of proteins that create an indirect interaction between integrins and the actin cytoskeleton (e.g. vinculin, FAK, paxillin). For instance, talin binds to integrins and the actin cytoskeleton, creating a direct connection between both. On the contrary, vinculin binds to the actin-cytoskeleton and talin, creating an indirect link (37,38). The natural assembly of these proteins into FAs depends on ECM properties such as stiffness (8,37) or viscosity (39). Those matrix features determine cell behaviour (e.g. attachment, proliferation and differentiation) and also cellular

mechanical properties (e.g. cell shape, cytoskeleton organisation, F-actin assembling and force loading) (40,41) (Figure 1-4). How cells interact with the ECM depending on its mechanical properties, as well as FAs assembling and their engage and disengage dynamics, can be explained by the *molecular clutch* model (38,39,42). On soft or low viscous surfaces, the nucleus is relaxed, it appears round, and its pores are closed. Plus, the cell circularly increases and cells present a poor cytoskeleton organisation (37,39,43,44) (Figure 1-4A). Under these circumstances, talin is folded and vinculin is not recruited. FAs are weakly assembled, which leads to a slow force generation. The bond ECM protein-integrin ends up dissociated before the force can be loaded (44–46). On the other hand, as stiffness and viscosity increase, the bond with the matrix is firmer, giving the cells time to load enough forces on the FAs. This force loading leads to talin unfolding and vinculin recruitment, which strengthens the clutch actin-FA-ECM (37,39,42) (Figure 1-4B).

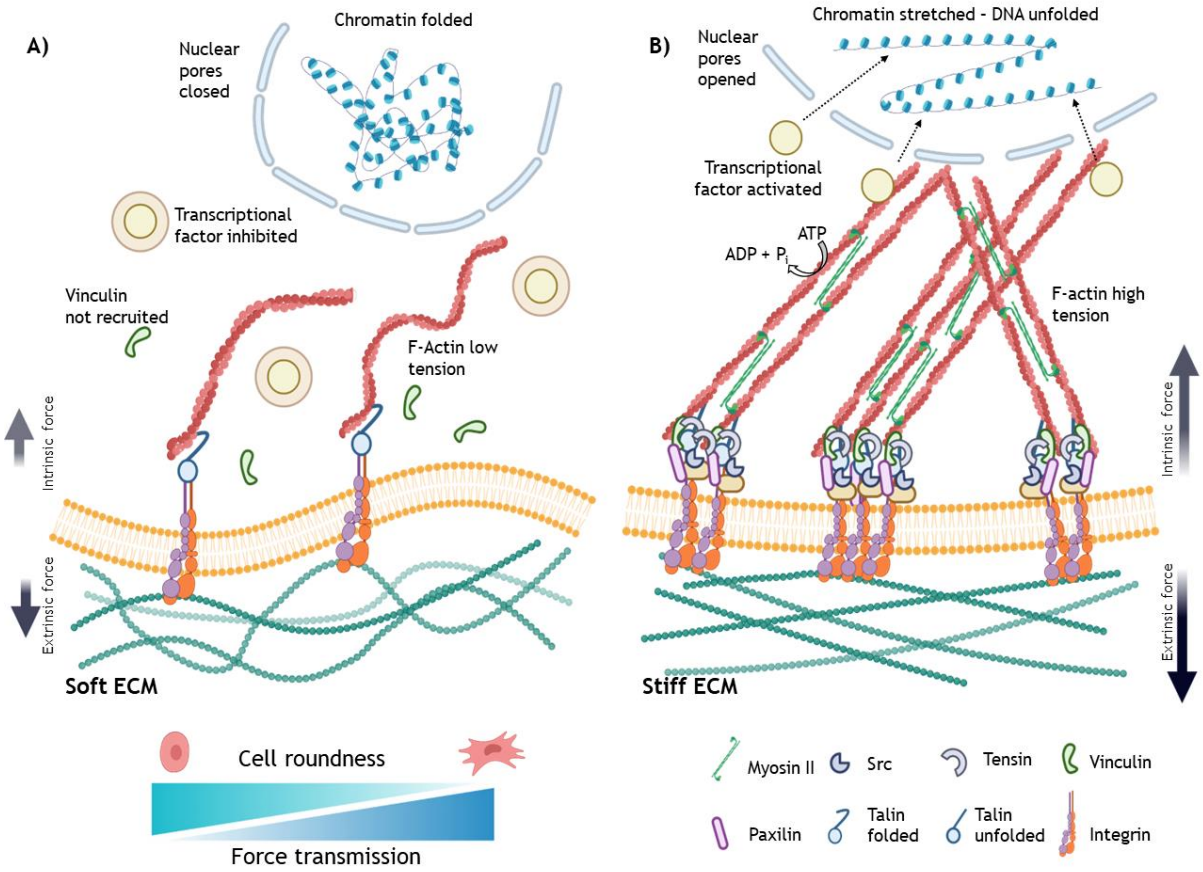

Figure 1-4. Mechanical forces and FAs reinforcement increase with surface stiffness (Biorender made). *A) On soft matrices, cells do not have enough*

strength to generate mature focal adhesions. Talin remains unfold and vinculin is not recruited to the FAs. The cells are rounder as well as the nucleus. The nuclear pores are closed and chromatin remains unfolded. Transcriptional factors are inactive in the cytoplasm. Actin fibres (F-actin) are not tense, and the intracellular tension is low. B) On stiff surfaces, talin unfolds and vinculin can be recruited to the focal adhesions along with other proteins involved in the molecular clutch, forming mature FAs. Actin cytoskeleton is established and cells can contract by hydrolysing ATP. Cells are more spread and the nucleus stretch opening the pores. Transcriptional factors are activated and capable to enter the nucleus and bind to the DNA.

The molecular mechanism to detect rigidity and trigger downstream signalling has been widely investigated. Integrins play an essential role as they are the direct link between actin-cytoskeleton and the ECM (Figure 1-4). Also, their binding and unbinding rate works as a rigidity sensor (4,45,46). Moreover, there is a wide variety of identified integrins with different binding rates to the same ECM components, what could be an important rigidity adaptation mechanism. Furthermore, not all cell lines express the same type of integrins or at the same density, what changes the cellular response to a same surface. The density of ECM proteins on the substrate will also have an impact on the forces that the cells exert (43,47,48). In summary, the total force loaded is determined by the protein concentration and the density of integrins available for interaction (49).

As well as stiffness and protein density, matrix degradability plays an important role in cell behaviour. In order to migrate and proliferate, cells have to break the ECM network. To remodel the ECM, it is necessary the action of matrix metalloproteinases (MMP), which are enzymes that are able to recognise specific domains in the ECM proteins and cleave them. These enzymes can be secreted or be bound to the membrane (known as MT-MMP). The Table 1-1 taken from Cabral Pacharo G. et al. 2020 (50) describes the main MMPs classified by structure and the main substrate where they act.

Table 1-1. Classification of metaloproteinases depending on their structure and the substrate where they act. Taken from (50).

Feature	Subgroup	Description	MMPs
Structure	Minimal domain MMPs	Secreted	MMP-7, MMP-26
	Simple Hemopexin domain-containing MMPs	Secreted	MMP-1, -3, -8, 10, -12, -13, -18, -19, -22, -20, 27
	Gelating binding MMPs	Secreted	MMP-2, MMP-9
	Furin-activated MMPs	Secreted	MMP-11, MMP-28
	Vitronectin-like insert MMPs	Secreted	MMP-21
	Transmembrane MMPs (with cytoplasmic domain)	Membrane-type MMPs	TM: MMP-14, -15, -16, -24.
	glycosylphosphatidylinositol (GPI)-anchored MMPs	Membrane-type MMPs	MMP-17, MMP-25
	Type II transmembrane MMPs (cysteine array and immunoglobulin-like domains)	Membrane-type MMPs	MMP-23
Substrate	Collagenases (1–4)	Substrates: Col II, II, III, VIII, X, gelatins, aggrecan, entactin	MMP-1, -8,-13, -18
	Gelatinases (A and B)	Substrates: gelatins, collagens I, IV, V, VII, X, XI, fibronectin elastin, laminin, vitronectin, proMMPs-9 and 13	MMP-2, MMP-9
	Stromelysins (1–3)	Substrates: proteoglycans, laminin, gelatins, fibronectin, entactin, collagens III, IV, V, IX, X, XI, proMMPs 1, 8, 9 and 13, vitronectin, α 1-proteinase inhibitor	MMP-3, -10, -11
	Matrilysin	Substrates: proteoglycans, laminin, fibronectin, gelatins, entactin, collagen IV, elastin, tenascin	MMP-7, MMP-26
	Membrane-type MMPs (MT-MMP-1, -3, -4)	Substrates: col I, II, III, gelatins, fibronectin, laminin, proteoglycans, proMMP-2 and 13	MMP-14,-15, -16, -17, -24, -25

These specific domains that can be recognised by the MMPs can be engineered to create proteolytically cleavable crosslinkers, which will be incorporated in the hydrogel to create a biodegradable network. This will change the matrix stiffness and, hence, how cells sense the matrix. It has been shown that the higher biodegradability, the higher cell circularity and cell viability, while cell density and area decrease. Biodegradation makes the hydrogels softer, therefore, the cell differentiation pattern changes (51,52).

Matrix degradability is of special interest in 3D systems. Cells need to degrade the matrix to be able to migrate and proliferate (34,53). Depending on the biodegradation rate of the matrix, MSCs will present a different differentiation pattern. Cells cultured in a non-biodegradable gel will not be able to migrate and proliferate, being confined in the hydrogel. In those cases, cells adopt a more rounded shape and tend to differentiate into softer tissues, such as adipose tissue (54). However, when a biodegradable crosslinker is added to the system, MSCs can cut the network by secreting metalloproteinases. Thus, they will be able to migrate, proliferate and expand, which allows the cells to generate more force tension and, hence, differentiate into stiffer tissues such as bone (55,56). This is because, in non-degradable 3D systems, MSCs cannot form mature FAs and, hence, load enough forces to deform the matrix. It has been also observed that this behaviour can be reversed with high RGD density. In those cases, cells will be able to generate more FAs and exert enough traction forces to differentiate into bone, when the stiffness is 11-20 kPa (44,57). All these outcomes provide important insight into the importance of degradability and force generation in 3D systems.

Even though the implication of matrix degradability has not been fully studied on 2D systems, there are few studies that have seen differences in cell behaviour (58). It has been shown that adipogenesis is enhanced on softer surfaces, independent of degradability. Surprisingly, there has been observed an upregulation of osteogenesis as the degradation rate increases (51). Matrix degradability has been shown to play an important role in cancer cell invasion. In a metastasis study carried out by Dvir et, al, they observed that cancer cells with high metastatic potential are able to indent either on degradable or non-

degradable surfaces regardless of the stiffness. However, the indentation depth and the forces applied were higher on stiff degradable matrices (58).

To recapitulate, MSCs differentiation depends on ECM characteristics such as stiffness or degradability. Taking this into account, controlling the rigidity and degradability of the scaffold makes it possible to direct cell differentiation into a specific cell type to be used in tissue regeneration.

1.1.4. Cell contractility has an essential role in cell attachment, force generation and differentiation

Cells must contract their actin cytoskeleton to generate the forces needed to remodel the ECM. This actin structure is directly linked to FAs responsible for force transmission from inside the cell to the matrix. Cells on stiff surfaces present a well-organised cytoskeleton, with high expression of F-actin fibres, which allows them to generate higher traction forces (42,49). However, we should not confuse cytoskeleton organisation with cell shape. Even though on stiff surfaces cells tend to present a more elongated shape, the cellular shape is not an indicator of force magnitude generated by the cell, as it happens with the cytoskeleton (a more organised cytoskeleton leads to higher contractility and force generation). Cells change shape while they are indenting and penetrating the surfaces while they are applying mechanical forces, hence, cell shape is not related to force magnitude (58,59).

The proteins present in these FAs, such as non-muscle myosin II isoforms, are the ones that sense matrix elasticity and drive lineage differentiation. Therefore, inhibition of non-muscle myosin II blocks all elasticity directed lineage specification, without strongly perturbing many other aspects of cell function and shape (60,61).

Blebbistatin is a specific inhibitor of the ATPase activity of non-muscle myosin II (62,63), a hexameric actin-binding protein formed by two heavy chains with ATPase activity in its head domains (64). Blebbistatin binds to the ATPase when this one is in a complex myosin-ADP-Pi, slowing down the ATP molecule release

(Figure 1-5). It does not interfere with the actin-myosin bonding or with ATP-induced actomyosin dissociation (62) (Figure 1-5). Therefore, the presence of blebbistatin decreases cell contractility by disrupting the actin retrograde flow.

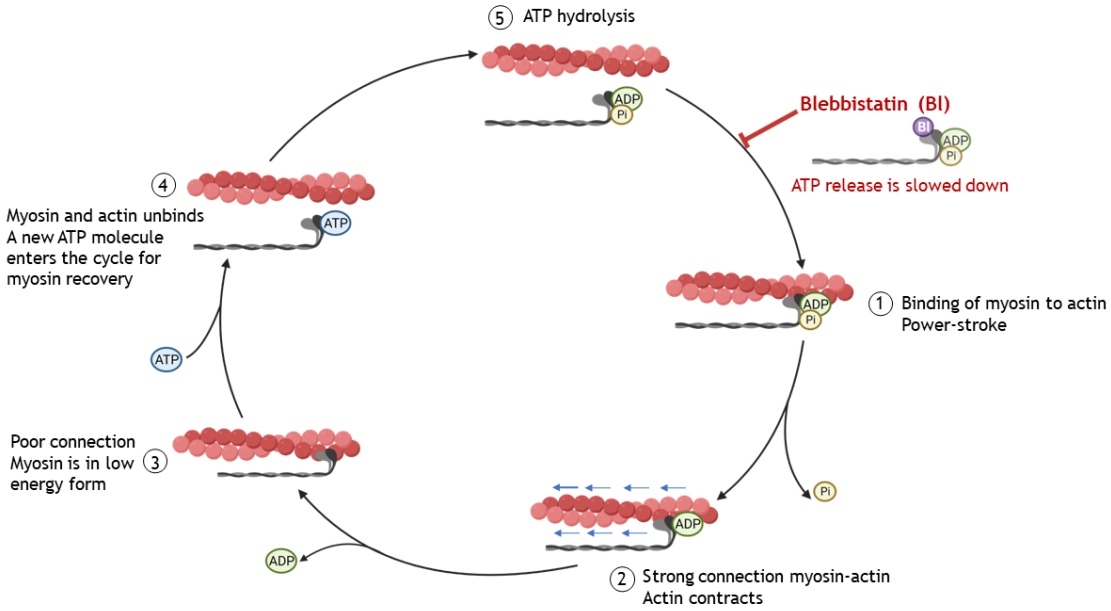

Figure 1-5. The mechanism of action of blebbistatin (Biorender made). *Blebbistatin is a non-muscular myosin II inhibitor. It binds to the ATPase of the myosin II when it is in a complex myosin-ADP-Pi, slowing down the ATP molecule renovation in the contractile cycle.*

In MSCs, treatment with inhibitors of actomyosin contractile units blocks osteogenesis in favour of adipogenesis, regardless of surface stiffness (65,66) (Figure 1-6). These observations indicate that mechanically driven cell fate determination relies on the contractility of the actomyosin cytoskeleton. Moreover, as matrix stiffness increases, MSCs alter their non-muscle myosin II expression to prepare their actin-cytoskeleton to generate an appropriate force rate to deform the matrix. But this behaviour is not shown in cells treated with blebbistatin. This inhibition not only prevents cell contractility but also makes the cells unable to migrate and blocks cytokinesis (1).

MSCs differentiation is also regulated by the RhoA-dependent actomyosin contractility (67,68). Higher contractility is linked to an increase in RhoA expression, and this triggers osteogenic differentiation. RhoA is a GTPase protein

that activates ROCK. ROCK phosphorylates myosin light chain enhancing actomyosin contraction. Thus, as happens with blebbistatin, inhibiting actomyosin contractility with a ROCK inhibitor, such as Y-27632, favours adipogenesis and down regulates the expression of osteogenic markers (69). In support of ROCK activity, the myosin light chain can be also phosphorylated by Ca^{2+}/ calmodulin (CaM)-dependent myosin light-chain kinase (MLCK) (70). The activity of this enzyme can be specifically inhibited using ML-7 (71).

Based on these studies, inhibition of cell contractility has big consequences on mechanosensing and cell differentiation. In most cases, cells tend to behave as they were on soft surfaces, being adipogenesis upregulated over osteogenesis.

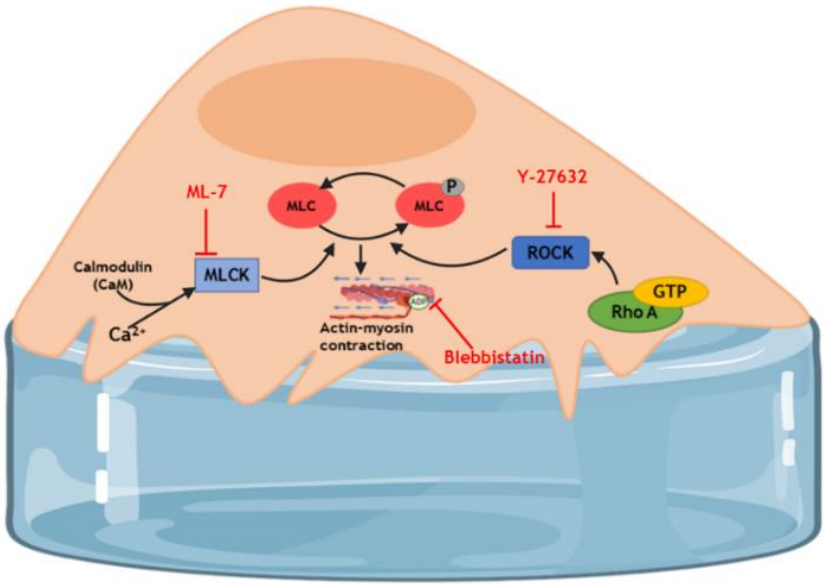

Figure 1-6. The implication of actomyosin contractility and FAs alteration in cell differentiation and actomyosin contractility inhibition (Biorender made). *There are multiple compounds that can inhibit cell contractility at different points such as blebbistatin which act at non-muscle myosin II A level, while Y27632 blocks RhoA activity, or ML-7 which inhibits MLCK. The inhibition of cell contractility will change how cells sense the surface.*

1.2. YAP: AN IMPORTANT MECHANOTRANSDUCTION FACTOR

Cells create adequate FAs to be able to communicate with the ECM. The activity of the focal adhesion kinase (FAK) in FAs is essential to transmit the signals gathered from the ECM through the cytoskeleton to the nucleus. This enzyme phosphorylates and activates mechanoresponsive signalling elements, which leads to an increase in cellular contractility and the nuclear translocation of transcriptional factors (e.g. Yes-associated protein (YAP) and transcriptional co-activator with PDZ-binding motif (TAZ)) as well as activation of lamina proteins in the nucleus (e.g. LMNA) regulating transcription pathways (34). One of the most widely studied mechanosensing transcriptional factors is YAP. This protein remains phosphorylated in the cytoplasm as its inactive form. Under the pertinent stimuli, can be dephosphorylated into its active form through different pathways (e.g. Hippo Pathway inhibition, RhoA activation), form a dimer with TAZ (transcriptional coactivator with PDZ-binding motif) and migrate into the nucleus. Once inside the nucleus, YAP/TAZ will join to specific domains of the DNA by activating and forming a complex with. transcriptional enhanced associate domain (TEAD) protein. This interaction triggers the expression of genes involved in multiple cellular processes including cell proliferation and differentiation (39,61,72,73). YAP/TAZ activity is involved in cytoskeleton stability and FAs assembly, thereby it is important to control cellular tension and mechanics (74).

The number of FAs and YAP translocation are related to the adhesion area and the cell area (Figure 1-7). Nardone. G. et al showed that FAs assembly depends on adhesion area and YAP activation. On the other hand, YAP nuclear translocation, even though it is triggered by FA-cytoskeleton stabilisation, is independent of FA formation and dependent on cell area through the activation of the Rho/ROCK mechanosensing pathway (74,75). YAP nuclear translocation activates gene expression involved in FA reinforcement. The disruption of the YAP/TAZ mechanical pathway leads to cytoskeleton disorganisation, a decrease in cell stiffness, failure in cell attachment and a complete disruption in cellular mechanical cues to respond to ECM signals (74).

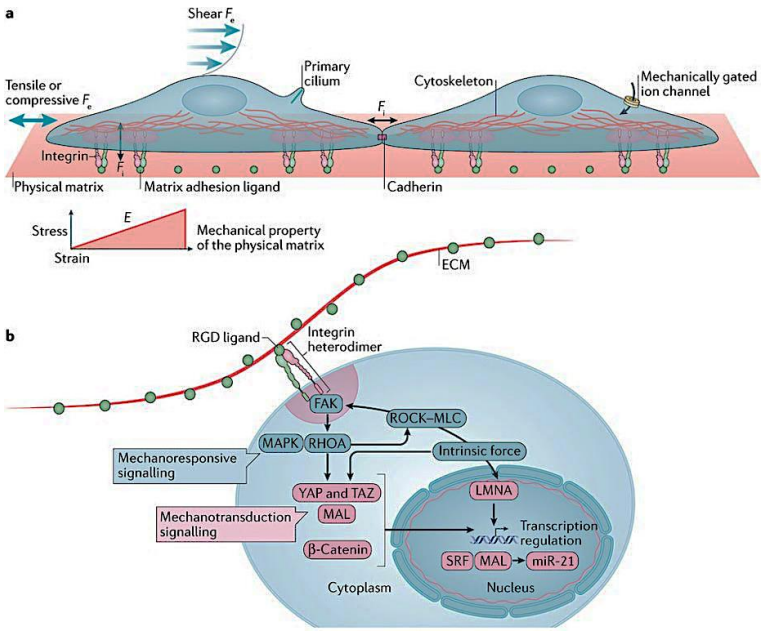

Figure 1-7. Mechanotransduction within the cell (image taken from (34)***).*** *A) Cells interact with the ECM through integrins and with other cells through cadherins. Through these connections, they are able to exert forces and sense external forces. B) The information gathered by the integrins is going to trigger different intracellular pathways to generate an ultimate response to the initial stimulus.* (34).

Depending on how stiff cells detect the surface, YAP nuclear translocation varies (75) (Figure 1-8). On stiffer matrices, YAP translocates into the nucleus and favours osteogenic differentiation (Figure 1-8B). Whereas, on softer substrates, YAP is phosphorylated and excluded from the nucleus remaining cytoplasmatic, being adipogenesis differentiation enhanced (61,75–77) (Figure 1-8A). This behaviour is directly related to actin-cytoskeleton contractility. On soft surfaces, cells present low contractility, there is low F-actin fibres expression, and the nucleus remains round (Figure 1-4A). YAP cannot translocate to the nucleus and remains trapped in the cytoplasm (11). On the other hand, as surface stiffness increases, cells load higher forces by the generation of further F-actin stress fibres and contraction. The increment of tension within the cell provokes nucleus flattering and nucleus pores stretching, leaning to YAP nuclear translocation (11,77) (Figure 1-4B). This same behaviour that appears on rigid surfaces also happens when a force is applied to the cell (11).

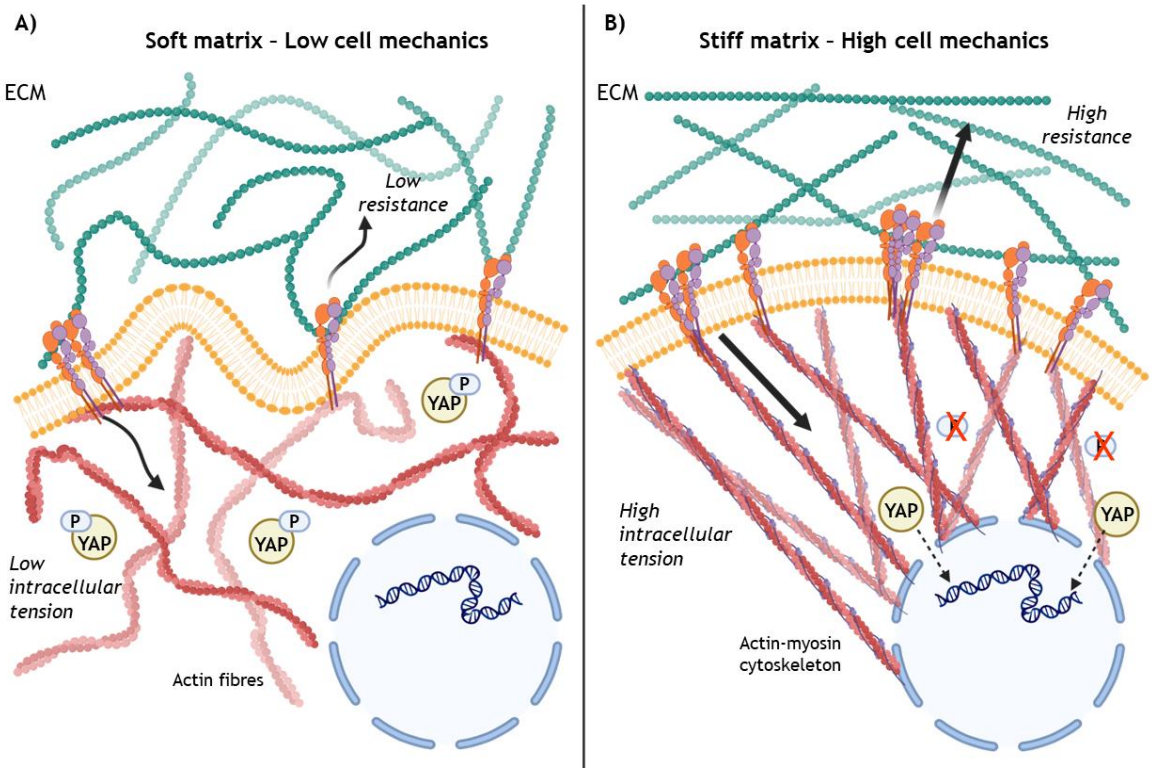

Figure 1-8. YAP translocation relies on ECM stiffness and cell contractility (Biorender made). *a) When cells find low resistance in the ECM (soft) the tension rate decrease, and YAP remains cytoplasmic phosphorylated (inactive). b) When the ECM resistance increase (stiff matrices), the actomyosin contractility is higher, allowing YAP to dephosphorylate and translocate into the nucleus where it binds to the DNA.*

YAP nuclear translocation is different in 2D and 3D models. As described above, in cells cultured in 2D, YAP translocates into the nucleus on stiffer hydrogels (75). However, when cells are embedded in a hydrogel (3D model), YAP nuclear translocation increases with matrix degradability and lower stiffnesses (78,79). Contrary to what happens in 2D, cells encapsulated in stiff hydrogels are not able to elongate and YAP appears in the cytoplasm (75). These discrepancies between 2D and 3D might explain the difficulty to translate what we observe *in vitro* with what is happening *in vivo*(75).

Regardless of surface stiffness, YAP translocation is also influenced by cell attachment. Modifying cell attachment by changing the ligand available for cells to attach to the surface, as well as its density is going to have an effect in cell

mechanotransduction. For instance, coating the surface with poly-L-lysine (PLL) reduces FAs formation, cell area and favours adipogenesis (75). In another study done by Stanton A et at., they demonstrated that in cells seeded in polyacrylamide gel functionalised with fibronectin, YAP translocation is influenced by surface stiffness only in intermediate ligand densities (80). However, on low or high ligand density YAP is going to remain cytoplasmatic or translocate into the nucleus, respectively, regardless of the surface stiffness. This has also an effect on cell differentiation, increasing the fibronectin density favours osteogenesis over adipogenesis differentiation (80). Furthermore, cell contractility and integrin expression influence YAP translocation (80). Lee et. al. studied YAP localisation after the knockdown of two integrins β_1 and β_4. When integrin β_1 was knocked down, cells could not spread, and YAP remained cytoplasmatic which confirms the influence of cells spreading in YAP translocation. However, cells with integrin β_4 knocked out did not present a decrease in the cell area, but YAP nuclear translocation was affected, which indicated that cell spreading is not the only factor to have in consideration in YAP activity (77).

YAP localisation can also vary depending on cell density. In a high confluent scenario, cell-cell contact through cadherins increases, while cell-ECM link through integrins decreases (81). Regardless of matrix stiffness, YAP starts to accumulate in the cytoplasm. Also, densely plated cells express fewer stress fibres compared with the widespread plated ones which present a well-organised cytoskeleton (77).

1.3. CELL METABOLISM

Metabolism is the series of biochemical reactions mediated by enzymes that occurs within the cells and are essential for life-sustaining. The intermediate or final products generated in this process are known as metabolites. These molecules can be categorised as primary metabolites if they are directly involved in cell growth and development; or secondary metabolites, generated from the primary metabolites and without a direct implication in cellular function maintenance.

The different metabolic pathways can lead to the biosynthesis of small molecules, known as anabolism (e.g. protein synthesis), or their breakdown, called catabolism (e.g. cellular respiration). In general, anabolic reactions consume energy, while catabolic reactions release it. These reactions occur thanks to enzymes: proteins that catalyse the metabolic reactions and couple the anabolic pathways with the catabolism ones. Those enzymes provide energy released during the catabolism, generally, in the form of ATP to the anabolic processes (82).

1.3.1. Cellular respiration influences cell differentiation

Glycolysis is an oxygen-independent metabolic pathway that occurs in the cytoplasm (Figure 1-9A). Through this process one molecule of glucose is broken into 2 molecules of pyruvate, yielding 2 ATP and 2 NADH (83). Depending on the oxygen available, pyruvate can follow two different pathways: anaerobic (fermentation, also known as anaerobic glycolysis) (Figure 1-9C) or aerobic (oxidative phosphorylation) (Figure 1-9B) (84). Under the presence of enough levels of oxygen, aerobic organisms use pyruvate to create energy through oxidative phosphorylation (OXPHOS), a life-sustaining process that occurs in the mitochondria to generate energy in form of ATP by transferring electrons from NADH or $FADH_2$ to oxygen (O_2). Commonly, the set of all these reactions is known as cellular respiration.

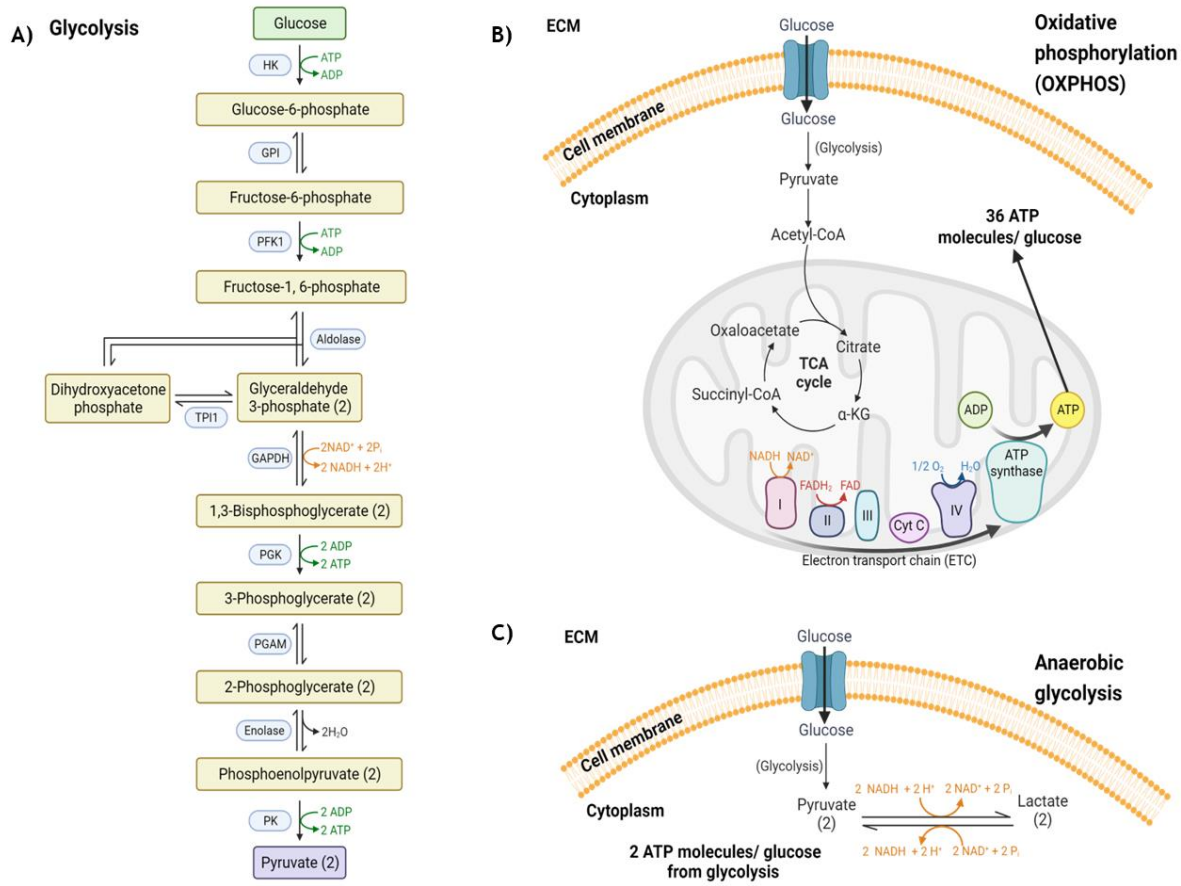

Figure 1-9. Cell metabolism under aerobic and anaerobic conditions. *Pathways templates taken from BioRender. A) Glycolysis: glucose metabolism to pyruvate. In total the process yields 2 molecules of ATP. Enzymes involved: hexokinase (HK), phosphoglucose isomerase (GPI), phosphofructokinase-1 (PFK1), aldolase, triosephosphate isomerase (TPI1), glyceraldehyde 3-phosphate deshydrogenase (GAPDH), phosphoglycerate kinase (PGK), phosphoglyceromutase (PGAM), enolase and pyruvate kinase (PK). B) Under aerobic conditions, pyruvate is converted into acetil-CoA by the pyruvate deshydrogenase. Acetyl-CoA enters into the mitochondria to me metabolised in the tricarboxylic acid cycle. ATP is generated in the electron transport chain by the reduction of oxygen in a process called oxidative phosphorylation (OXPHOS). At the end of this process around 36 ATP molecules are generated. C) Under anaerobic conditions where the oxygen available is limited, pyruvate will be converted into lactate in a reversible reaction by the lactate dehydrogenase.*

Mitochondrial activity and oxidative metabolism play an important role in stem cell pluripotency control. It has been shown that during differentiation oxidative

phosphorylation increases (85). Cells regulate their respiratory rate and mitochondria activity and number, depending on how they sense the environment. Pluripotent stem cells and also mesenchymal stem cells mainly have a glycolysis metabolism (83). They present a low number of mitochondria which are poorly developed. In their naïve environment, stem cells have a low proliferation rate and high differentiation potency capacity. However, during cell maturation and differentiation, the proliferation rate increases, as it does mitochondria expression (there is an increment in mitochondrial DNA and mass). Glycolysis-based cell metabolism shifts to OXPHOS-based metabolism (83). Differentiated cells have a higher demand for oxygen, which translated to an increase in respiratory rate and, hence, in intracellular ATP content. However, during stemness reprogramming of pluripotent stem cells from adult tissue, there is a setback, the metabolism shifts from oxidative phosphorylation to glycolysis. Also, cells in hypoxia enter into a glycolytic quiescent state protecting the tissues from reactive oxygen species (ROS) generation and ensuring tissue regenerative capacity. Interestingly, if MSCs are cultured in normoxia the proliferation and senescence increase while they lose their stemness (86).

On the other hand, osteogenic differentiation requires OXPHOS activity (87). During differentiation, MSCs express fewer pluripotency genes and start to upregulate terminal-specific genes. At the same time, they go through a metabolic switch, respiratory metabolic enzymes are expressed and mitochondria DNA increases. Glycolysis markers, such as hypoxia-inducible factor (HIF)-1a, start to decrease and the oxygen consumption rate increases (83). Recently, Guo et. al. have shown that by transferring mitochondria from a donor bone marrow MSCs to a recipient bone marrow MSCs, osteogenic differentiation and wound healing are enhanced. After mitochondria transfer, modified MSCs showed higher osteogenic markers (Runx2, ALP, and BMP2) after 14 days of culture compared with the control (88). Furthermore, those mitochondria-recipient MSCs have been demonstrated to heal bone defects in vivo faster than the control cells. When the metabolism activity of mitochondria transfer cells was investigated, a greater OXPHOS activity and ATP production were found (83,88). Under any cellular stress situation as could be applied forces, a defect on the bone or skin, the respiratory rate increases. This study has demonstrated that an upregulated mitochondria

activity could improve cell viability by decreasing cell senescence and enhancing cell proliferation and migration, yielding a faster and greater recovery(88).

In their natural niche, MSCs are in hypoxia conditions (89,90). They present a glycolysis-based metabolism with the downregulation of respiratory enzymes and oxygen consumption rate decrease. Hypoxia allows stem cells to proliferate, maintaining their self-renewal and potency abilities. MSCs are still able to differentiate into chondrocytes, adipocytes or cardiomyocytes under hypoxic or ischemic conditions (83). Notice that in a hypoxia environment, ROS levels are enabled and osteogenesis differentiation of hMSCS will be inhibited in favour of adipogenesis. Also, ROS levels have an implication on senescence and stemness, hMSCs will remain undifferentiated and maintain their self-renewal and multipotency abilities. However, to maintain low levels of ROS is necessary to reduce mitochondrial activity (83,86).

1.3.2. ATP: the energy currency of the cells

ATP is the principal source of energy in life sustainability. It is mainly produced during cell respiration. The highest amount of ATP is produced in the electron transport chain, situated in the inner membrane of the mitochondria during OXPHOS. Other pathways which also contribute to the overall amount of ATP, are the metabolism of fatty acids through ß-oxidation or during ketosis. Under situations of low oxygen, ATP is also produced in a much lower amount. One example would be the fermentation of glucose into lactic acid which yields only 2 molecules of ATP compared with 36 molecules obtained in aerobic cell respiration (OXPHOS) (Figure 1-9). There are multiple molecules from where ATP can be obtained. However, the one that yields more ATP is glucose. Cells use the energy accumulated in ATP bonds by breaking the molecule into ADP or further into AMP.

ATP is implicated in multiple processes of cell mechanics and metabolism. One molecule of ATP must be hydrolysed into ADP and Pi to get actin-myosin coupling and the consequent pulling of the actin filaments to contract. Furthermore, ATP is essential to establish FAs and, in the cytoskeleton remodelling and cell spreading. As well as in cell-cell interactions (91). In epithelial cells, applied

mechanical forces increase the formation of cell-cell adhesions through E-cadherin. This reinforcement of cell connections required remodelling of the actin cytoskeleton for which they need energy supplied by ATP (92). However, when cells are in glucose starvation, they cannot produce enough levels of ATP showing a decrease in FAs formation, less cellular spreading and cytoskeleton organisation. Therefore, cells required glucose to maintain an adequate level of ATP. Also, inhibiting cytoskeleton remodelling with Cytochalasin D (CytoD), which blocks actin polymerisation, leads to a diminution in ATP consumption. Under these circumstances, cells could not form their actin-cytoskeleton and spread. When CytoD is washed out, cells recover their activity and ATP levels decrease, confirming that this molecule is essential for actin-cytoskeleton formation and spreading (91). A similar pattern occurs when cellular contractility is inhibited with blebbistatin or ROCK inhibitor Y27632, ATP levels remain constant over time, but cellular contraction decreases, and cells appear more round (91). ATP is also involved in cell migration. Mousawi et. al. showed that MSCs treated with Yoda1, an activator of the ion channel Piezo 1, caused an increase in ATP release with the subsequent activation of the mitogen-activated protein kinase/extracellular signal-regulated kinase (MEK/ERK) implicated in cell migration (93).

Cellular energetic levels are altered when there is DNA damage. Milanese et.al have demonstrated that interrupting the DNA repair pathways (transcription-coupled DNA repair (TCR) and nucleotide excision repair (NER)) leads to an increase in ATP levels and a decrease in DNA transcription (94). As an adaptive response, glycolysis is inhibited and glucose is directed to the pentose phosphate pathway, changing the cell metabolism completely (94). Through this pathway, cells are capable to reduce redox stress and NADPH is produced as a reducing equivalent to supply the energy requirements under these circumstances (94,95). This underlines the importance of ATP in DNA repair, transcription and translation.

Another process where ATP plays an important role is in protein metabolism. During protein synthesis, one molecule of ATP is hydrolysed into AMP and PP_i by the aminoacyl tRNA synthetase. This enzyme binds the corresponding amino acid in the gene code of the protein being synthesised, to the transfer RNA (tRNA). Later, the tRNA enters the ribosome, couples to the messenger RNA (mRNA) and

transfers that amino acid to the elongating protein in synthesis. Therefore, any alteration in ATP synthesis is going to have an effect on protein synthesis.

ATP does not only act as in intracellular signalling molecule. It has been demonstrated its implication in multiple extracellular processes. It acts as a neurotransmitter in neurotoxicity (96) or in the activation of sensory nerves terminal in the gastrointestinal tract (97). Under brain damage, ATP is released to the extracellular space. Once there it interacts with different neuronal receptors (e.g. P2X7R) to trigger pro-inflammatory pathways (e.g. release IF-β or cytokines) to reduce the neurotoxicity (96). Recently, it has been shown that extracellular ATP is one of the main sources of pyrophosphate, which is the main endogenous inhibitor of vascular calcification. Therefore, the ATP/pyrophosphate metabolism could be a potential target to reduce vascular calcification (98).

To sum up, ATP is essential for cell survival. If ATP metabolism is dysregulated it can lead to multiple pathologies. For instance, it has been shown that during tumorigenic processes there is an increase in the uptake of glucose which leads to a higher production of ATP and a faster tumour growth (99). Hence, targeting glucose metabolism could reduce cancer progression.

1.3.3. AMPK acts as an energy regulator

When the levels of ATP are too low to sustain cell life, AMPK is activated. This usually happens under mitochondrial stress. Cells enter into a low-energy consumption mode increasing nutrient intake and activating alternative energy source pathways (e.g. turning macromolecules into nutrients) (100).

AMP can sense the amount of energy available by an allosteric mechanism. When the ratio AMP/ATP increases the kinase activity of the enzyme is activated. It directs cellular metabolism towards catabolism pathways to generate nutrients from where energy can be obtained and decreases anabolism to reduce ATP usage (92,100). Once AMPK is activated, it phosphorylates key metabolism enzymes and triggers the expression of different transcription factors (e.g. GLUT1 and GLUT4 which increases glucose intake). For instance, AMPK phosphorylates the enzyme HMG-CoA reductase (HMGCR) and the acetyl-CoA carboxylases ACC1 and ACC2,

inhibiting cholesterol and lipid synthesis respectively (100). Lipid synthesis is also inhibited by phosphorylating the transcriptional factor sterol regulatory element binding proteins 1c (SREBP-1a) in hepatocytes. When this transcriptional factor is phosphorylated, it cannot be cleaved and translocated into the nucleus to activate the expression of lipid synthesis genes (101).

The AMPK pathway is directly linked with the mechanistic Target of Rapamycin (mTOR) pathway. mTOR acts as a regulator of cell growth and metabolism. It adapts the cellular functions depending on the nutrients available (102). In normal situations where there is a good supply of nutrients, AMPK is inactive while mTOR promotes cell growth and anabolism increasing the production of protein, lipids, nucleotides and ATP (100). On the other hand, under a lack of nutrients, AMPK is activated, and it inactivates mTOR by phosphorylating its subunit RAPTOR and indirectly by activating its negative regulator tuberin (TSC2) (100,102). As described above, in a situation of cell starvation catabolism primes over anabolism, and cell growth decrease whereas cell autophagy increases to get more nutrients (100).

AMPK plays an important role in cell homeostasis. Most importantly, it regulates the levels of ATP in situations of cellular stress. Understanding how AMPK works could provide a better knowledge of the cellular metabolism in different environments.

1.4. CELLULAR MECHANICS AND METABOLISM ARE NOT SEPARATED PROCESSES

The connection between mechanotransduction and metabolism has not been fully addressed yet. However, they are not independent of one another. In the last years, there have been arising multiple studies where the link between cellular mechanotransduction and metabolism has been demonstrated. In order to resist the stress caused by applied forces, cells have to couple and reinforce the actin-cytoskeleton and the FAs (103,104). To do so they increase enzymatic activity, actin polymerization and cell contractility which requires ATP energy (104,105). L. Bays et al. have demonstrated that when a force is applied on E-cadherins in

epithelial cells leads to AMPK recruitment and activation. As a result, cell contractility via RhoA and glucose uptake increase to produce more ATP. Interestingly, AMPK recruitment to the E-cadherin junction is also favoured by cell contractility. Cells treated with blebbistatin cannot transmit the mechanical force signal through the cell cytoskeleton, showing a lower level of AMPK recruitment to E-cadherin (104). Actomyosin contractility also regulates lipid metabolism. Romani et al. show that when cell contractility was inhibited via ROCK by Y27632 there was a lipid and cholesterol accumulation. Genes involved in lipid synthesis (e.g. SREBP) were upregulated. This also coincides with a decrease in YAP/TAZ nuclear translocation. A similar pattern appears in cells seeded on soft substrates which present low contractility (106) (107).

In addition to the connection between the mechanical and metabolic activity of the cells, there is a regulation of mitochondria ATP levels in relation to surface stiffness (108). One example is the recycling of ATP through the phosphocreatine (pCr)-creatine kinase (CK) system. which plays an essential role in mechanotransduction. Stiff surfaces not only promote an increase in mitochondria number and activity but also triggers ATP recycling though the pCr-CK system. This system depends on arginine flux through the urea cycle, which is reflected by the increased incorporation of carbon and nitrogen from L-arginine into creatine and phosphocreatine on stiff matrix (109).

Depending on how the cells sense the stiffness of the surface when they stablish FAs is going to direct cell fate. The tension generated when cells attach is going to be transmitted from the FAs to the nucleus through the actin-cytoskeleton, this connection is also known as the linker of nucleoskeleton and cytoskeleton (LINC) (10). On stiff surfaces, cells present a more spread shape and more mechanical forces are generated. This tension leads to a flatter nucleus and hence, wider pores (10,12). Chromatin is stretched and transcriptional factors enter into the nucleus more easily and bind to the DNA, which triggers the expression of mechanosensitive genes (12,110). As a result, cells undergo an adaptation of their mechanics and metabolism depending on the information gathered from the ECM in the first place. Nonetheless, mechanical forces are not only going to change the shape and morphology of the nucleus but of different organelles changing the cell

activity completely. Furthermore, on stiff surfaces, molecules involved in glycolysis (e.g. TRIM21) are going to be trapped within the actin fibres incapable to act. Under these circumstances, glycolysis is going to be triggered to supply the energy demand (111). On the other hand, on soft surfaces, the actin filaments are not formed and these molecules are released and free to act (111). Thereby, the higher stress fibres density and actin-cytoskeleton contractility on stiff surfaces correlate with an upregulation of metabolites implicated in glycolysis and tricarboxylic acid cycle (TCA). Whereas on soft surfaces cells adopted a lower contractility and an accumulation of glucose-6-phosphate indicates inhibition of early stages of glycolysis (111).

Understanding how cells metabolomics and mechanotransduction are going to change depending on the mechanical properties of the substrate and environment conditions provides a complete overview of cellular behaviour. All this knowledge can be used later in regenerative medicine to develop the most adequate scaffold to direct cell differentiation to the tissue of interest.

1.5. ENGINEERING THE EXTRACELLULAR MATRIX (ECM)

A well-known method to mimic the ECM characteristics and have complete control of the mechanical properties is through hydrogels. Generally, hydrogels are viscoelastic networks which can swell without dissolving in water (112). It is possible to incorporate biologically active molecules like ECM proteins to allow cell attachment or other molecules such as growth factors to drive cell differentiation (113). As a result, hydrogels can be easily controlled to have certain physicochemical and biochemical properties, being a suitable scaffold for cell biology studies while mimicking certain aspects of the natural ECM (66,114). Furthermore, they are also a perfect scaffold for cell culture as they can be used either in 2D or 3D culture.

Hydrogels can be obtained from natural or synthetic sources, depending on if they derivate from animals or plants, or have been originated by crosslinking polymers using chemical reactions respectively.

1.5.1. Matrigel: a widely used natural hydrogel

Natural hydrogels coming from mammalian cells are normally obtained by extracting the cells and antigens of the ECM using detergents. The main advantage of this method is that the composition of the ECM is preserved. The same proteins, adhesion ligands and soluble molecules that were on the original tissue or organ remain intact, making the hydrogel an environment closer to reality.

One example of a natural hydrogel widely used to study cell behaviour *in vitro* is Matrigel, a commercial matrix obtained from an Engelbreth-Holm-Swarm mouse tumour (115,116). This is a chondrosarcoma which produces large amounts of the basement membrane, a type of extracellular matrix characteristic of epithelial and endothelial cells. This matrix is really rich in collagen, among other cell adhesion proteins such as laminin, and soluble molecules (e.g. growth factors and cytokines). These properties make it suitable to study cell attachment and differentiation (116). Also, it can be used directly in 3D models providing the physiological requirements to allow cell proliferation, migration and differentiation (115,116). It has been also useful to study angiogenesis in mice (117,118).

Nonetheless, Matrigel has a series of disadvantages. As they come from a natural source, there are multiple variables that cannot be controllable and can cause off-target effects. It cannot be used for clinical purposes due to its murine origin, plus it can be tumorigenic(115). That is why, synthetic hydrogels are a more suitable tool for tissue regeneration as they can be manipulated to be used *in vitro* and *in vivo* with the characteristics of interest.

1.5.2. Synthetic hydrogels: a suitable tool in regenerative medicine.

Synthetic hydrogels have a series of advantages over natural ones. They are bioinert, which means that they are not hazard for the cells, and malleable, which makes easier the manipulation of their chemistry, shape and properties. However, due to their bioinert nature, cells cannot attach to synthetic hydrogels

themselves. Thereby hydrogels must be tethered to biologically active compounds like proteins naturally found in ECM such as fibronectin. Moreover, synthetic hydrogels are not degradable, which limits cell migration, proliferation and differentiation (113). To make them degradable it is necessary to include crosslinkers with a domain recognisable by metalloproteinases (MMPs) secreted by the cells. For example, VPM (GCRDVPMSMRGGDRCG) is a cysteine-flanked enzyme-sensitive peptide sequence that can be degraded by MMP-1and MMP-2 (119). Once these enzymes are secreted to the extracellular space, they recognise and cut these specific domains in the matrix network, allowing cell migration, proliferation and differentiation within the system. These processes of introducing molecules recognisable by the cells in the hydrogel is known as bioactivation.

After the bioactivation of the hydrogel, cells can behave as they usually do *in vivo*, they sense the surface and create FAs through which they exert forces of different magnitude depending on the mechanical properties of the surface. This triggers different mechanical and metabolic pathways within cells leading to different cellular behaviours. Being able to manipulate the nature of the matrix starting with a bioinert material can be a big advantage as it is possible to elucidate how cells behave mechanically and metabolically depending on the matrix properties. Furthermore, it will be possible to generate optimum scaffolds *in vitro* that can be used *in vivo for* regenerative medicine.

1.5.2.1. Polyacrylamide (PAA) hydrogels

Since they were first described in 1997 by Pelham and Wang (120), polyacrylamide (PAA) hydrogels have been widely used to study cell mechanobiology. They have been highly characterised, being one of the most reproducible hydrogels. It also provides total control of the mechanical properties under physiological conditions. Polyacrylamide hydrogels consist of a covalent crosslinking of the main polymer acrylamide with the crosslinker bisacrylamide in an aqueous medium. The polymerisation takes place when the gel solution is irradiated with UV light which initiates a free radical polymerisation, yielding a purely elastic system. PAA hydrogels can be easily bioactivated to allow cell attachment by covalently linking proteins from the ECM.

Recently it has been described a method to produce a viscoelastic PAA hydrogel. The ECM is not purely elastic, also this elasticity is variable among the different tissues. Furthermore, it has a viscous component that affects cellular response. Being able to recreate a viscoelastic system *in vitro* permits us to get a better understating of cell-ECM interactions and their implications in cellular response. This viscoelasticity is created by entrapping a linear PAA molecule in the network acrylamide-bisacrylamide (121,122). By changing the concentration of the linear PAA and the polymers it is possible to vary the viscoelastic properties of the hydrogel (121).

The main disadvantage of PAA hydrogels is that the polymer network cannot be broken by the cellular metalloproteinases. Therefore, these hydrogels cannot be used in 3D culture, as cells will not be able to migrate and proliferate within the system. Also, these hydrogels are not bioinert, being impossible to be used *in vivo*.

1.5.2.2. Poly-(ethylene)glycol (PEG) hydrogels

PEG hydrogels are one of the most common synthetic hydrogels used. They have the advantage of being biocompatible, non-toxic and bioinert, allowing to control cell adhesion and protein adsorption with minimum unspecific bindings. Furthermore, they can be crosslinked under mild or physiological conditions. All these characteristics make it possible to include cells *in situ* and used the scaffold developed *in vivo*.

PEG can be found with a linear or multi-arm structure. The basic PEG structure is PEG diol with two hydroxyl end groups. These end groups can be substituted with a functional group e.g. methyloxyl, carboxyl, amine, thiol, azide, vinyl sulfone, azide, acetylene or acrylate; and in this way PEG molecules can crosslink (Figure 1-10). PEG works in a wide range of pHs and its hydrophilic nature provides similar characteristics to the ECM. Thereby, PEG hydrogels are a high tuneable model to construct the most ideal environment for the cells.

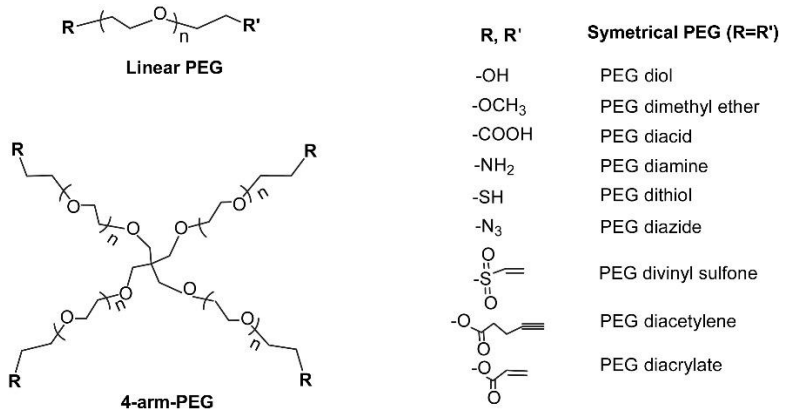

Figure 1-10. PEG linear and 4-arm structure, and possible functional end groups (image taken from (113)***). PEG is a polymer widely used for hydrogels synthesis. The basic structure is PEG diol with two hydroxyl end groups. These end groups can be substituted with multiple functional groups*** (113)

There are three possible methods of PEG polymerisation:

1. **Free-radical photopolymerisation.** This polymerisation reaction occurs in the presence of UV light which split initiator molecules into free radicals. These free radicals can react with acrylate or vinyl groups on PEG molecules (123).
2. **Step-growth polymerisation.** The reaction takes place at physiological conditions between two reactive groups (e.g. Michael-type addition) (124).
3. **Mixed-mode polymerisation**. This method involves the initiation of a thiol-acrylate polymerization upon UV light irradiation, without the requirement for a photoinitiator (125).

For this project, the method selected was photopolymerisation as it is a suitable technique to get a good gel structure before it starts polymerising.

Photopolymerisation

The photopolymerisation technique uses UV light to crosslink the polymer and form the hydrogel at physiological temperature and pH. It consists in a free radical polymerisation that occurs within minutes under controllable circumstances. Photopolymerisation is being widely used lately due to its advantages: i) allows to

control of the spatial and temporal formation of the scaffolds in situ without damaging the surroundings, and ii) cells can be encapsulated with other biological agents during the polymerisation process. The main advantage of this technique in tissue regeneration is that it can be used *in vivo* (126,127).

A photoinitiator is needed to start the polymerisation. Those are molecules with high absorption at a specific wavelength of light, once are induced with UV they will produce free radicals, which initiate the polymerisation by crosslinking the polymer. There are three types of photoinitiators depending on the photolysis mechanism: radical photopolymerisation through photocleavage, hydrogen absorption and cationic photopolymerization. This last method is not recommended in tissue engineering as can generate protonic acids (127). A widely used photoinitiator is 2-Hydroxy-4'-(2-hydroxyethoxy)-2-methylpropiophenone, known as Irgacure 2959, is a photoinitiator that undergoes cleavage when exposed to UV light, yielding free radicals to promote the polymerisation reaction.

Bioactive modification of PEG-hydrogels to mimic ECM

As has been pointed out before, cells cannot attach to synthetic hydrogels if they do not incorporate biologically active molecules that the cells can recognise. Cell attachment peptides can be chemically bound to the hydrogel and come from ECM proteins: FN (e.g. REDV), laminin (e.g. IKVAV), collagen (e.g. DGEA, GFOGER) and elastin (e.g. VAPG). Although, RGD is the cell adhesive peptide more widely used and can be obtained from FN, laminin o collagen (128).

It is important to know how cells interact with the ECM proteins, as cellular response changes depending on what ECM peptides are incorporated into the hydrogel. For instance, it has been shown that on surfaces functionalised with both gelatin and FN, cells reduce the level of traction forces on FN, being mainly applied on the gelatin. Interestingly, the traction forces on surfaces coated with FN alone (without gelatin) are higher than on surfaces functionalised with both proteins (129).

Nowadays, it is possible to covalently link full proteins into synthetic hydrogels. One possible procedure to do this is through a method known as PEGylation

(69,130). The possibility to have the entire molecule in the hydrogel will provide better protein recognition by the cells and a closer image of the natural ECM (131). Karuri and co-workers have described two methods of FN PEGylation: via lysine (132) or cysteine amino acids, both do not have an effect on cell attachment and FN-fibrinollogenesis in 2D (69,130).

Our group has developed a third PEGylation technique based on a Michael-type addition reaction between the maleimide (133) groups of a PEG functionalised polymer and the cysteines from the FN. One of the advantages of this technique is that the growth factor binding site of FN is available to be used as a synergic domain to promote either cell differentiation as migration, what will have a big implication in 3D culture. Also, as the reaction occurs with the cysteines of the proteins, we can make sure that the PEGylation will happen at specific sites within the FN. This high specificity occurs because the cysteines are not abundant in nature, so the reaction is concentrated in the protein with minimum loss of biological activity. These reactive groups are hidden inside the molecule, hence the protein has to be unfolded to react. Moreover, this process can happen at physiological pH which reduces the side effects and facilitate the reaction (134).

To summarise, PEG-hydrogels are a promising scaffold in tissue regeneration due to their facility to be modified physically and chemically. PEG-hydrogels are completely compatible with cells due to their bioinert nature. Furthermore, the fact that they must be bioactivated, allows the incorporation of bioactive molecules that can provide a better understanding of how cells interact with their environment. Furthermore, one of the main advantages is that can be used for 2D and 3D cultures which gives the possibility to form the gel in situ.

1.6. TRACTION FORCE MICROSCOPY (TFM)

Cells remodel their surrounding matrix either by proteolysis or mechanically. This kind of behaviour underlines the importance of matrix remodelling in cell-ECM interactions, cell migration and differentiation (54). To do this, cells generate traction forces to deform the matrix. However, the overall forces change depending on the ECM characteristics. Other factors, such as cell confluency, also

have an effect on the transmission of forces. It has been shown that force transmission is mainly occurring between cells when they are forming a cluster. Whereas in absence of cell-cell contact, force transmission is mainly between the cell and the substrate (135). Also, cells mechanically adapt to the surface in a different way depending on the surface coating (129). Studying what are the forces that cells exerted on the matrix provides a better knowledge of cellular mechanical behaviour and their relation with the ECM.

Traction force microscopy (TFM) is a technique that measures cellular forces exerted on elastic substrates. It consists of the quantification and analysis of elastic substrate deformation by the cells, generating map stresses (force per unit area) when these deformations are converted into traction forces.

This technique has some advantages: i) it is easy to set up and perform, ii) there is not a specific size or force scale, so by adjusting the substrate stiffness and the imaging technique a wide range of length and force scale can be measured. (iii) As it measures spatially, interfacial forces across the cells can be also quantified. All this makes TFM an easy and versatile technique to measure interfacial forces compare to others.

In general, for TFM experiments, cells interact with a hydrogel which has a functionalised protein adsorbed on the surface and fluorescent beads embedded. The position of these beads during the pulling of the cells is imaged to quantify the displacement. Later, TFM analysis software compares two images: one corresponds to the material relaxed (no cellular forces applied) and another one of the materials under stress (cells are pulling) (Figure 1-11). From these two images, it is possible to analyse the displacement of the pixels from the relaxed to the stressed position. One of the most common methods to calculate this displacement is using Particle Image Velocity (PIV). Combining the calculated displacement and the hydrogel mechanical properties it is possible to calculate the traction forces by Fourier Transform Traction Cytometry (FTTC) (136). Finally, a stress map will be generated which gives information about what forces are the cells ejecting (136,137).

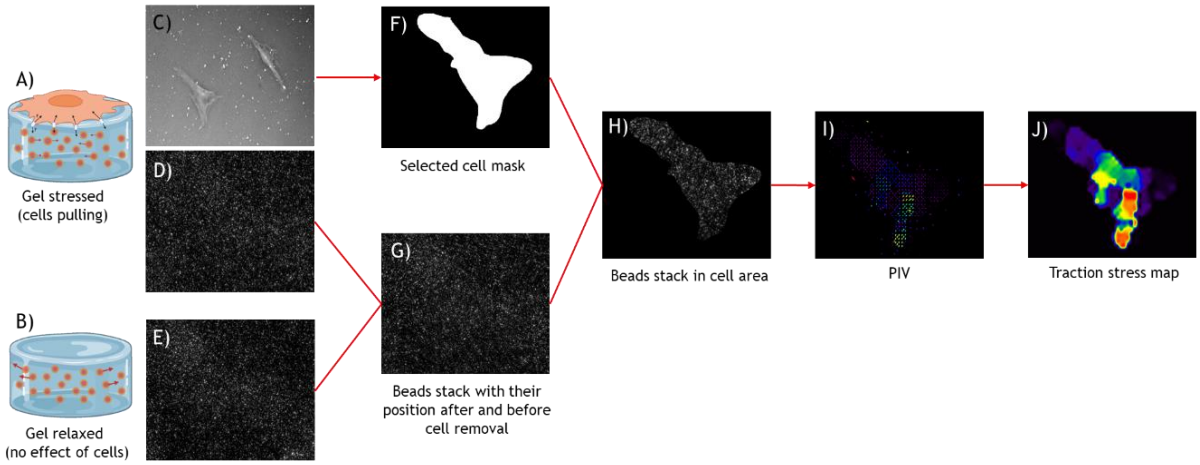

Figure 1-11. Traction Force Microscopy (TFM) analysis scheme (Biorender made). *Cells seeded on a hydrogel (A) attach to it through focal adhesions (light blue rectangle). Through these focal adhesions they exert forces (black arrows) and pull, drawing the fluorescent beads embedded in the hydrogel (red arrows). In this moment a picture of the cells (C) and the position of the beads (D) are taken. After cells are removed, the gel relaxes (B), allowing the beads to come back to their original position (red arrows). This time, a picture of the position of the beads without the influence of the cells (E) is taken. From the cells picture one is selected, and a mask is done (F). To be able to compare the position of the beads, a stack of the cells after and before cell removal is done (G). To only have into consideration the cells influenced by the studied cell, the beads stack is cut using the cell mask (H). The displacement of the beads is calculated through the stack (I) and from the displacement data a stress map is generated (J).*

Originally, TFM measured the 2D force field exerted by a single cell seeded on top of a 2D surface. It is possible to go further and measure multicellular clusters on 2D substrates at the same time. However, this is not accurate enough as cells exert forces in three directions and not only in two, even when they are seeded in 2D. In the last few years, methods to analyse 3D forces in 2D surfaces (often known as 2.5 tractions) have been studied (119,138).

Even though, TFM is a promising technique to study cellular forces that can help to understand better the mechanobiology, it has limitations. The main limitation is that TFM techniques do not allow the characterisation of the mechanical properties (e.g. deformability, viscosity or stiffness). Also, 2D TFM only provides

information on the forces applied on the apical flat surface of the hydrogel. Although, the recent experiments of 2.5 and 3D TFM, the actual techniques are not yet well-stabilised, and they need further investigations (139). Another big problem is the tracking of the beads over time. The density of the beads must be enough to cover the whole surface, so if there are parts without beads, when the traction forces are applied, part of the displacement information is lost. However, if the bead density is too high, the signal of the beads in different planes can overlap. This makes it difficult to analyse the displacement and hence, information is lost. On top of this, beads lose fluorescent emission over time. Consequently, TFM is tight to an optimal bead density that can provide all the displacement information across the gel to be able to analyse the traction field applied by the cells (140).

There are different study lines that are working to solve these problems. One example would be a new type of TFM known as STED-TFM (STFM) which uses optimal super-resolution stimulated emission depletion (STED) microscopy (140). This technique allows a better quantification of cellular tractions. However, it still has the limitations of other optical techniques (e.g. the density of the beads within the gel, beads tracking and the fluorescence light sensitivity of the biological specimen). To measure the displacement, there are two types of methods: the ones that track a single particle and the techniques that depend on correlating displacements within regions of an image (e.g. particle image velocity (PIV)). In relation to the expected nature of the forces and the density of beads used one of the two methods is going to be more suitable for the experiment in question (140).

Besides its limitations, TFM is a very promising technique to understand the forces exerted by the cells and the ones applied inside the cells by the organelles or individual receptors. Traction force quantification has a huge implication in the understanding of the role of mechanics in many disciplines e.g. tissue regeneration.

1.7. AIMS AND OBJECTIVES

ECM mechanical properties have a direct effect on cellular fate. When this ECM-cell interaction is disrupted, a pathology can be developed (2). Understanding these interactions would provide a better understanding to tackle tissue damage and diseases.

Cells respond to the physicochemical properties of the material (e.g. stiffness, degradability, viscosity). Recently, it is being studied cellular force transmission during cell attachment using TFM (9,34,141). Other studies have been more focused on cell metabolism (95,142) as well as cell respiration and ATP production in response to different mechanical properties of the surface (143). However, it has not been fully addressed the connection between the mechanical and the metabolic response of the cells to the ECM.

The main objective of this work is to study at the same time the mechanical and metabolic activity of cells during their attachment to the ECM. Observing the respiration rate, ATP production and metabolic profile when cells exert forces on surfaces with different stiffness will provide a complete overview of the cellular response to different environments. To carry out this study different cell types (L929 fibroblasts, MSCs and 3T3-L1) were seeded on full-length FN-PEG, PAA and Matrigel hydrogels. Incorporating full-length FN hydrogels improves cell attachment and it provides more similar scenario to the natural ECM. Also, it can be brought to 3D studies.

The specific aims of this work are:

- To investigate cell adhesion looking at FAs assembly and the traction forces exerted in relation to matrix stiffness and degradability.
- To investigate the mechanical cues triggered during force exertion, in particular YAP nuclear translocation.
- To establish a metabolic profile during cell-ECM interactions.
- To explore the implications of cellular contractility inhibition in cell attachment, traction force exertion and cell metabolomics.

- To determine if there is any correlation among TFM, FAs assembly, cell mechanotransduction, metabolite generation and cell respiration.

CHAPTER 2 : MATERIAL AND METHODS

2.1. MATERIALS

The materials used in this project are listed in the following tables:

Table 2-1. List of silanes

Reagent	Product	Provider
(3-Mercaptopropyl)-trimethoxysilane	175617	Sigma
3-(Acryloyloxy) propyltrimethoxysilane, 94%	L16400	Alfa Aesar

Table 2-2. List of materials used for full-length FN-PEG hydrogels

Reagent	Product	Provider	Notes
4-arm-PEG-Maleimide	4arm-PEG-MAL-20K-5g	LaysanBio	PEG-(4)-MAL, 20 kDa
Fibronectin	663	YoProteins	Human, from plasma
Tris(2-carboxyethyl) phosphine hydrochloride	75259-5G	Sigma	TCEP
Urea	U5378	Sigma	
Iodoacetamide	I1149-5G	Sigma	IAA
NaOH	S/4920/53	Fisher	
4-arm-PEG-Acrylamide	4arm-PEG-ACRL-10K-5g	LaysanBio	PEG-(4)-ACRL, 10 kDa
PEG-dithiol	PSB-613	Creative PEGworks	SH-PEG-SH, 2 kDa
VPM peptide	Custom synthesised	GensScript	GCRDVPMSMRGGDRCG
2-Hydroxy-4′-(2-hydroxyethoxy)-2-methylpropiophenone	410896-10G	Sigma	Irgacure-2959

Table 2-3. List of reagents used in polyacrylamide hydrogels.

Reagent	Product	Provider	Notes
Acrylamide 40%	A4058-100ML	Sigma	AAm
N,N'-Methylene-Bis-Acrylamide 2%	M1533-25ML	Sigma	BisAAm
N,N,N',N'-Tetramethylethylenediamine	T9281-50ML	Sigma	TEMED
Ammonium persulfate	A3678-25G	Sigma	APS
Sulfo-SANPAH (sulfosuccinimidyl 6-(4'-azido-2' nitrophenylamino)hexanoate)	803332-50MG	Sigma	0.2 mg/ml in H_2O
HEPES ≥99.5% (titration)	H3375-1KG	Sigma	

Table 2-4.List of cells and cell culture reagents used

Reagent	Product	Provider	Notes
Fibroblasts	L929		Murine
Bone marrow hMSC	hMCS	PromoCell	Human, single donor
Fibroblasts	3T3-L1	Prof. Sirio Dupont's lab, University of Padua	Murine, adipocyte differentiation ability
Penicillin/Streptomycin	15140-122	Gibco	P/S
Foetal Bovine Serum	10500-064	Gibco	FBS
L-Glutamine			L-Glu
Non-essential aminoacids	11140-035	Gibco	MEM NEAA (100X)
Sodium pyruvate solution	S8636-100ML	Sigma	SP
Amphotericin B	15290-026	Gibco	Fungizone
Dulbecco's modified Eagle's medium	D5671	Sigma	DMEM
Dulbecco's modified Eagle's medium	41965-039	Gibco	DMEM

Table 2-5. List of kits

Reagent	Product	Provider	Notes
ATP Assay Kit (Colorimetric/Fluorometric)	ab83355	Abcam	
Luminescent ATP Detection Assay Kit	ab113849	Abcam	
Lipofectamine 3000	L3000001	ThermoFisher	Transfection reagent
PureLink™ HiPure Plasmid Filter Maxiprep Kit	K210017	ThermoFisher	DNA extraction

Table 2-6. List of Seahorse Reagents

Reagent	Product	Provider
Seahorse XF Cell Mito Stress Test Kit	103015-100	Agilent
Seahorse XF Cell Culture Microplates	102340-100	Agilent
Seahorse XF DMEM	103575-100	Agilent
Seahorse XF Calibrant	100840-000	Agilent

Table 2-7. List of plasmids

Reagent	Product	Provider
GW1-PercevalHR	49082	AddGene
GW1-pHRed	31473	AddGene
GW1-Peredox-mCherry-NLS	32381	AddGene
ExRai AMPKAR T-A		Dr. Zhang's Lab, UC San Diego
pcDNA3-ExRai-AMPKAR1		Dr. Zhang's Lab, UC San Diego
iNapC		Prof. Sirio Dupont's Lab, University of Padua

iNapI		Prof. Sirio Dupont's Lab, University of Padua

Table 2-8. List of restriction enzymes and buffer used

Reagent	Product	Provider	Notes
NdeI	R0111	New England Biolabs	5'…C A▼T A T G…3' 3'…G T A T▲A C …5'
XhoI	R0146	New England Biolabs	5'…C▼T C G A G…3' 3'…G A G C T▲C…5'
HindIII-HF	R3104	New England Biolabs	5'…A▼A G C T T…3' 3'…T T C G A▲A…5'
EcoRI-HF	R3101	New England Biolabs	5'…G▼A A T T C…3' 3'…C T T A A▲G…5'
BsaI-HFv2	R3733	New England Biolabs	5'… G G T C T C (N)$_1$▼…3' 3'…C C A G A G (N)$_5$▲…5'
ApaI	R0114	New England Biolabs	5'…G G G C C▼C…3' 3'…C▲C C G G G…5'
ScaI-HF	R3122	New England Biolabs	5'…A G T▼A C T…3' 3'…T C A▲T G A…5'
rCutSmart Buffer	B6004S	New England Biolabs	

Table 2-9. Immunostaining antibodies and reagents used

Reagent	Product	Provider	Notes
Mouse-anti-YAP (monoclonal)	Sc-101199	Santa Cruz	Dilution 1:100
Mouse-anti-vinculin (monoclonal)	V9131	Sigma	Dilution 1:400
Rabbit-anti-mouse-Cy3	315-165-003	Jackson Immunoresearch	Dilution 1:200
Alexa Fluor 488 Phalloidin	A12379	ThermoFisher	Dilution 1:100

Triton-X100	T8787	Sigma	
Tween 20	P2287	Sigma	
Vectashield with DAPI	H-1200-10	Vectorlabs	
Bovine Serum Albumin	A7979	Sigma	BSA

Table 2-10. List of other reagents used

Reagent	Product	Provider	Notes
Rain-X	80199200	Rain-X	
Anhydrous Dimethyl Sulfoxide	276855	Sigma	DMSO
Dulbecco's Phosphate buffer solution	14190-094	Gibco	PBS
Trypsin-EDTA	T4049-100ML	Sigma	0.25%
Sodium dodecyl sulfate	L5750	Sigma	0.5% SDS
FluoSpheres™ Carboxylate-Modified Microspheres	F8810	ThermoFisher	0.2 µm, red (580/605)
Matrigel	356234	BD Bioscience	
DMEM, no glucose, no glutamine, no phenol red	A1443001	Gibco	

2.2. METHODS

2.2.1. Silanisation

Silanisation is the process through which a surface, such as glass, is functionalised with a monolayer of silanes in order to make the surface hydrophobic or to act as a coupling agent between the hydrogel and the surface. In this project, the silanisation process was essential to couple the hydrogel to a glass coverslip.

Round coverslips were cleaned following a RCA cleaning protocol. These glass coverslips were submerged in a solution of H_2O:H_2O_2:NH_4^+ (5:1:1) during 10 minutes to remove all the organic material on their surface.

Depending on what type of gels were going to be fabricated, two different types of silanisation were used.

2.2.1.1. Thiol-silanisation

For full-length FN-PEG hydrogels, glass coverslips were coated using a vapour thiol-silanisation. Cleaned coverslips were placed in a desiccator, next to a glass slide with few drops of (3-Mercaptopropyl)-trimethoxysilane (Sigma) (Figure 2-1A). Vacuum was applied for 3 hours to allow silanisation at room temperature. Afterwards, the silanised coverslips were cured in the oven for 1 h at 70°C. Silanised coverslips (Figure 2-1B) were stored at room temperature under nitrogen inert atmosphere until use.

The acrylate groups of the PEG polymer react with the thiol groups of the silane in a reaction 1:1 (Figure 2-1C), allowing the gel to attach to the coverslip. The thiol groups of the crosslinker (SH-PEH-SH or VPM) can react with the silane forming disulphide bonds (Figure 2-1D).

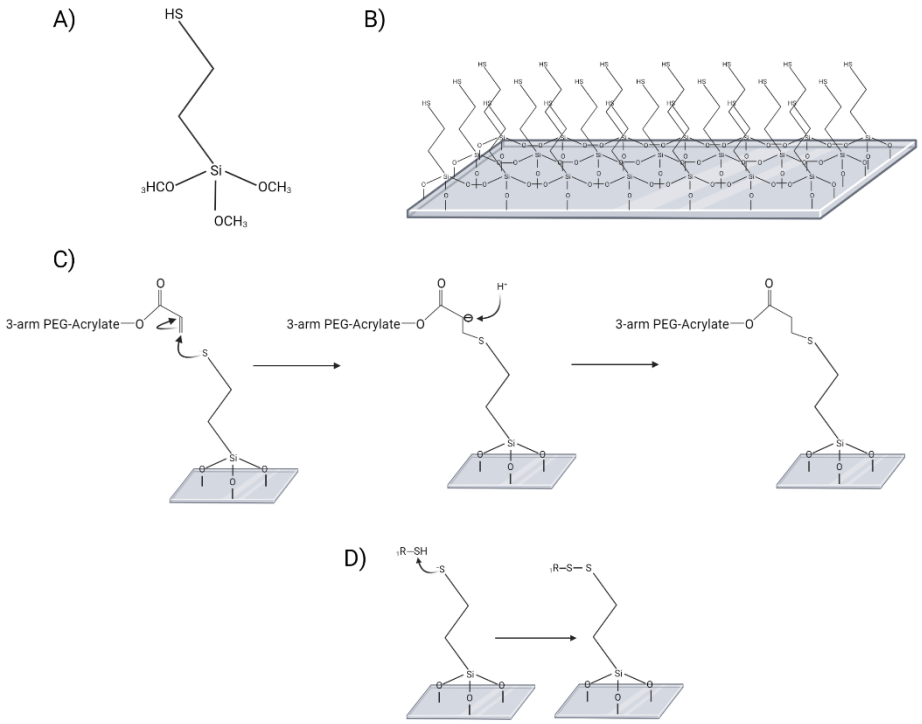

Figure 2-1. Thiol-silanisation*. A) Thiol-silane chemical formula. B) Depiction of a glass coverslip silanised. C) 4-arm PEG-Acrylate reaction with the thiol of the silane. Essential interaction in order to attach the PEG-hydrogel to the coverslip. D) Possible reaction between the thiol group of the silane and the crosslinker of the PEG-hydrogel (SH-PEH-SH or VPM). This reaction would yield a disulphide bond.*

2.2.1.2. Acryl-silanisation

In the case of PAA hydrogels, coverslips were coated using acrylsilanisation. In this occasion, a solution of 50 mL ethanol, 2.5 mL H_2O and 0.231 mL acylsilane (3-(Acryloyloxy)propyltrimethoxysilane, 94%, stab. with 100ppm BHT, Alfa Aesar) was prepared and the coverslips were submerged for 2 – 3 hours (Figure 2-2A). After this time, they were rinsed with water twice. The silanised coverslips were cured in the oven for 1 h at 70°C and stored in the fridge in inert atmosphere of nitrogen until use.

During gel formation, the acrylamide groups of the polymer react with the acrylic acid ester group of the silanes. This reaction is possible for the presence of a

catalyser (tetramethylethylenediamine, TEMED) and an initiator ammonium persulfate (APS), both incorporated in the gel solution (Figure **2-2**B). This reaction will be explained in detail in the polyacrylamide hydrogels section.

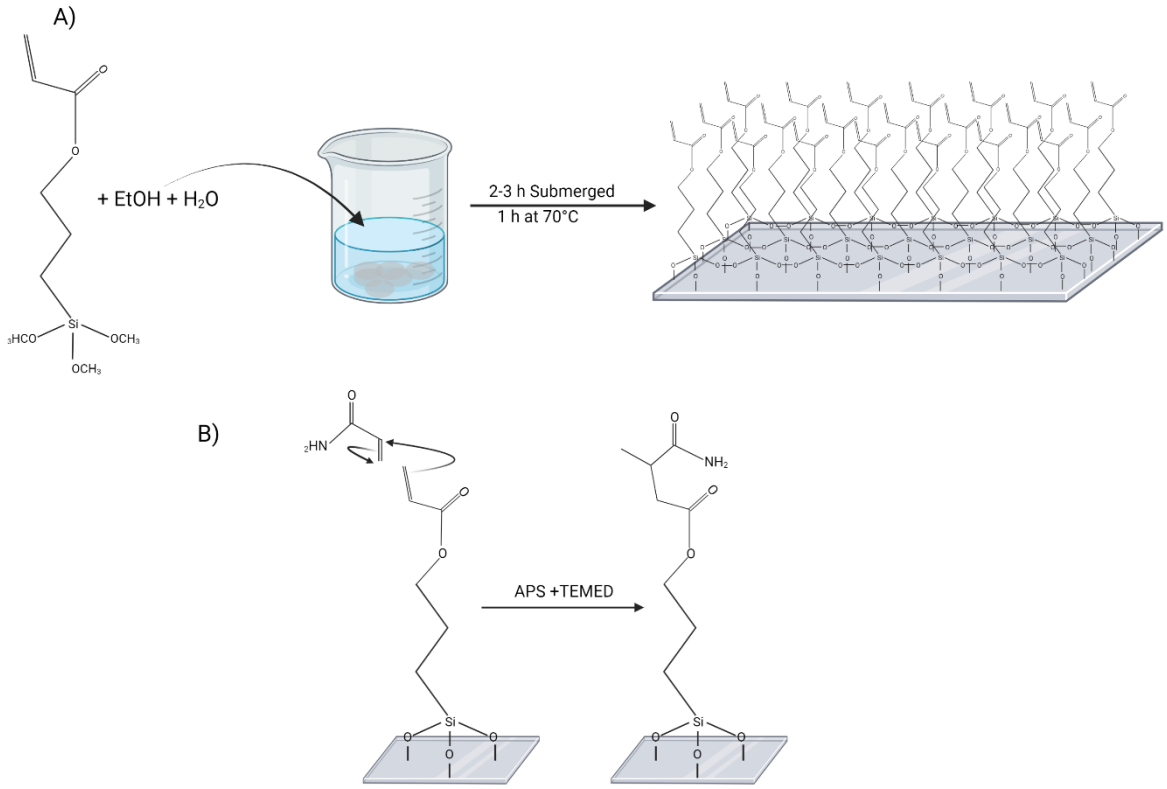

Figure 2-2. Acrylsilanisation*. A) Coverslips are silanised submerging them in a solution prepared with acrylsilane, absolute ethanol and H_20. The reaction takes place for 2-3 hours at room temperature. Later, the coverslips are cured for 1 hour at 70°C. B) The acrylamide group of the polymer and crosslinker of the gel solution will react with the acrylate group of the silane. In order for this reaction to happen two initiators are required (TEMED and APS).*

2.2.2. Fibronectin PEGylation

Prior to gel formation, fibronectin was functionalised to be able to covalently link it to the PEG network. For PEGylation, fibronectin was bound to 4-arm-PEG-Maleimide molecules (PEG-(4)-MAL, LaysanBio,20 KDa) through Michael-type addition reaction (i.e. via thiol groups of FN cysteines) (Figure 2-3).

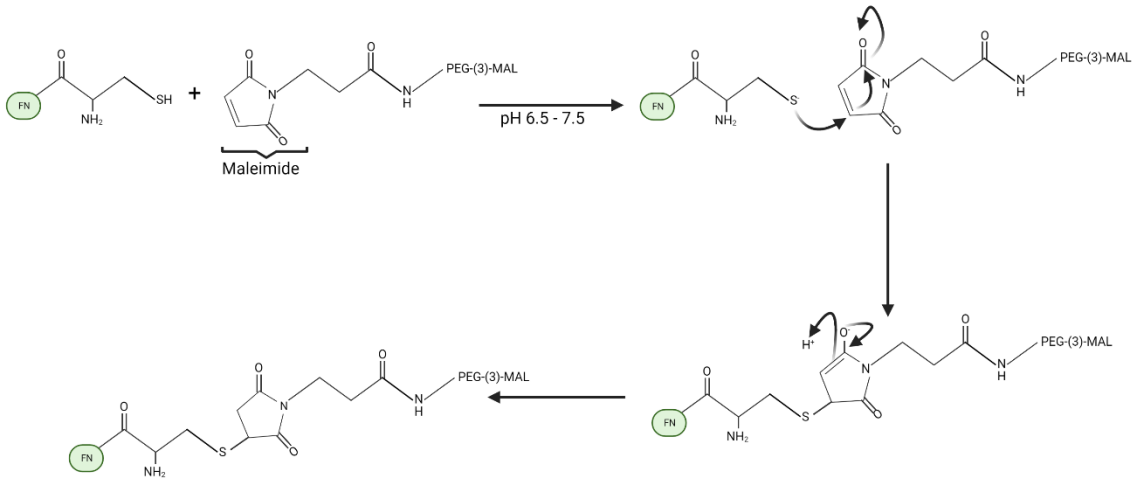

Figure 2-3. Michael-type addition reaction for FN-PEGylation. *The maleimides attached to PEG will react with the thiol groups of the FN´s cysteines in a ratio 1:1.*

First, fibronectin was denatured to expose its thiol groups. The required amount of fibronectin (YO proteins, 3 mg/ml stock) to get 50 µg of fibronectin per 50 µL gel (final concentration of 1mg/mL) was added and mixed with urea 8M (Fisher) to unfold the fibronectin. To get the thiol groups of the fibronectin available to react, tris(2-carboxyethyl)phosphine hydrochloride (TCEP) (stock 0.1M, pH 7, sigma) was added. The mixture was let to react for 15 min at room temperature (RT).

Afterwards, PEG-(4)-MAL was added (LaysanBio, 20 KDa) to have a molar ratio of 1:4 FN:PEG-(4)-MAL. It was kept shaking at room temperature for 30 min. After this time, the reaction was stopped with 0.5 µL NaOH (Fisher, 1M stock).

The following step was protein alkylation. In this step, 14 mM of iodoacetamide (Sigma) was added. The reaction was left for 2 hours at room temperature, shaking and covered from light. The iodoacetamide blocks the unreacted fibronectin's thiol groups. The PEGylated FN was dialysed (Mini-A-Lyzer, MWCO 10KDa, ThermoFisher) for 1 hour at RT against phosphate-buffered saline (PBS).

For protein precipitation, 9 volumes of cold absolute ethanol were added, and the mixture was left at -20°C for 24 hours. The following day, all the samples were

centrifuged at 15000 g and 4°C for 15 minutes. The supernatant was removed, and the pellet was washed with 90% cold ethanol (200 µL). All the tubes were centrifuged again at 15000 g, 4°C for 5 minutes. The supernatant was discarded, and the pellet was dried in the fume hood. When the pellet was completely dried, it was resuspended in 8M sterile urea to a final concentration of 2.5 mg/mL of fibronectin. Finally, the protein was dialysed again against PBS for 1 hour at room temperature. The total amount collected was measured to calculate the final fibronectin concentration.

The final concentration of FN is calculated multiplying the initial amount of FN that was added in each tube (50 µg) by the total number of tubes used (Ntubes), and then divided by the total volume collected from all the tubes (Vtotal). The final protein solution was stored at -20°C.

Equation 2-1. FN-PEGylated concentration

$$[FN]_f = \frac{50\ \mu g\ of\ FN/tube * N_{tubes}}{V_{total}\ collected}$$

2.2.3. PEG-Acrylate hydrogel preparation

PEG hydrogels were formed at room temperature and physiological pH by photopolymerization (Table 2-11). Three different percentages of 4 arm polyethylene glycol-acrylate (PEG-(4)-ACRL) (3%, 5% and 10% wt, LaysanBio, 10kDa) were used to get the different stiffnesses. A constant concentration of FN-PEG of 0.5 mg/mL was kept among all stiffnesses.

To obtain gels with different degradability, SH-PEG-SH (Creative PEG works, 2kDa) or a protease-degradable peptide (VPM peptide, GCRDVPMSMRGGDRCG, purity 96.9%, Mw 1696.96 Da, GenScript) were added as crosslinker, getting non-degradable and degradable gels respectively. Those react with the polymer 4arm PEG-Ac at a molar ratio 1:2. The reaction occurs following a Michael-type addition between the thiol groups of the crosslinker (2 groups in each) with the acrylate groups of the polymer (4 groups in total).

The reaction was initiated adding 0.5 mg/mL of the photoinitiator Irgacure 2959 (2-Hydroxy-4'-(2-hydroxyethoxy)- 2-methylpropiophenone, Sigma).

Table 2-11. Concentrations used in the different PEG gels expressed in mg/mL

REAGENT	3% wt PEG-(4)-ACRL	5% wt PEG-(4)-ACRL	10% wt PEG-(4)-ACRL
PEG-(4)-ACRL	30	50	100
VPM	12	20	40
SH-PEG-SH	12	20	40
FN-PEG	0.5		
Irgacure 2959	0.5		

For traction force microscopy, 1 µL of FluoSpheres™ Carboxylate-Modified Microspheres (0.2 µm, red fluorescent (580/605), 2% solids) diluted 1/10 in PBS was added to each gel solution. Once everything was properly mixed, the mixture drop was poured on a hydrophobic coverslip and the silanised coverslip placed on top. Everything was photopolymerised under the UV lamp, set at 10 mW/cm^2, for 10 min (Figure 2-4).

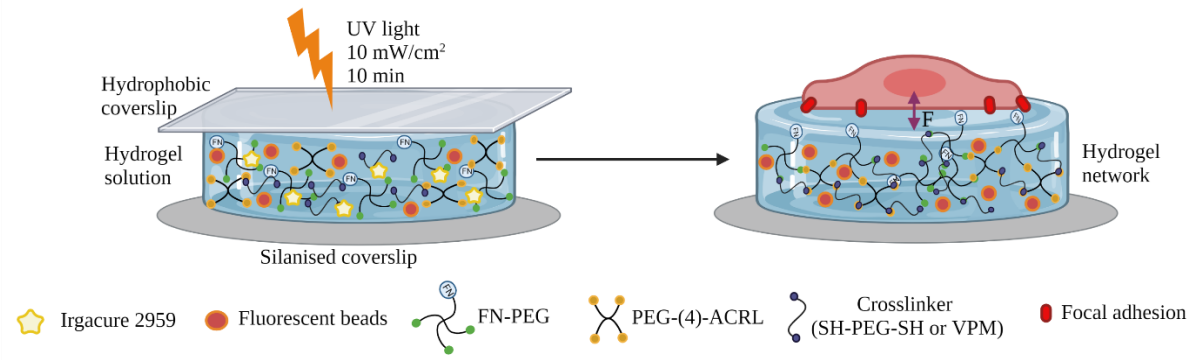

Figure 2-4. Proposed system. *The pre-gel solution contains the photoinitiator (Irgacure 2959), the polymer (4 arm PEG-Ac), crosslinker (SH-PEG-SH, for non-degradable gels, or VPM (GCRDVPMSMRGGDRCG), for degradable gels), full-length fibronectin (FN) pegylated (FN-PEG) and fluorescent beads. The solution is incorporated between two coverslips, one silanised and a hydrophobic one. The whole sandwich system irradiated with 10 mW/cm^2 UV light, for 10 min. After*

this time, the gel has been formed and the hydrophobic coverslip is removed. The cells seeded on top attach to the gel forming focal adhesions between their integrins and the FN in the gels (red rectangle). Cells will pull the hydrogel with a specific force. The final diameter of the gels was 12 mm and the heigh around 1 mm.

Photopholymerisation was selected due to the facility to go from 2D to 3D culture maintaining the same conditions and reagents.

2.2.4. Polyacrylamide (PAA) hydrogels

Polyacrylamide hydrogels were formed at room temperature and physiological pH under the fume hood. A commercial kit of 40% (w/w) acrylamide (monomer) and 2% (w/w) bis-acrylamide (crosslinker) was acquired from sigma. Firstly, a solution of 1.5 % (w/w) tetramethylethylenediamine (TEMED, sigma) and 5% (w/w) ammonium persulfate (APS, sigma) were prepared.

The reaction between the acrylamide and bis-acrylamide occurs between their vinyl groups. In order of this reaction to happen a catalyst, in this case the TEMED, is needed to create free radicals that can react to create the new bonds C-C (144). To start this reaction and allow the TEMED to work, an initiator is required. Thereby, the reaction is not going to happen unless the APS is present (144).

Three different stiffnesses 3 kPa (±0.4), 9 kPa (±0.7) and 35 kPa (±4) were obtained following the ratios described in Justin R.Tse and Adam J.Engler work (145).

2.2.5. Rheology

Hydrogels are formed by a polymer network. Depending on the physical structure of this network, gels have different stiffness and, hence, different cellular behaviour on the surface will be observed. In order to characterize the properties of the gels, full-length FN-PEG hydrogels with different stiffness were subjected to a changing frequency (to measure stress when a force is applied) and a changing

strain (to measure deformation of the gel) in a rotational MCR302 rheometer (Anton Paar) using a parallel-plate of 15 mm diameter geometry.

The gel was placed on the bottom fixed plate. The upper plate was mobile and going to approach at a determined frequency and strain. A constant temperature of 25°C was set during the assessment and solvent was added frequently to avoid evaporation.

Firstly, measurements were taken with an angular frequency sweep from 100 to 1 rad/s, keeping the amplitude gamma constant at 0.06%. Afterwards, we measure the same gel again changing the strain and maintaining the frequency. This time, we used an amplitude gamma sweep from 0.01 to 1% and a constant frequency of 10 rad/s.

In order to study the influence of the beads embedded in the gel, both, gel with and without beads, were analysed.

2.2.6. Nanoindentation

The results obtained in rheology were compared with nanoindentation. A nanoindenter (Chiaro, Optics11) mounted on top of an inverted phase contrast microscope (Evos XL Core, Thermofisher) was used. This is a new technique to measure the mechanical properties of the material. It is versatile method that allow to measure a large number of samples in less time. A spherical glass tip with a specific area is approached to the surface, once this one is reached a nanoindentation is done at a specific load and depth. Analysing the surface deformation, mechanical details such as Young´s Modulus (E), storage (E') and loss moduli (E'') were provided.

2.2.7. Cell culture

The first experiments were carried out with L929 mouse fibroblasts. They are easy to work with and grow fast what made them suitable for the protocol optimisation and to fulfil all the requirements before moving to mesenchymal stem cells.

L929 fibroblasts were cultured in a 75 cm^2 flask until confluence, in 10 mL of Dulbecco's Modified Eagle Medium (DMEM, Gibco) (4.5 g/L glucose without pyruvate) complemented with 10% fetal bovine serum (FBS, Gibco) and 1% antibiotics (Penicillin/Streptomycin, Gibco). The media was changed one day after the cells were defrosted and exchanged every two days and one day before the seeding.

For the traction force microscopy experiments, 10000 L929 cells per cm^2 were seeded in a 24 well plate with the gels attached to the bottom. The cells were cultured with 1 mL of DMEM (4.5 g/L glucose without pyruvate) complemented with 10% FBS and 1% Penicillin/Streptomycin for 24 hours before imaging.

To study the behaviour of MSCs during cell adhesion, MSCs were seeded at 4000 cells per cm^2 on top of full-length FN-PEG hydrogels for 24 hours before imaging or fixation. Commercial human MSCs harvested from bone marrow from PromoCell were used. They are obtained from human individual donors and has been tested for their ability to differentiate in vitro into adipocytes, chondrocytes and osteoblasts.

MCSs were cultured in DMEM (4.5 g/L glucose without pyruvate, Sigma) complemented with 10% FBS, 1% Sodium pyruvate (Sigma), 1% non-essential amino acids (ThermoFisher) and 2% mix of L-Glutamine: Penicillin/Streptomycin: Fungizone (150:100:12.5). Generally, MSCs were used in a passage 2-5, with media change every two days MSCs were serum starved (1% FBS) the day before seeding, synchronising their cell cycle and metabolic activity. (146).

Due to the difficulty of transfecting MSCs, 3T3-L1 murine fibroblast were used to carry out ratiometric experiments. The election of these cells was done for their ability to differentiate into adipocytes, following a MSCs like behaviour. 3T3-L1 cells were culture in 125 cm^2 flasks upon confluency in high glucose DMEM media supplied with 1% sodium pyruvate (Gibco), 2mM glutamine, 20% FBS and 1%Penicillin/Streptomycin. To study the expression of proteins under different conditions we use ratiometric reporters. Those are useful tools to measure the relative abundance of proteins by fluorescence. For these ratiometric experiments, 3T3-L1 cells were seeded on 96 well Falcon plates coated with

Matrigel, to test their behaviour on soft matrices, or directly on the well plate. The following day, they were transfected using Lipofectamine 3000 (Invitrogen) and incubated overnight at 37°C. The media was changed before imaging to DMEM supplied with the appropriate supplement depending on the sensor which was going to be observed. The transfection success was confirmed looking at the fluorescent cells in the well after 24h using a conventional fluoresce microscopy (ZEISS AxioObserver Z.1).

To study the cellular response to matrix stiffness, cells were seeded in three different types of hydrogels PAA (3, 9 and 35 kPa), full-length FN-PEG (2.5, 8 and 26 kPa) and commercial Matrigel (0.2 kPa and 1 GPa) (Table 2-12).

For contractility inhibition experiments, cells were treated with 10 μM blebbistatin (Sigma) 1 hour before imaging or fixation. Blebbistatin inhibits non-muscle myosin II interrupting cell-contractility (62,63).

Table 2-12. Cell types used, describing at what density and on what substrates they were cultured in the different experiments

Cell type	Density (cells/cm^2)	Substrate	Experiment
L929	10000	Full-length FN-PEG gels	TFM
MSCs	4000	Full-length FN-PEG gels	TFM, vinculin staining, YAP staining, metabolomics
		PAA hydrogels functionalised with FN	TFM, YAP staining
	15000	Matrigel	Seahorse
3T3-L1	15000	Matrigel	Seahorse
	5000	Matrigel	ATP assay, ratiometric sensors
	5000	PAA hydrogels functionalised with FN	Vinculin staining, YAP staining, ATP assay

2.2.8. Metabolomics

To extract the MSCs metabolites a cold solution of chloroform: methanol: water (1:3:1) was prepared in advance. After removing the growing media, 400 µL of cold solution was added per 1.5 cm well diameter in a P24 well-plate. The solution was left for one hour at 4°C. After this time the wells were scraped to improve the metabolites extraction. All the solution in the well was transferred to a clean eppendorf tube and vortex at 4°C for 5 min. Straight after, the eppendorf tubes were centrifuged for 3 min at 4°C. The supernatant was collected and storage at -80°C until it was sent for analysis. The pellet was dried and resuspended with milliQ water for protein analysis. The protein values would be used for normalisation.

The -80°C frozen samples collected were send to the Polynomic facilities in the university for analysis. Liquid chromatography (LC)–mass spectroscopy (MS)-based metabolomics with a ZIC-pHILIC column was used for it. The equipments available were three Thermo Orbitrap instruments: an Exactive, a Q-Exactive, and an Orbitrap Elite.

Metabolomic data analysis was carried out using Metaboanalyst (v.0.5) and Pathos (http://motif.gla.ac.uk/Pathos/index.html). The data introduced in these programs was pre-analysed using IDEOM, which was used to do the normalisation between samples using the protein values. Different analysis by time points were done: i) all time points ii) 24h iii) day 7. In all these comparisons day 0 was the control.

2.2.9. Seahorse

The respiration rate of MSCs and 3T3-L1 fibroblasts was tested using Agilent Seahorse XF Cell Mito Stress Test. This assay measures the oxygen consumption rate (OCR) of alive cells at real time by injecting sequentially different drugs that interfere in the normal mitochondrial functionality.

The day before running the assay the MSCs and 3T3-L1 cells were seeded on the Seahorse Cell Culture Microplate at an optimum density to get a monolayer (15000

cells/cm^2). Some of the wells were coated with collagen or Matrigel, to study the effect of this protein and the stiffness of the surface, respectively, in the cellular respiration rate. For soft surfaces (E ≈ 250 Pa) we used pure Matrigel gelled at 37°C for 20 min. On the other hand, 2% (v/v) Matrigel in PBS was used to get a stiff surface (E ≈ 1GPa). The cells were kept in growth media at 37°C overnight (147). Also, a sensor cartridge was hydrated in Seahorse XF Calibrant at 37°C in a non-CO_2 incubator overnight.

The following day, Seahorse XF DMEM was supplemented with 1mM pyruvate, 2mM glutamine, 10mM glucose and 1% Penicillium/Streptomycin. The pH was adjusted to 7.4 and the medium was warmed up to 37°C. The different drugs were prepared at the desire concentration in the prepared medium (Table 2-13).

Table 2-13. Drugs used and concentration

Drug	**Final Concentration**
Olygomicin	8 µM
Carbonyl cyanide-4 (trifluoromethoxy) phenylhydrazone (FCCP)	9 µM
Rotatone + Antimycin	10 µM (both)

Following the indications of the company, the different drugs were loaded in the indicated ports of the hydrated cartridge. It was kept at 37°C until reading the plate.

The plate with the cells was observed under the microscope to confirm that a monolayer was formed. Confirming the cells viability, the growth media was changed to the Seahorse XF DMEM, pH 7.4 previously prepared. The plate was incubated for one hour at 37°C in non-CO_2 incubator.

After this time, the cartridge with the drugs was loaded in the equipment and after calibration the plate with the cells was introduced and the assay run.

Seahorse is a good technique to study the mitochondria state. It also helps to understand if the cell metabolism might be glycolytic or OXPHOS based.

2.2.10. Ratiometric sensors

Perceval, pH-Red and Peredox plasmids were acquired through Addgene. All of them were produced in GW1 vector (Figure 2-5). The plasmids were received as an agar stab in bacteria resistant to ampicillin. After arrival, the bacteria were grown at 37°C on agar with ampicillin doing serial dilutions. The following day 3 colonies were selected and grown in 5 ml of lysogeny broth with ampicillin at 37°C overnight. The following day the falcons were centrifuged for 10 min at maximum speed at 4°C. The pellet was resuspended in 700 µl of lysogeny broth growth media.

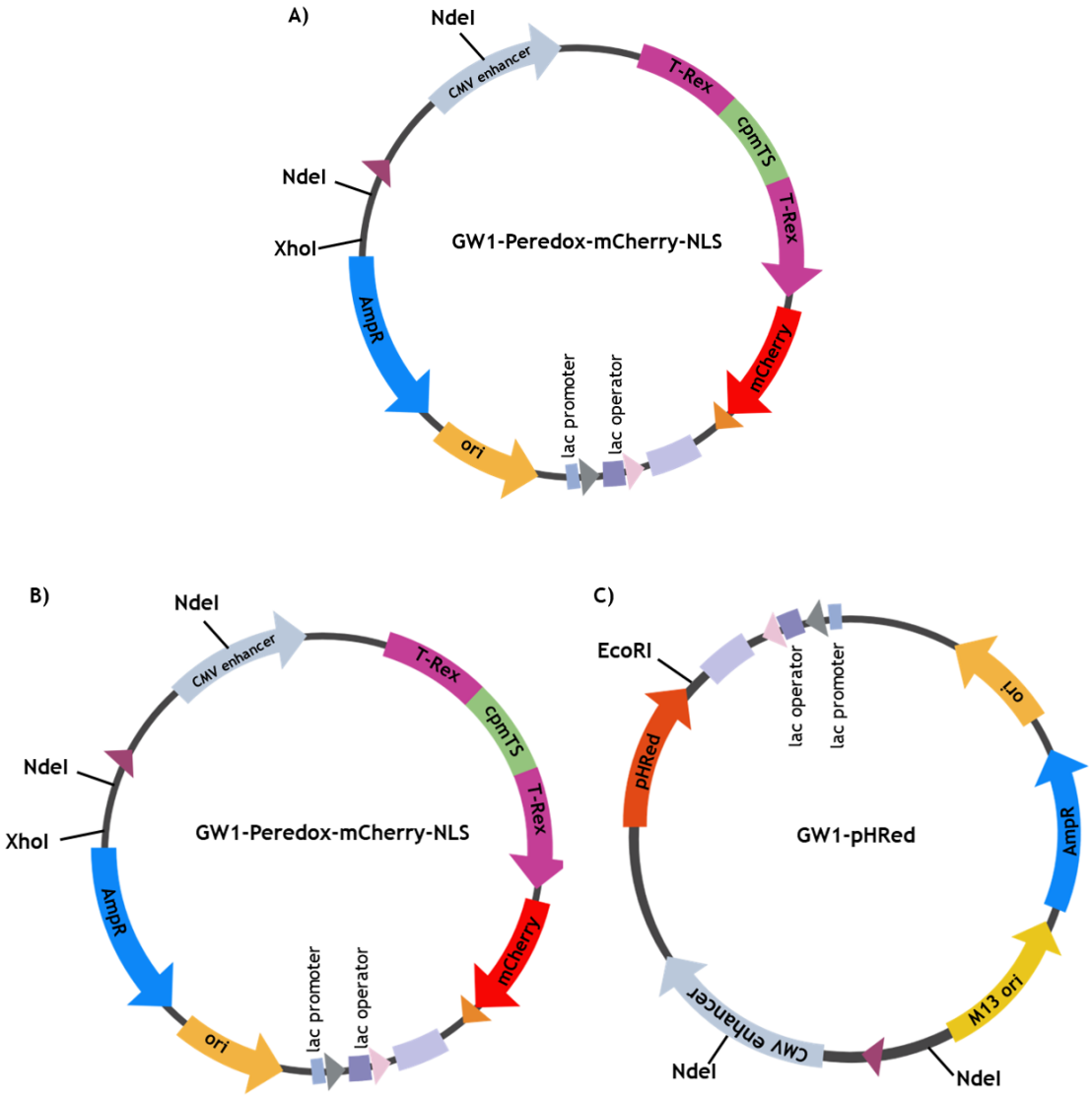

Figure 2-5. Addgene Plasmids maps showing restriction enzymes used. Made in Biorender. *A) Plasmid map of Peredox showing cutting sides for NdeI and XhoI.*

B) Plasmid map of PercevalHR showing cutting sites for HindIII and XhoI. C) Plasmid map of pHRed showing the cutting enzymes EcoRI and NdeI

From the total volume, 600 µL were used for diagnostics. Different enzyme restrictions were selected from the plasmid map (Figure 2-5) obtained from Addgene website (Table 2-14).

Table 2-14. Restriction enzymes used for the diagnostics of the sensors.

Plasmid	Restrictions enzymes
Peredox	Nde I and XhoI
Perceval HR	Hind III and Xho I
pHRed	Nde I and EcoRI

The plasmids DNA was extracted using ZR Plasmid Miniprep kit (Zymo Research). At the end of the protocol the DNA was dissolved in 30 µL of pure water. The amount of DNA was measured using a Nanodrop ThermoFisher equipment. A solution of 100 ng/µl of DNA was prepared for the diagnostics. The diagnostics solution as prepared accordingly the following indications on (Table 2-15).

Table 2-15. Digestion solution for plasmids diagnostics.

Plasmid DNA (500 ng)	5µl (from 100 ng/µl dilution)
Buffer (10x)	3 µl
Enzymes (s)	0.5 µl/enzyme
H_2O	Up to 30 µl

The buffer used is essential to ensure the activity of the restriction enzymes. These buffers contain recombinant albumin and are usually supplied with the enzymes. Not all the enzymes work in the same buffer, therefore it is essential to select restriction endonucleases that work in the same restriction buffer. In this case, the enzymes selected work in rCutSmart Buffer (New England BioLabs).

The enzymes were added in the reaction solution the last, to assure they start to act when all the components are incorporated.

The whole solution was incubated at 37°C in the water bath for an hour. After this time, the solution of each enzyme was loaded in a different column of an electrophoresis gel. The samples were run through the gel at 110 mW. The gel was imaged, and the different fragments were compared with a reference guide to certify that the plasmids received were correct (Figure 2-6).

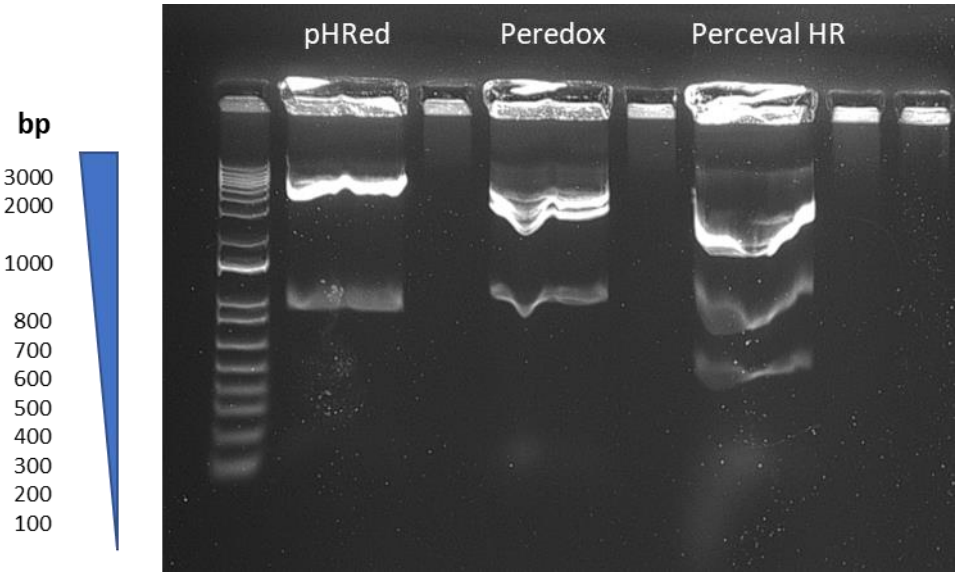

Figure 2-6. Addgene plasmids diagnostics. *After restriction enzymes' plasmid digestion, the fragments were run in an electrophoresis gel to identify their size and certify the plasmids.*

The rest 100 µl were used to isolate plasmids DNA using PureLink HiPure Plasmid Filter Maxiprep kit (ThermoFisher). The entire volume was added to 200 mL growth media supplemented with ampicillin. The colonies were left to grow overnight at 37°C. The next day, the liquid was transferred to a plastic bottle and centrifuged for 10 min at 4°C at 4100 rpm and 9 speed acceleration. The resultant pellet was resuspended with 10 ml of resuspension buffer. Later 10 ml of lysis buffer and incubated at room temperature for 5 min. After this time, 10 ml of precipitation buffer was added and mixed by inversion. The mix was loaded in a filter column to wash the DNA. To increase the purification of the DNA in the column, 10 ml of wash buffer was incorporated and left to flow through. The part

of the column with all the residuals was discarded and the part with the DNA adsorbed was washed with other 50 mL of washing buffer. To elucidate the DNA 10.5 ml of cold isopropanol was added into the column. The isopropanol decreases the DNA solubility, avoiding that it reacts with other possible materials. The DNA dissolved in the isopropanol was collected in a falcon, which was centrifuged at 12000 g for 5 min at 4°C. The supernatant was discarded, and the pellet was washed with 70% ethanol and centrifuged again for 5 min at 4 °C. The ethanol was discarded, and the pellet dried down at 37°C. When the pellet was completely dry it was resuspended in 500 µL of milliQ water.

The representative and mutant plasmids ExRai AMPKAR were provided by Jin Zhang laboratory from Centre for Cell Signalling San Diego (Figure 2-7). The mutant plasmid has mutated the phosphorylation site changing a threonine to alanine (T/A). Thereby, the phosphorylation activity is lost, and the response of this biosensor would be minimal. The mutant plasmid will be referred as ExRai AMPKAR T/A (Figure 2-7B), while the responder is indicated as ExRai AMPKAR. The plasmids were received on a paper. After arrival the part of the paper with the plasmid was cut and introduced in an Eppendorf tube. To wash the plasmid from the paper, 10 mM Tris pH7.6 was added to the eppendorf tube, then vortexed and left the paper to hydrate for 5 min. *Escherichia coli* bacteria were incubated with 50 µl of the elucidated plasmid from the paper for half an hour in ice. This step allows the plasmid DNA to approximate to the bacteria walls. To incorporate the plasmids into the bacteria, the Eppendorf tubes were incubated for 1 min at 37°C. Immediately after, they were brought back to ice for 2 min to leave the bacteria recover. After this time, 250 µl of lysogeny broth were added to the Eppendorf and left at room temperature for 30 min. This step allows the membrane of the bacteria to seal. Before seeding the transfected bacteria on agar with ampicillin, they were left for other 30 min at 37°C. The colonies grown on the agar were collected and proceed as described before for the diagnostics and maxiprep.

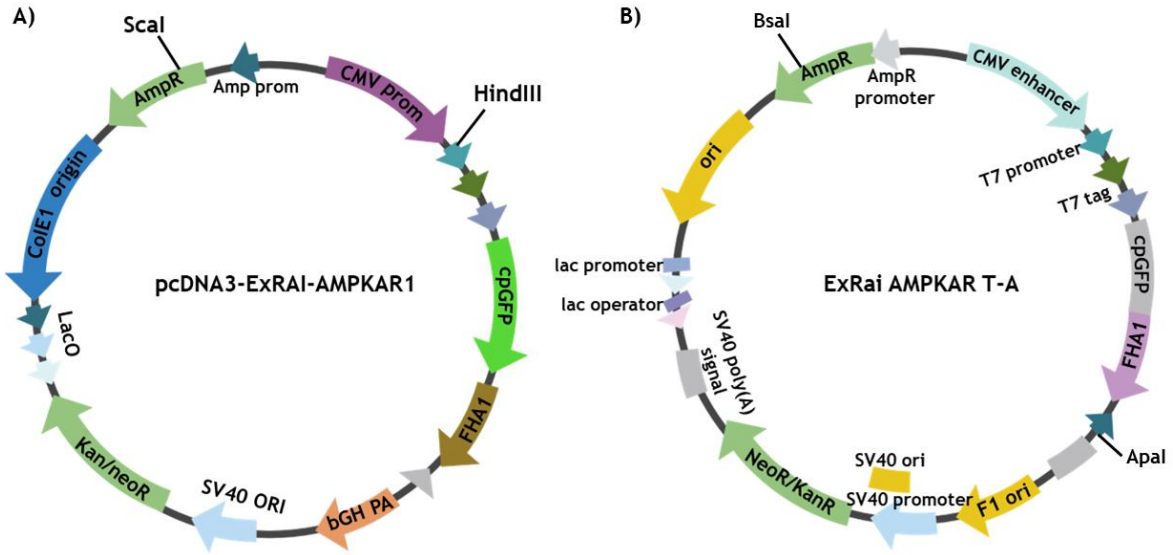

Figure 2-7. Plasmids ExRai AMPKAR maps. *A) Representative plasmid ExRai-AMPKAR1 showing the cutting sites for the restriction enzymes ScaI and HindIII. B) Mutant plasmid ExRai-AMPKAR T/A showing cutting sites for the restriction enzymes BsaI and ApaI.*

The restriction enzymes for the diagnostics were selected from the plasmids' maps (Figure 2-7) provided by Jin Zhang's group (Table 2-16).

Table 2-16. Restriction enzymes for ExRAi AMPKAR plasmids diagnostics.

Plasmid	**Restriction Enzymes**
ExRai AMPKAR	Sca I and Hind III
ExRai AMPKAR T/A	Bsa I and Apa I

The fragments after the enzymes' digestion were run in an electrophoresis gel as described before (Figure 2-8).

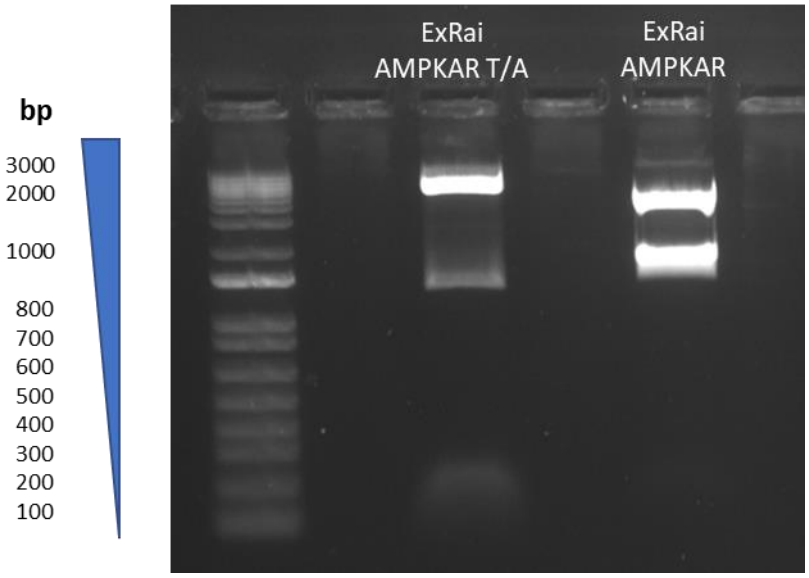

Figure 2-8. ExRai AMPKAR T/A and ExRai AMPKAR diagnostics.

To compare and have a better understanding of the results obtained with Peredox, we incorporated another plasmid iNAp1 and iNapC provided by Sirio Dupont's lab, who provided the plasmid DNA already extracted and analysed, therefore, no extraction or diagnostics was needed.

The plasmids DNA was used to transfect 3T3-L1 fibroblasts cells with lipofectamine 3000 (ThermorFisher). The day after the transfection the cells were visualised in an Operetta CLS microscope (PerkinElmer). To stimulate the movement of the biosensors within the 3T3-L1 cells the media was change using different conditions (Table 2-17).

Table 2-17. Medium conditions per ratiometric sensor.

Plamids	Media conditions
Perceval and pHRed	- High glucose DMEM with 1% sodium pyruvate, 2mM glutamine, 20% FBS and 1%Penicillin/Streptomycin (control). - High glucose DMEM (no other supplements). - DMEM + 2mM glutamine. - DMEM + 20X Sodium pyruvate - DMEM + 50 mm 2-DG

	- DMEM + 4.5 g/L glucose
ExRai AMPKAR and ExRai AMPKAR T/A	- High glucose DMEM with 1% sodium pyruvate, 2mM glutamine, 20% FBS and 1%Penicillin/Streptomycin (control). - Control media + 50mM 2-deoxy-glucose (2-DG). - Control media + 50mM 2-DG + 20 µM dorsomorphin (Compound C) - Control media + 100 µM AICAR - Control media + 20 µM YM (ROCK inhibitor, Y27632; and myosin light chain kinase inhibitor, ML7)
Peredox	- High glucose DMEM with 1% sodium pyruvate, 2mM glutamine, 20% FBS and 1%Penicillin/Streptomycin (control). - DMEM + 10 mM lactic acid - DMEM + 20 mM Sodium pyruvate
iNap	- High glucose DMEM with 1% sodium pyruvate, 2mM glutamine, 20% FBS and 1%Penicillin/Streptomycin (control). - DMEM + 10 mM lactic acid - DMEM + 20 mM Sodium pyruvate - Control media + DD (50 µM DIA + 150 mM DEA)

DMEM media used differently to the control is DMEM only supplemented with L-Glutamine (L-Glu) and P/S.

2.2.11. Traction Force Microscopy (TFM)

The gels were imaged with an EVOS™ FL Auto and EVOS™ M7000 Imaging System (ThermoFisher) at 20x magnification. The incubator of the microscope was set at 37°C and CO2 concentration at 5% while the images were taken.

Different beacons in the gel were selected and a Z-Stack was run. To get the position of the beads a TexasRed channel was used and bright field to visualise the cells. Then, the cells were removed using 0.5wt% Sodium dodecyl sulphate (SDS). The same beacons than before were imaged again without the cells to get the photo of the position of the beads without the influence of the cell. The alignment of the beads' images after and before cell removal, was made in ImageJ 1.53p (National Institutes of Health, US) for each cell. Afterwards, the traction forces were analysed using a software in MATLAB developed by Pompe T (148). and colleagues of the Leibniz Institute of Polymer Research Dresden (IPF) (149). Due to different problems with this program we decided to change the traction force analysis to ImageJ 1.53p (National Institutes of Health, US) using the plugins for TFM developed by Qingzong Tseng (150).

First, a cell mask and the position of the beads before and after the trypsinisation were aligned using 'align slices in stack' plug-in. Then the displacement of the beads in the cell area was calculated by particle image velocity (PIV). This plug in uses a normalised correlation coefficient algorithm to calculate the displacement, what means that an individual interrogation window is compared with a larger searching window. This minimise a false correlation peak due when there are insufficient beads presented in an interrogation window.

The errors due to an insufficient number of beads in the field was filtered running a dynamic mean test and replacing the invalid displacement vectors by the mean. A displacement file was generated after each PIV analysis. This document was used to reconstruct the traction force field implementing the Fourier transform traction cytometry (FTTC) method, which has been included as a plugin in ImageJ. To be able to set a more accurate scale for the stress map obtained in ImageJ, this one was modified in ParaView (v5.8.0, Kitware).

2.2.12. Immunostaining

Cells were fixed with fixative buffer (4% paraformaldehyde in PBS) for 30 min at RT. The permeabilization was done with 0.1% Triton x100 for 5 min. After washing

the cells with PBS twice, samples were blocked using blocking buffer (1% Bovine serum albumin, BSA, Sigma) for 30 min at room temperature.

To investigate the mechanotransduction activity of the cells, we looked at YAP translocation. The primary antibody mouse monoclonal anti-YAP (SantaCruz) was added in a 1:100 dilution in blocking buffer. The reaction was left for 1 hour at RT and washed with 0.5% tween 20 three times. The second antibody donkey-anti-mouse Cy3 (Jackson Immuno Research,1:200) together with the phalloidin (Alexa488, 1:100), were incubated for 1 hour at room temperature, both diluted in blocking buffer. The cells were washed 5 times with 0.5% tween 20 and then mounted with VECTASHIELD mounting media with DAPI (Vector Laboratories). Images were taken with a ZEISS AxioObserver Z.1 at 20X and 40X magnifications.

Vinculin staining was carried out to study the formation of the focal adhesions in MSCs. The procedure followed was similar to the one described above for YAP. After cell permeabilization and blocking, in this case, we used as a primary antibody mouse anti-vinculin diluted 1:400. As before cells were incubated with the primary antibody for 1 hour at RT. After washing three times with 0.5% tween 20, the secondary antibodies were added. The secondary antibodies used were the same ones used for YAP: donkey-anti-mouse Cy3 (Jackson Immuno Research,1:200) and phalloidin (Alexa488, 1:100). Once the cells were incubated for 1hour in the darked and washed 5 times with 0.5% tween 20, the samples were mounted VECTACHIELD with DAPI. The images were taken with the ZEISS AxioObserver Z.1 at 20X and 40X magnifications.

2.2.13. Image analysis

Cell area

Cell area was calculated using ImageJ 1.53p. A threshold was applied in the actin cytoskeleton images to binarized the images. This step allows to select the outline of the cells with the wand tracing tool. Once the desired outline was selected, the cell area was calculated running the measure function.

FA analysis

The images taken from the vinculin staining were uploaded in ImageJ for analysis. The cells in the images were analysed one by one. First, the images were prepared using the functions *subtract background* and *enhance local contrast (CLAHE)*. The next step was applied a threshold to create a binary image. After that, the images were analysed using the tool *analyse particles*. From the result sheet obtained, the data used were area. Number of particles analysed and major for the length of the FA.

YAP localisation

Yap localisation was measured in ImageJ using the fluorescence images. The intensity of the signal in the cell and in the nucleus was calculated to do the ratio nuclear/cytoplasm following the equation 2-2.

Equation 2-2. YAP's integrated density fluorescence nuclear/cytoplasm ratio

$$YAP_{nuc/cyt}ratio = \frac{YAP_{nuc}/Area_{nuc}}{YAP_{nuc}/Area_{cyt}}$$

The integrated density of YAP in the nucleus (YAP_{nuc}) is normalised by the area of the nucleus ($Area_{nuc}$). Everything is divided by the integrated density of YAP in the cytoplasm (YAP_{cyt}) normalised by the area of the cytoplasm ($Area_{cyt}$). The integrated density of Yap in the cytoplasm and the area of the cytoplasm are calculated as described in the equations 2-3 and 2-4.

Equation 2-3. YAP's integrated density in the cytoplasm

$$YAP_{cyt} = YAP_{cell} - YAP_{nuc}$$

The integrated density obtained in the nucleus is subtracted from YAP's integrated density in the entire cell (YAP_{cell}).

Equation 2-4. Cytoplasm area calculation

$$Area_{cyt} = Area_{Cell} - Area_{nuc}$$

The area of the cytoplasm is calculated deducting the nucleus area from the area of the entire cell ($Area_{cell}$)

2.2.14. Statistical analysis

The statistical analysis was performed using GraphPad Prism v8.2.1 software. All the conditions were done in triplicates and an average of n=20 cells were analysed per condition. The mean ± standard deviation (SD) is represented in all the graphs unless otherwise noted. To study if the data follow a normal distribution a D'Agostino-Pearson Normality test was assessed.

When three or more groups were compared, normal distributed populations were analysed by two-way ANOVA test and Tukey's multiple comparisons test. In cases of populations without normal distribution, a Kruskal-Wallis test was used with a Dunn's post hoc test to correct for multiple comparisons.

When only two groups were compared, a t-test analysis was performed in normal distributions and as nonparametric test, we used Mann-Whitney for populations that did not follow a normal distribution.

Differences among groups are stated as follows: for p-values <0.05 (*), when p-values <0.01 (**), for p-values < 0.005 (***), for p-values < 0.001 (****), when differences between groups are not statistically significant (n.s).

CHAPTER 3 : INFLUENCE OF DEGRADABILITY AND STIFFNESS IN CELL MECHANOSENSING

3.1. INTRODUCTION

Cells create multiprotein complexes known as FAs when they enter in contact with the ECM. It is through these connections that cells perceive the physical and mechanical cues from their surroundings (e.g. ECM stiffness) (114). One of the main proteins in the FAs is vinculin, an actin-binding protein. When it is inactive, vinculin has a cytoplasmatic location. After being activated, it is recruited to the FAs to bind to talin, an adaptor protein that has to unfold to interact with vinculin. Once, vinculin binds to talin, it anchors the actin filaments to the rest of the FAs complex. This link allows to transfer the signals gathered from the ECM to the nucleus, where the information is processed (66,114). A widely studied pathway involved in transferring the information collected in the FAs to the nucleus is YAP/TAZ signalling cascade (61,73,77). Of these two proteins this study focalised in YAP, a transcriptional factor with an important role in mechanotransduction (6,61,151). Depending on how cells sense their surroundings, YAP activates and migrates to the nucleus. First, it dephosphorylates in the cytoplasm to be able to enter the nucleus. Once in the nucleus YAP binds to the DNA and trigger different pathways to create a response to the signals received through the FAs (151). YAP regulates the formation of focal adhesions to control the mechanical cues. Initially, YAP nuclear translocation is indirectly induced by Rho/ROCK pathway, which is involved in actin cytoskeleton assembling. When the actin fibres are formed, cells create tension which activates YAP nuclear translocation (11,74,152). In a study carried out by Nardone et. al. they observed that MSCs seeded on FN-coated micropattern, YAP translocated into the nucleus always that cells were able to spread and form the actin cytoskeleton, regardless the density of FAs (74). In turn, when YAP is located in the nucleus together with TAZ, they bind to DNA transcriptional factors (e.g. TEAD), initiating the expression of genes involved in FAs formation and cytoskeleton stability (e.g. genes involved in Rho/ROCK) (74,152). All this create a reinforcement loop to maintain cell attachment and cellular tension. Furthermore, either FAs formation and YAP nuclear translocation are influenced by ECM mechanical properties (e.g.

stiffness). As surface stiffness increases FAs assembling is favoured, cells are spread and they present a well-organised cytoskeleton; cellular tension increase and YAP nuclear translocation is activated (11,61)

In response to all these activation pathways, cells generated forces that are exerted to the ECM through the FAs. The magnitude of these forces changes depending on how cells feel the environment. *In vitro* it is possible to study the mechanical behaviour of cells looking at the material deformation (9).

This study has brought together YAP nuclear translocation and FAs formation to put them in relation with the traction forces exerted by the cells. The experiments were done in different cell types (L939 fibroblasts, MSCs and 3T3-L1) seeded on full-length FN-PEG hydrogels and PAA hydrogels of different stiffnesses. Moreover, to study the influence of cell contractility in cellular mechanotransduction and force generation, myosin II was inhibited using blebbistatin. As described in the general introduction blebbistatin is a specific inhibitor of non-muscle myosin II that blocks cell actin-cytoskeleton's contractility (153). This changes the way cells sense the ECM and how they exert forces. YAP nuclear translocation and FA assembling were explored by immunostaining, using monoclonal antibodies which target YAP and vinculin respectively. To determine the traction forces exerted by the cells, traction force microscopy (TFM) has been used. This technique measures the elastic substrates deformation by single cells and converts it into forces, generating stress (force per unit area) maps (154).

3.2. HYDROGELS CHARACTERISATION

In this thesis three different type of gels have been used: full-length FN-PEG hydrogels, polyacrylamide (PAA) and Matrigel. PAA hydrogels and Matrigel have been characterised before and the same the parameters described in the literature were followed (145,147). The stiffness for the PAA hydrogels were 3 kPa (±0.4), 9 kPa (±0.7) and 35 kPa (±4) (145); and for Matrigel 0.2 kPa and 1 GPa (147). On the contrary, the full-length FN-PEG hydrogels were developed in the lab. They were characterised using rheology and nanoindentation. The gels used in each experiment of the thesis are described in Table 3-1.

Table 3-1. Type of gels and cells used in each experiment of the thesis

Type of gel used	Experiment description	Type of cells	Chapter
Full-length FN-PEG	FN immunostaining	-	3
	Vinculin immunostaining	MSCs	3
	YAP immunostaining		
	General metabolomics	MSCs and L939	4
	TFM		3
PAA	Vinculin immunostaining	3T3-L1	3
	YAP immunostaining	MSCs and 3T3-L1	
	TFM	MSCs	3
	ATP assay	3T3-L1	4
Matrigel	Seahorse	MSCs and 3T3-L1	4
	ATP assay	3T3-L1	4
	Ratiometric sensors		

3.2.1. Mechanical characterisation

Full-length FN-peg gels were characterised in the lab using rheology and nanoindentation. The stiffnesses described in the thesis (2.5, 8 and 26 kPa) are the average of the results obtained in rheology and nanoindentation together (Table 3-2). Unfortunately, 3% wt PEG-(4)-ACRL degradable hydrogels were not possible to measure their stiffness with any of these techniques. This type of gel cannot resist the pressure between the two plates in rheology. The degradable network breaks easily when the plates come together yielding inaccurate measurements. Also, this gel is sticky, hence the needle in the nanoindentor cannot do a proper indentation and it stayed stuck in the gel. Therefore, as in the other stiffnesses the results between degradable and non-degradable were similar. The same assumption was taken for the soft condition (3%wt PEG-(4)-ACRL).

Table 3-2. Young's Modulus obtained in rheology and nanoindentation for the full-length FN-PEG hydrogels

Percentage of PEG-(4)-ACRL	Rheology Young's Modulus (kPa)		Nanoindentation Young's Modulus (kPa)		MEAN (kPa)	+/- SD
	Degradable (VPM)	Non-degradable (SH-PEH-SH)	Degradable (VPM)	Non-degradable (SH-PEH-SH)		
3% wt	X	2.3	X	3	2.5	0.4
5% wt	8	7.5	8	9	8	0.7
10% wt	22	25	29	22	26	4

3.2.2. FN immunostaining

PEG hydrogels were functionalised with full-length FN protein to allow cell attachment. To ensure the protein incorporation into the gels a regular FN staining was performed (Figure 3-1). As a control, the native protein, acquired from YoProteins (Figure 3-1B), and the PEGylated FN were absorbed in a 20 µg/ml concentration on glass coverslips (Figure 3-1C). PEG-ACRL gels were functionalised with 50 µg/mL of PEGylated FN of three different stiffnesses (2.5, 8 and 26 kPa) (Figure 3-1). The lowest protein fluorescence intensity was found on PEGylated FN adsorbed on glass. While the highest signal was obtained on the native protein from YoProteins on glass (Figure 3-1A). FN intensity in the different gels were similar, what is a good indication that the protein is being successfully incorporated in the gel and available for cell attachment (Figure 3-1A).

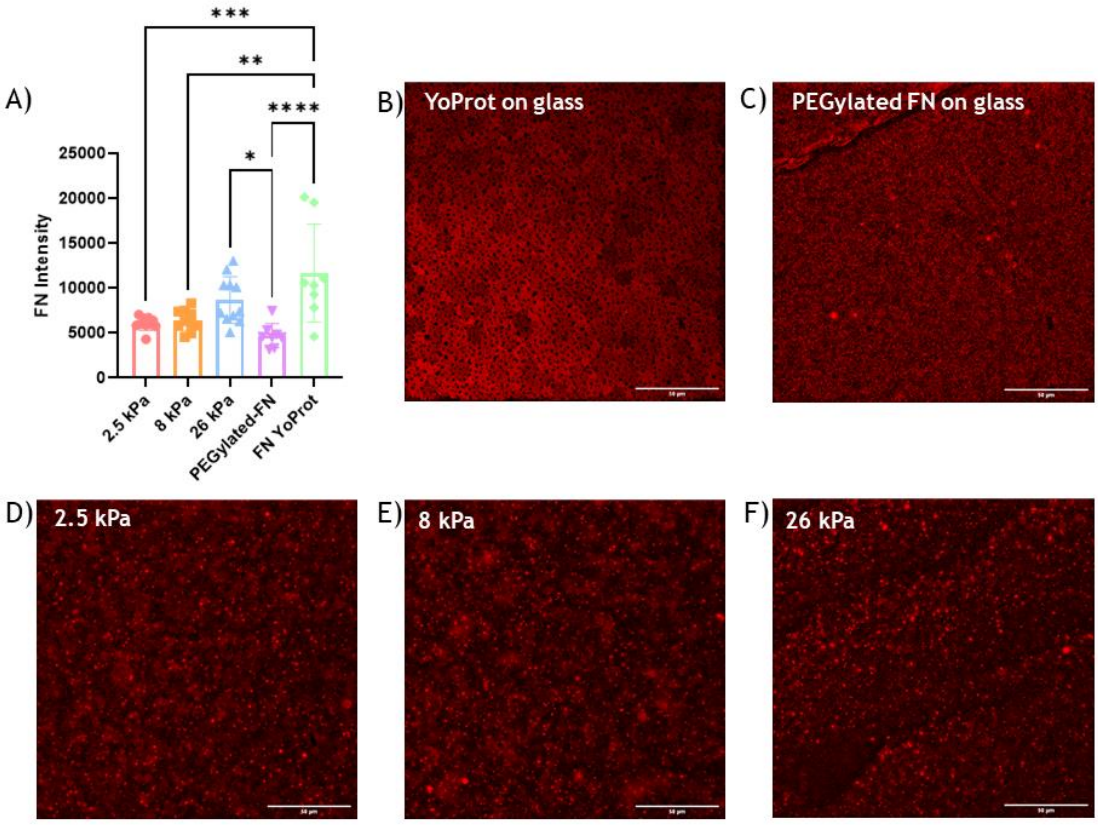

Figure 3-1. FN staining on different surfaces. *A) There were no significant differences among hydrogels. Significant differences were obtained for FN YoProtein (highest intensity) and FN-PEG on glass (lowest intensity).*P=0.02, **P=0.001, ***P=0.0007, ****P<0.0001. B) Native protein from YoProteins adsorb on a glass coverslip. C) Fluorescence image of PEGylated FN adsorb in glass. D) FN intensity image in 2.5 kPa PEG-ACRL hydrogels. E) FN intensity in 8 kPa PEG-ACRL hydrogels. F) FN intensity in 26 kPa PEG-ACRL hydrogels. Scale bar 50 µm.*

These results might indicate that the protein loses binding sites during protein PEGylation. In a study made by Trujillo et al. they observed that the collagen binding domain of the FN was hindered after PEGylation while the cell adhesion and growth factor binding domains remain available (133). Therefore, less adsorption of the PEGylated FN on glass than of the native protein was observed. During PEGylation, the protein is denaturalised and some of the SH groups react with PEG-MAL. Therefore, protein adsorption might be weaker, being easier to lose protein during the washes during the immunostaining. Moreover, the immunostaining was done with an anti-FN polyclonal antibody in a concentration 1:400 which binds to the whole protein. As during the PEGylation process some

binding sites are restrained, it can lead to less antibody binding and subsequently, to less fluorescence intensity measured. On the other hand, when the protein is incorporated into the hydrogels, the remain SH groups will react with the acrylate groups of the PEG-ACRL and the thiols groups in the crosslinker. These bonds are much stronger, ensuring the protein is trapped in the hydrogel. Hence, there would be more PEGylated FN retained in the hydrogels than when it is just adsorbed on the glass.

3.3. VINCULIN IMMUNOSTAINING

3.3.1. The formation of FAs in MSCs increases on stiffer surfaces

Once it was confirmed that fibronectin was correctly incorporated into the hydrogels, MSCs were seeded on full-length FN-PEG hydrogels of 2.5, 8 and 26 kPa for 24 hours. After this time a DAPI-actin-vinculin staining was performed to characterise FAs' formation (Figure 3-2). On soft surfaces, MSCs do not spread and remain poorly attach. FAs cannot be properly formed, and vinculin remains dispersed in the cytoplasm (Figure 3-2, first row). On the contrary, on stiffer surfaces MSCs were able to develop mature FAs (Figure 3-2, second row, red dots). Vinculin on the stiffest surfaces is mainly localised in the FAs (Figure 3-2, third row).

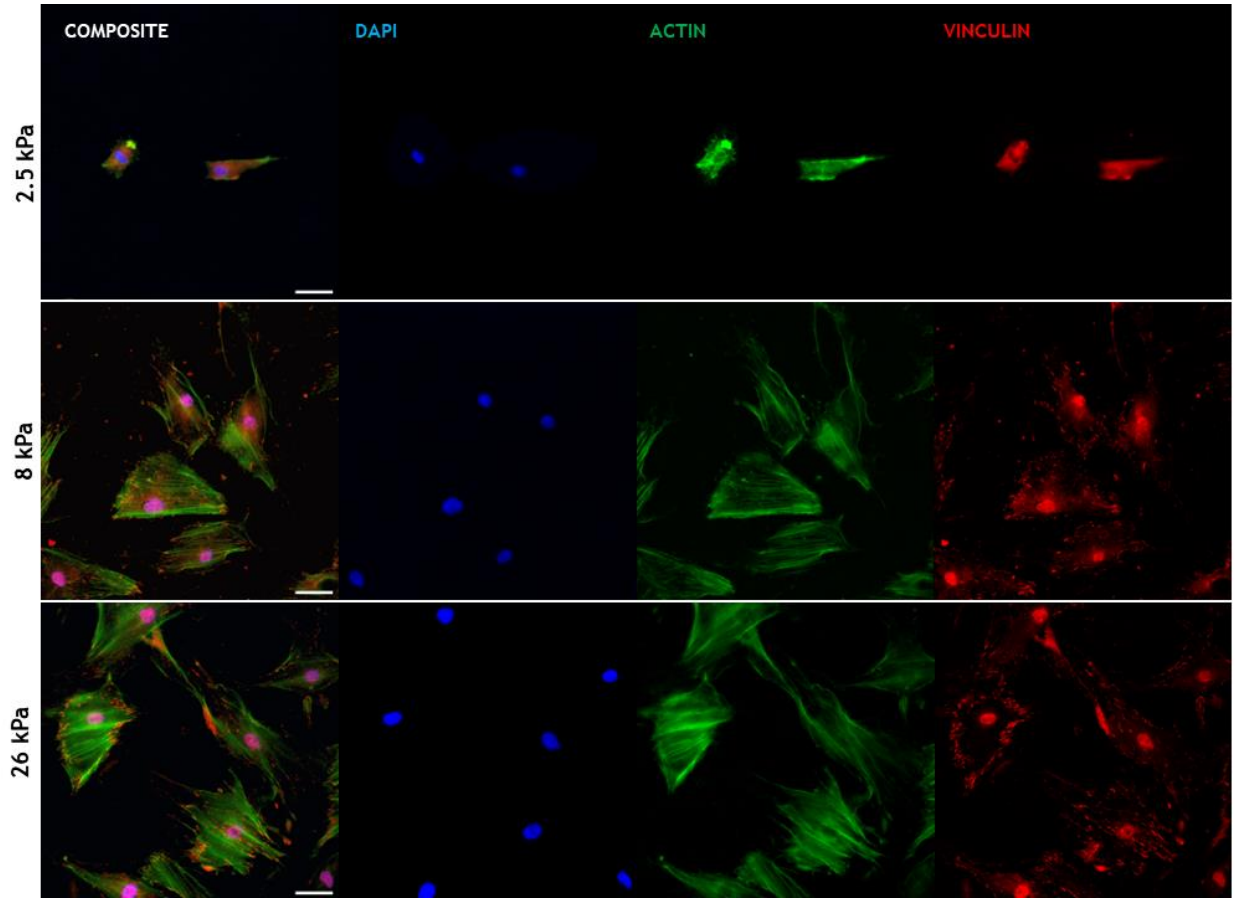

Figure 3-2. Vinculin staining of MSC seeded on full-length FN-PEG hydrogels. *Immunostaining for DAPI (blue), actin (green) and vinculin (red). In MSCs seeded for 24 hours on soft surfaces (2.5 kPa, first row) the highest fluoresce signal was in the cytoplasm. On stiffer surfaces (8 kPa, second row) vinculin is localised in the FAs. The highest localisation of vinculin in the FAs was found on the stiffest surfaces (26 kPa, third row). Scale bar 50 μm.*

Cell contractility plays an essential role in cell attachment. When cells are not able to polymerise the actin filaments and contract, as it happens on soft surfaces, the force loading in the FAs is very low. As a consequence, talin protein remains unfolded and it cannot bind to vinculin, which connects the actin filaments to the focal adhesions. Due to the low tension, FAs are not reinforced and the bond between integrins and the ECM is disrupted (37,155). By inhibiting MSCs contractility with 10 μM blebbistatin for an hour before imaging, FAs are not formed and vinculin remained in the cytoplasm regardless of matrix stiffness (Figure 3-3).

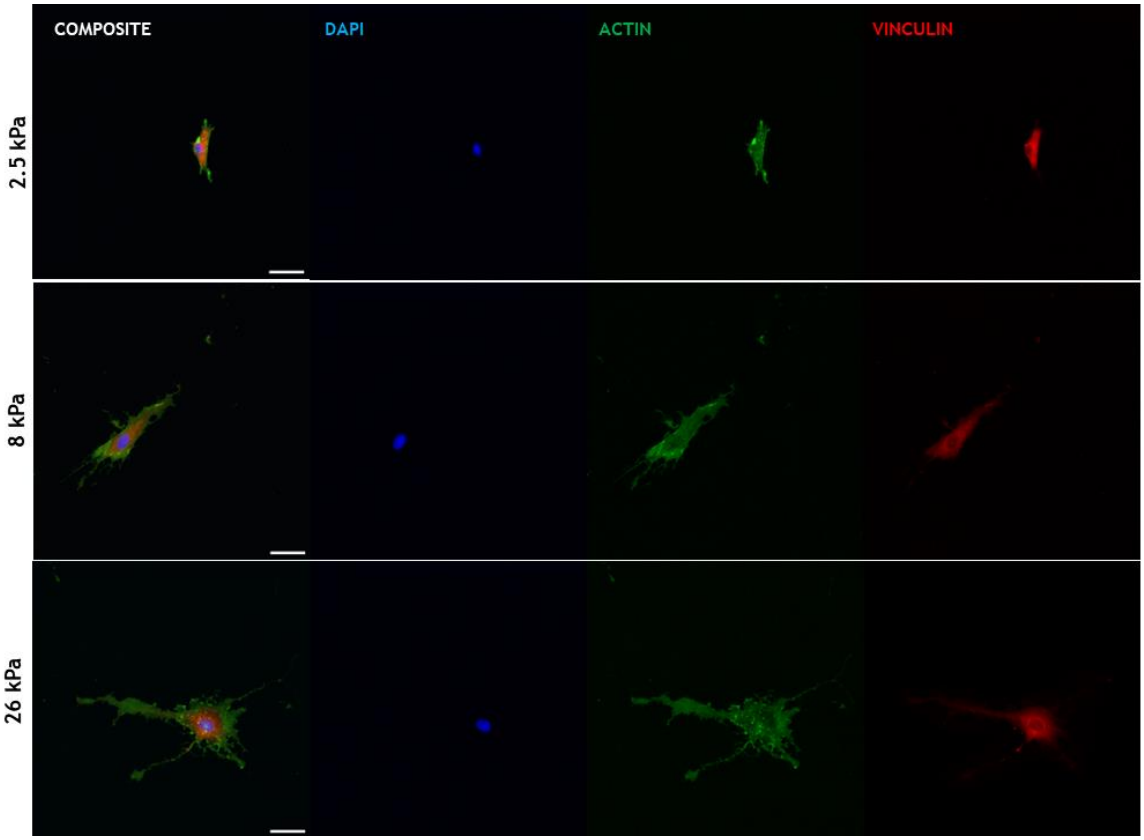

Figure 3-3. Blebbistatin blocks vinculin translocation to FAs. *Immunostaining for DAPI (blues), actin (green) and vinculin (red). When MSCs contractility is inhibited using blebbistatin, cells presented a more branched shape, even though, they kept being more spread on stiffer surfaces (8 and 26 kPa, second and third rows respectively). MSCs were cultured on the gels for 24hours and treated with 10 μM blebbistatin one hour before imaging. Blebbistatin blocked vinculin translocation to the FAs remaining dispersed in the cytoplasm. Scale bar 50 μm.*

Cell area and the number, area and length of FAs were quantified. The statistical analysis shows significant differences in cell area (Figure 3-4A). MSCs spread more on stiffer surfaces even when their contractility is inhibited. In the case of the FAs, MSCs created higher number of FAs on stiffer surfaces (Figure 3-4B). However, there were no significant differences between 8 and 26 kPa. In the case of FAs area and length (Figure 3-4C,D), the values increased with surface stiffness. For all the parameters investigated for FAs, when blebbistatin was presented in the medium, the values decayed (Figure 3-4B,C).

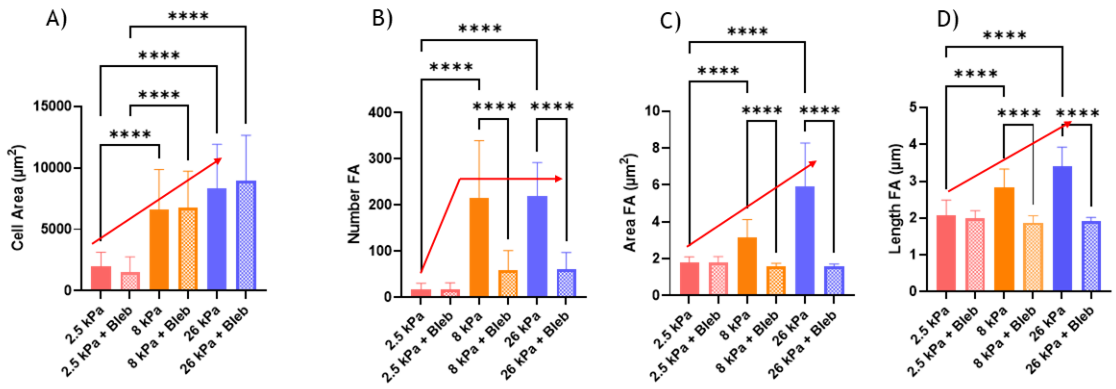

Figure 3-4. MSC create more FAs on stiffer surfaces*. MSCs were cultured for 24 hours on full-length FN-PEG gels. Blebbistatin treatment was done for one hours before imaging. A) MSCs spread more on stiffer surfaces regardless their contractility is inhibited with blebbistatin or not. B) The number of FAs increased on stiffer surfaces. However, MSCs are not able to form focal adhesions when their contractility is inhibited. When blebbistatin is added in the system the number of focal adhesions decreases. C) FAs area increased on stiffer surfaces. When cell contractility is inhibited using blebbistatin, the FAs area decays. D) The length of focal adhesions increases with the surface stiffness. This difference in the length disappears when blebbistatin is added into the system. Graphs shown mean ±SD of n≥10 of one experiment, differences were analysed via non-parametric ANOVA and t-test. **** P<0.0001.*

3.3.2. FAs assembling in 3T3-L1 cells is similar on hydrogels of different stiffness

Vinculin immunostaining was also performed in 3T3-L1 cells to compare them with MSCs. In this case, 3T3-L1 fibroblasts were seeded on PAA hydrogels of different stiffnesses (3, 9 and 35 kPa) and glass as a control, for 24 hours. Before imaging, selected samples of cells were treated with blebbistatin 10 µM for one hour.

Regardless the surface stiffness, 3T3-L1 cells were able to spread in all the surfaces and form mature FAs. Vinculin appeared gathered in FAs and in the cytoplasm (Figure 3-5). These results differ from the case of the MSCs (Figure 3-2), where vinculin disappeared from the cytoplasm on stiffer surfaces and was localised mainly in the FAs.

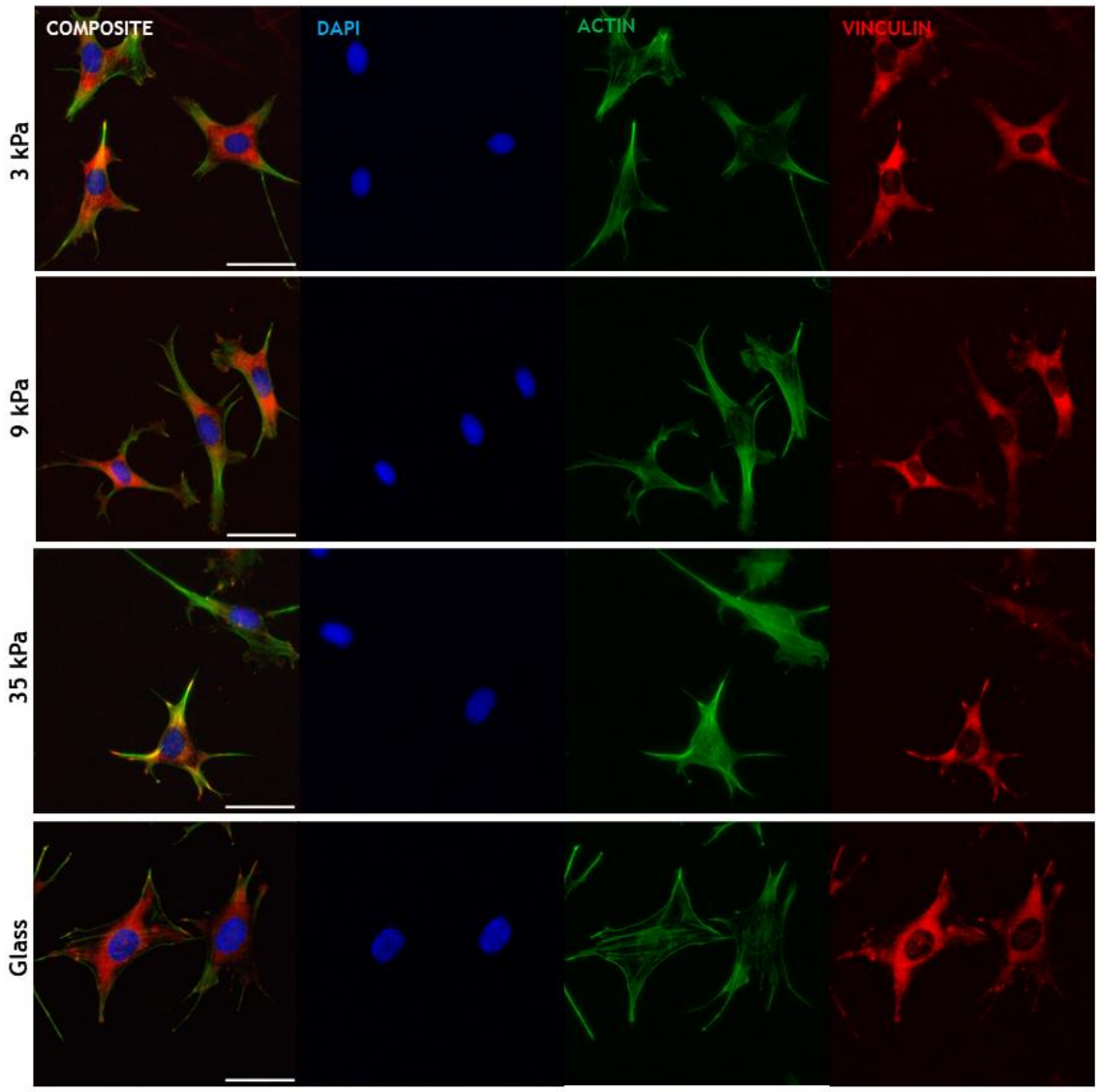

Figure 3-5. Fibroblast 3T3-L1 type form mature FAs in a stiffness range 3-35 kPa. *3T3-L1 cells were cultured for 24 hours on PAA gel functionalised with FN. From left to right, images correspond to composite of all filters, nuclei in blue (DAPI), cell cytoskeleton in green (actin) and vinculin in red. Every row of images are cells in a different stiffness going from soft (3 kPa) to the stiffest (glass). Scale bar is 50 μm. Looking at vinculin images, all the surfaces presented vinculin located in the cytoplasm and forming FAs.*

As it was observed in the case of the MSCs (Figure 3-3), when 3T3-L1 cells were treated with blebbistatin they appeared more branched (Figure 3-6). The actin filaments, which were visible before forming the cytoskeleton in 3T3-L1 cells without blebbistatin treatment, have been disintegrated with the drug treatment

(Figure 3-6, green images, third column from the left). No formed FAs were found, and vinculin was localised in the cytoplasm (Figure 3-6, images in red, very right column).

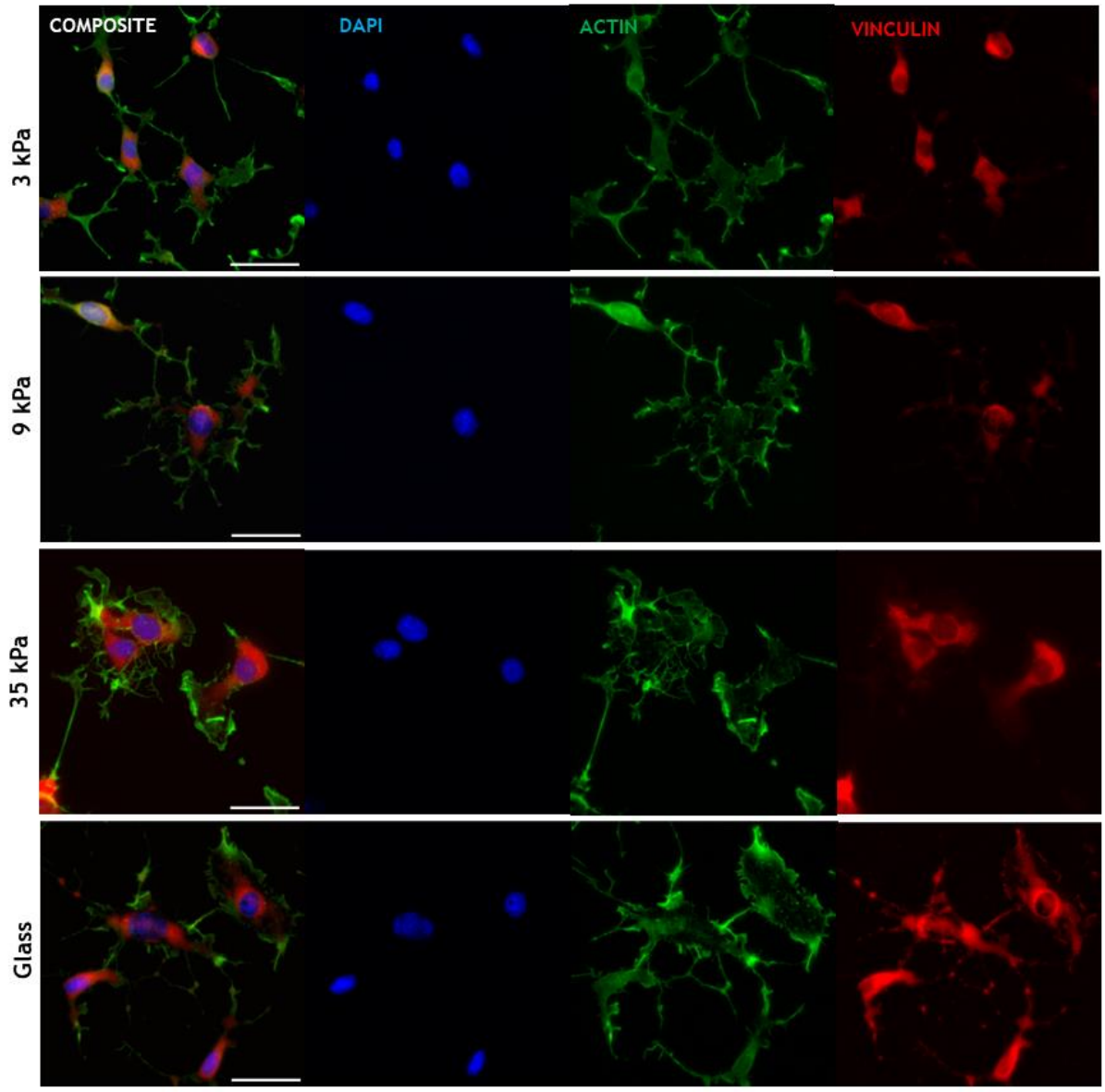

Figure 3-6. Fibroblast 3T3-L1 treated with blebbistatin are not able to form FAs. *3T3-L1 cells were treated with 10 μM blebbistatin for one hour before imaging. From left to right, images correspond to composite of all filters, nuclei in blue (DAPI), cell cytoskeleton in green (actin) and vinculin in red. Every row of images are 3T3-L1 cells in a different stiffness going from soft (3 kPa) to the stiffest (glass). Scale bar is 50 μm. Last column on the right, vinculin disappeared from the FAs and remained cytoplasmatic.*

When cell area was quantified for 3T3-L1 cells, no significant differences were found among different stiffnesses. The average cell area after blebbistatin treatment decreased (Figure 3-7A). Looking at the FAs formation, there were no significant differences for their area (Figure 3-7C) and the length (Figure 3-7D) among surfaces. However, in every surface stiffness there was a significant difference between the condition with and without blebbistatin treatment. The biggest variability among surfaces was in the number of FAs. 3T3-L1 presented higher number of FAs on glass. On the other hand, there were no significant variance among hydrogels stiffnesses (Figure 3-7B).

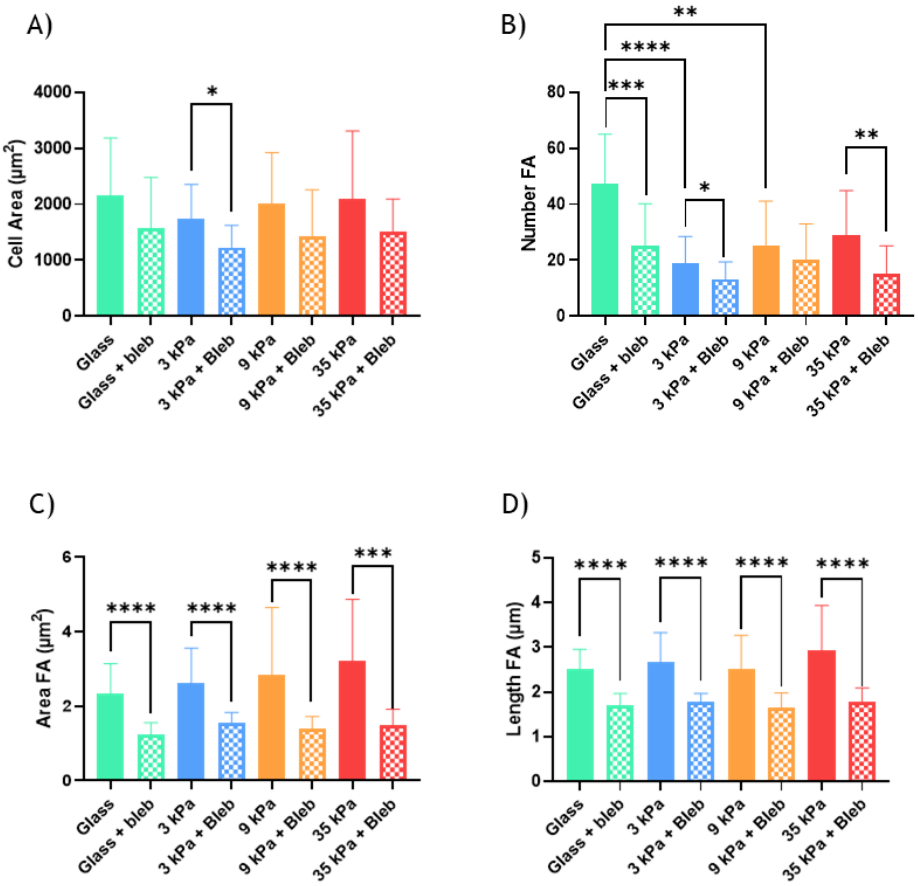

Figure 3-7. Similar values in FAs were found in 3T3-L1 cells seeded on different stiffnesses. *3T3-L1 cells were seeded on PAA gels functionalised with FN for 24 hours. Blebbistatin treatment was done for one hour before imaging. A) Average cell area does not have significant differences among surfaces. When 3T3-L1 cells were treated with blebbistatin for one hour, the area decreased minimally (* P<0.02). B) Average number of FAs was significantly higher on glass compare with the hydrogels. After treating cells with blebbistatin, the number*

*of FAs dropped down (*P<0.002, **P=0.002, ****P<0.0001). C) The area of FAs decreased significantly when 3T3-L1 cells were treated with blebbistatin. There were no significant differences among different surfaces (****P<0.0001). D) The values of FAs length were similar in all the surfaces. However, the values were lower with blebbistatin (****P<0.0001). Graphs shown mean ±SD of n≥10 from one experiment, differences were analysed via non-parametric ANOVA and t-test.*

3.4. YAP TRANSLOCATION

3.4.1. YAP nuclear translocation changes with surface degradability

A series of YAP stainings were performed to study the mechanotransduction of the MSCs and 3T3-L1 cells on different surfaces. When YAP is inactivated, it remains in the cytoplasm phosphorylated. Under certain stimuli it activates and translocates into the nucleus. It has been observed that on stiff surfaces YAP nuclear translocation increases (61,78).

In MSCs cultured on degradable FN-PEG gels, YAP remained in the cytoplasm on the softest surfaces, where also the cell area was the smallest. On the other hand, MSC appeared more spread on 8 kPa, 26 kPa and glass. On these surfaces YAP translocated into the nucleus (Figure 3-8). However, no significant differences between the two stiffer surfaces studied (8 and 26 kPa) and glass were observed (Figure 3-12).

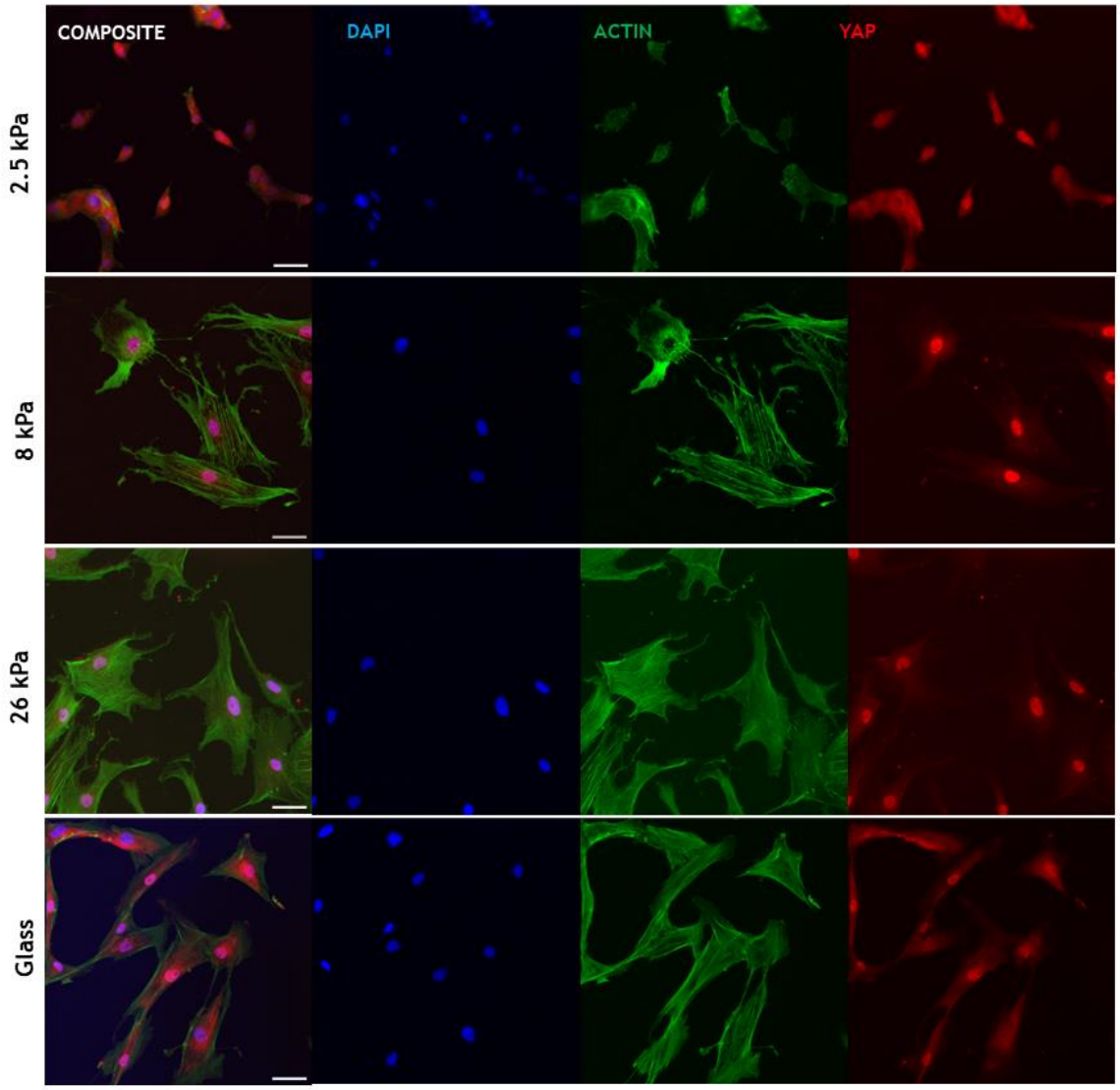

Figure 3-8. MSCs seeded on degradable surfaces present more YAP translocation as matrix stiffness increases. *The staining was made for the nucleus (DAPI, blue, second column), actin-cytoskeleton (green third column) and YAP (red, fourth column). Scale bar 50 µm. The first column corresponds to the composite. MSCs were seeded for 24 hours on degradable full-length FN-PEG hydrogels of different stiffnesses: 2.5 kPa (first row), 8 kPa (second row) and 26 kPA (third row). As a control they were also seeded on glass. YAP appeared localised in the nucleus on stiffer surfaces (8 kPa, 26 kPa and glass, last column red signal).*

On non-degradable FN-PEG gels, YAP nuclear translocation was also quantified. However, in comparison with the degradable gels, YAP also translocated into the nucleus on the softest surfaces (2.5 kPa) (Figure 3-9).

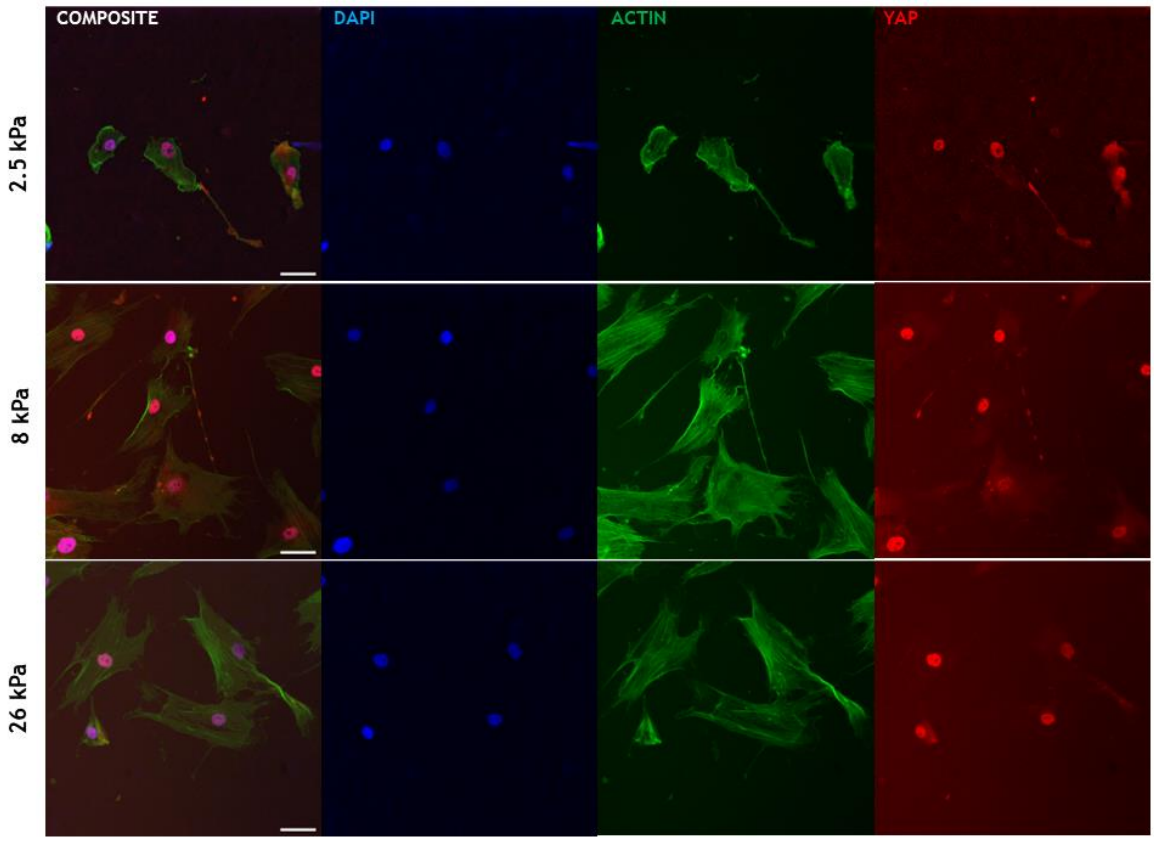

Figure 3-9. MSCs seeded on non-degradable surfaces showed nuclei YAP signal even on soft surfaces. *MSCs were seeded for 24 hours on non-degradable full-length FN-PEG gel. From left to right the columns correspond to composite (all channels together), nuclei signal (DAPI, blue), actin cytoskeletons (green) and YAP (red). Looking at the last column YAP appeared in the nucleus in all the surfaces. Scale bar 50 µm.*

When cell contractility was inhibited using 10 µM blebbistatin for one hour before imaging, YAP translocated into the nucleus and MSCs remained spread. The same response to the myosin II inhibitor was observed on degradable and non-degradable surfaces. Therefore, YAP nuclear translocation might be independent from myosin II inhibition and surface degradability (Figure 3-10 and Figure 3-11).

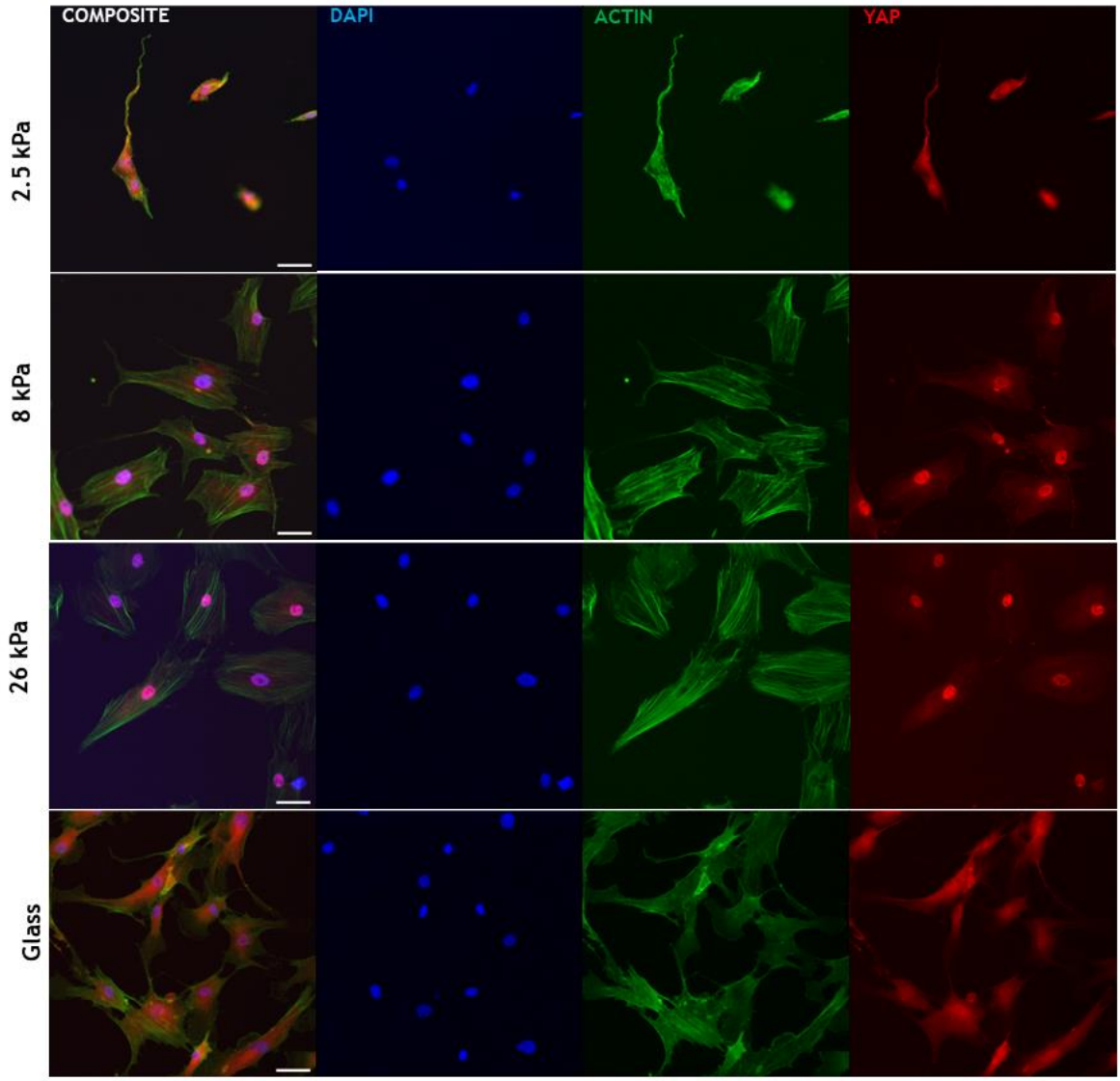

Figure 3-10. YAP continue translocating into the nucleus in MSCs seeded on degradable gels when their contractility is inhibited with blebbistatin. *MSCs seeded for 24 hours on degradable full-length FN-PEG gels and treated with 10 μM blebbistatin for 1 hour before imaging. From left to right the columns correspond to composite images, nuclei (DAPI, blue), actin-cytoskeleton (green), YAP signal (red). MSCs were seeded on degradable full-length FN-PEG gels of different stiffnesses (first row 2.5 kPa, second row 8 kPa, third row 26 kPa) and last on glass (last row). The contractility was inhibited using blebbistatin 10 μM. Scale bar 50 μm. Except from the softest surface, YAP kept translocated into the nucleus on stiffer surfaces (red signal, last column).*

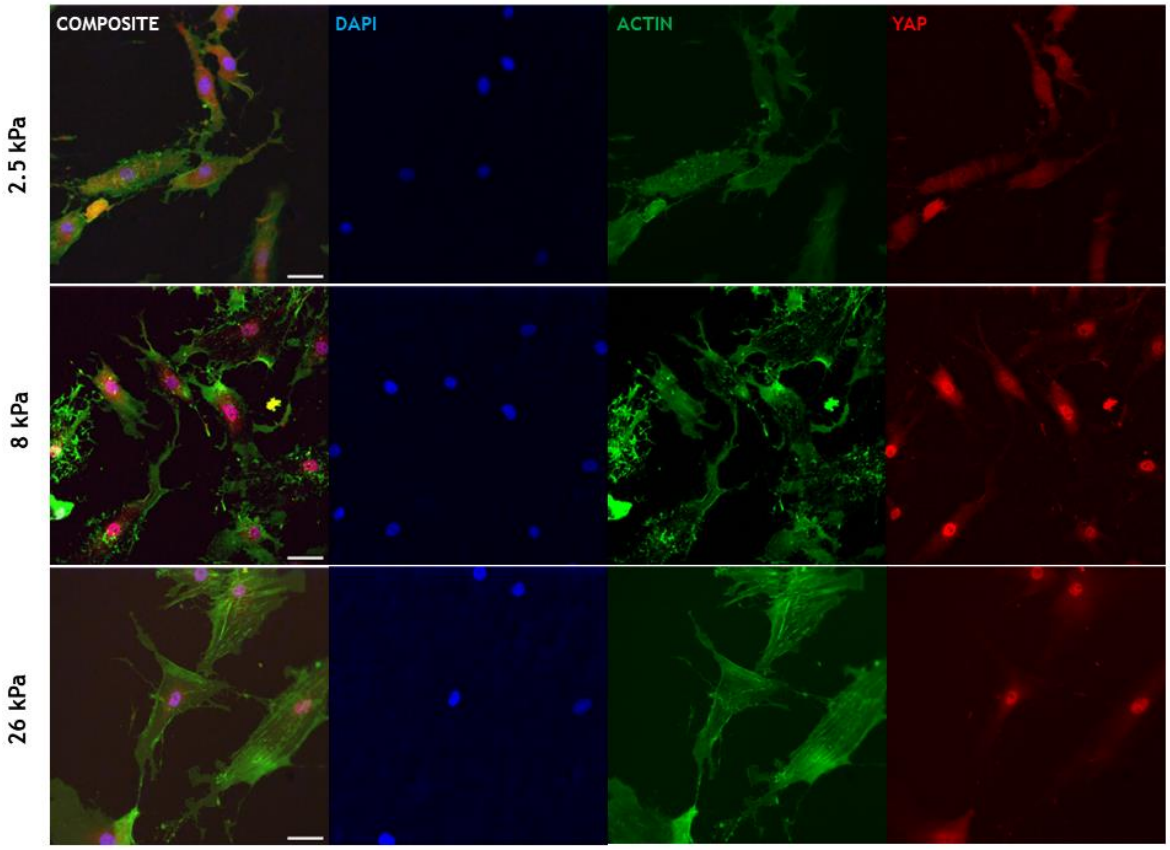

Figure 3-11. MSCs seeded on non-degradable surfaces keep presenting YAP in the nucleus after inhibiting their contractility with blebbistatin. *MSCs seeded for 24 hours on non-degradable full-length FN-PEG gels and treated with 10 µM blebbistatin for 1 hour before imaging. From left to right each column correspond to: the composite of all the channels, nuclei signal (DAPI blue), actin-cytoskeleton (green) and YAP (red). Each row corresponds to a surface stiffness 2.5 kPa (first row), 8 kPa (second row) and 26 kPa (last row). Scale bar 50 µm. MSCs seeded on full-length FN-PEG hydrogels were treated with blebbistatin to inhibit their contractility and YAP nuclear translocation was analysed. YAP nuclear signal appeared in all cases (last column, red).*

The statistical analysis showed differences between MSCs seeded on degradable and on non-degradable gels. On degradable surfaces, higher values of YAP nuclear /cytoplasm (n/c) ratio were obtained on stiffer surfaces. However, when they were compared with 2.5 kPa surfaces no significant differences appeared (Figure 3-12A). On the other hand, it was interesting to see a peak on YAP nuclear translocation on 8 kPa non-degradable surfaces, even though there were no significant differences between 2.5 kPa and 26 kPa (Figure 3-12B).

In both types of surfaces YAP translocated into the nucleus when the contractility of MSCs was inhibited with blebbistatin (Figure 3-12A,B). There was only a slightly difference on degradable 2.5 kPa FN-PEG gels (Figure 3-12A).

Cell area on degradable surfaces increased with stiffness up to 8 kPa. Afterwards, no significant differences were found between 8 and 26 kPa gels. When cell contractility was inhibited using blebbistatin the results changed depending on the surface. On the stiffest hydrogels (26 kPa) MSCs showed a decrease in size when blebbistatin was added into the media (Figure 3-12C).

On the contrary, no significant differences were found in MSCs area on non-degradable gels. Even when blebbistatin was added into the media, MSCs remained spread (Figure 3-12D).

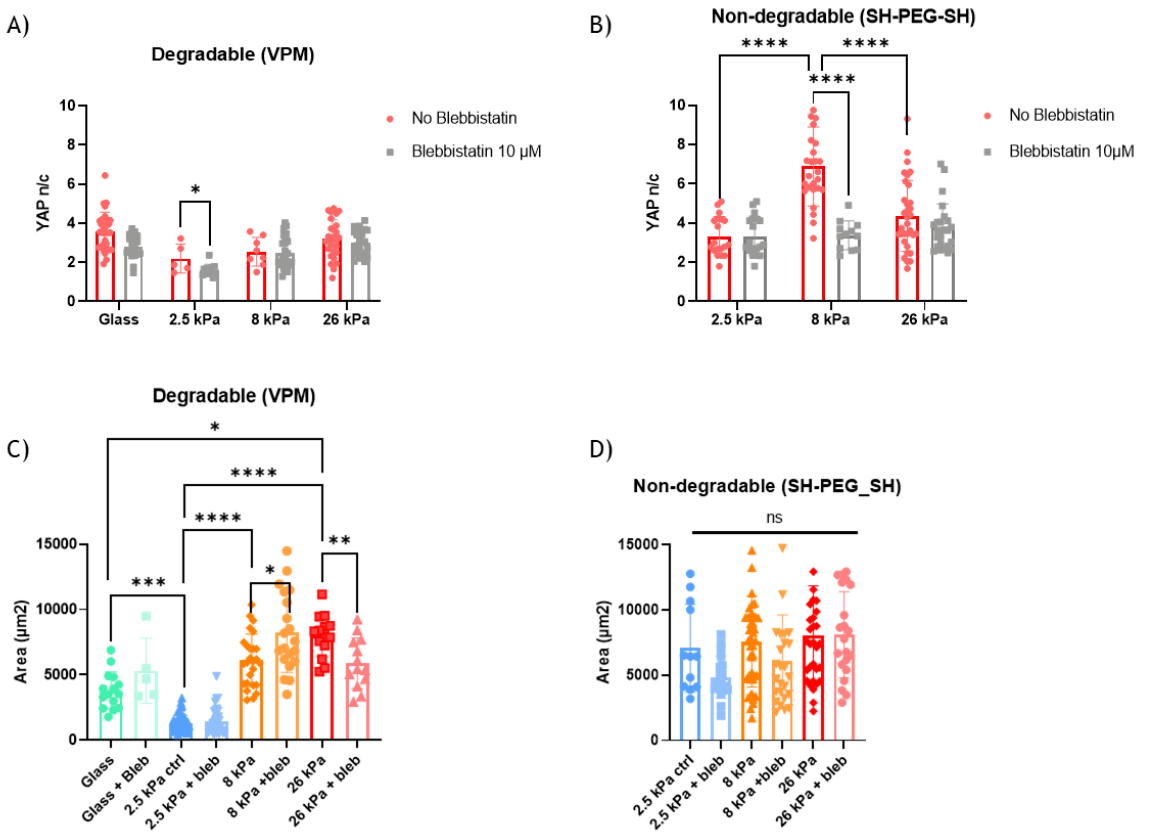

Figure 3-12. YAP translocates more into the nucleus in MSCs on stiffer surfaces, but it is not sensitive to cell contractility with blebbistatin. *A) No significant differences were found in YAP translocation into the nucleus in degradable surfaces. When contractility was inhibited using blebbistatin YAP kept*

*translocating into the nucleus. (*P=0.03). B) On non-degradable gels a peak in YAP translocation was found on gels of 8 kPa. For the other two stiffnesses, no significant differences were found. Also, there are no significant differences between the results with and without blebbistatin, apart from 8 kPa surfaces. (****P<0.0001). C) MSCs seeded on degradable gels spread more on stiffer surfaces. When blebbistatin is added into the system, cell area change, but MSCs keep spreading more on stiffer surfaces. (*P=0.04, **P=0.0066, ***P=0.0004, ****P<0.0001). D) On non-degradable surfaces no significant differences were found. Neither when blebbistatin was incorporated. (NS>0.9999). Graphs shown mean ±SD of n≥10 from one experiment, differences were analysed via non-parametric ANOVA and t-test.*

When these last results were intended to be replicated, a series of problem arose. The FN-PEG gels started to fail, and MSCs could not survive on them, while they could do on glass. MSCs remained rounded in all the hydrogels and YAP did not translocate into the nucleus, a pattern that it was not observed on glass functionalised with FN (Figure 3-13). The hydrogels seemed to not polymerase properly and some reagents, toxic for the cells, may have remained in the matrix.

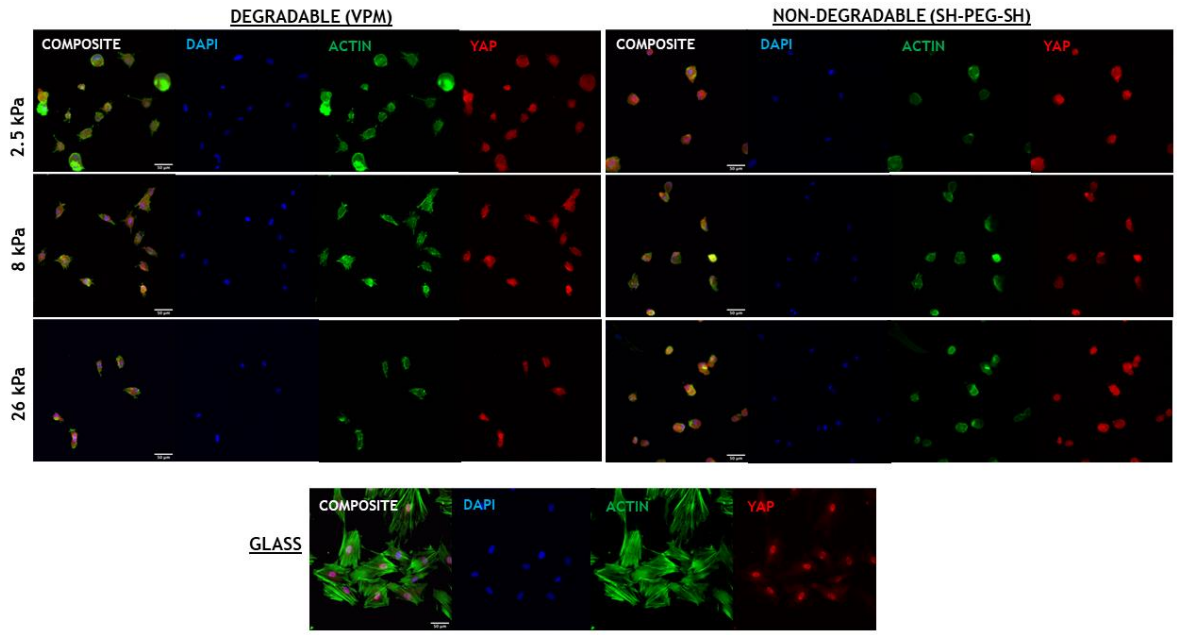

Figure 3-13. MSCs are not attaching properly to the surface. YAP does not translocate. *MSCs were cultured on the different gels for 24 hours. Set of four columns on the left corresponds to MSCs seeded on full-length FN-PEH hydrogels.*

The second set of four column on the right corresponds to MSCs seeded on non-degradable full-length FN-PEG hydrogels. IN both cases from left to right each column represents the composite, blue signal from the nuclei (DAPI), green signal from the actin-cytoskeleton and red signal from YAP. Set of four image sin the bottom corresponds to MSCs seeded on glass. The order of the images is the same as described before. Scale bar 50 µm. MSCs appeared completely rounded (third column, green, actin) and YAP dispersed in the cytoplasm (last column, red, YAP) in all the cases of the hydrogels regardless the degradability. YAP could translocate to the nucleus in MSCs seeded on glass.

3.4.2. MSC and 3T3-L1 cells on PAA gels are less mechanosensitive

While looking for a solution to the FN-PEG gels, cell mechanotransduction was kept being studied on PAA gels of 3, 9 and 36 kPa. This type of gels was selected because they are well-known, their protocol is well established and are easy to work with (145). Therefore, they were the best option to compare our previous results on full-length FN-PEG hydrogels.

In MSCs seeded on PAA hydrogels, YAP translocated into the nucleus in all the surfaces (Figure 3-14A). However, the translocation on the softest surfaces (3 kPa), was significantly different compared to 9 kPa and 35 kPa gels (Figure 3-14B). Cell area did not present significant differences among surfaces (Figure 3-14C). In all the cases, MSCs were able to spread and attach to the surface.

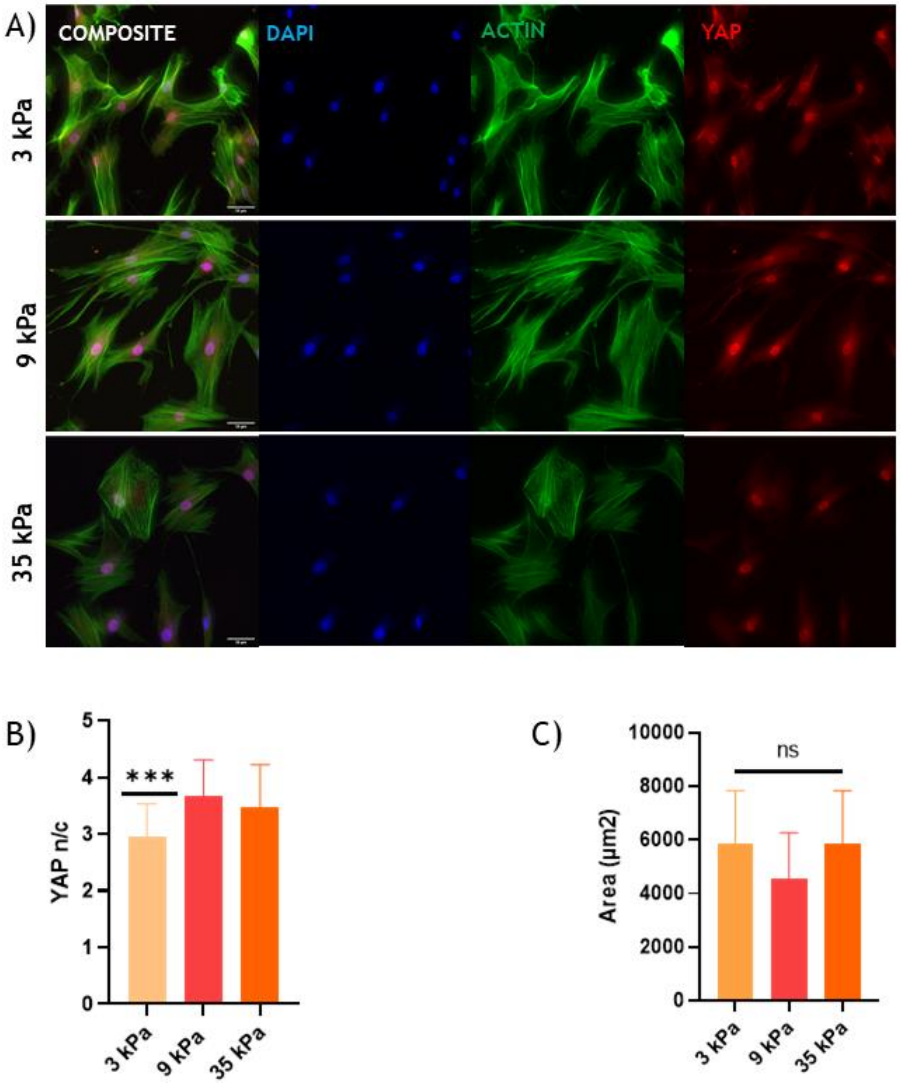

Figure 3-14. MSCs on PAA gels showed no difference in YAP translocation in different stiffnesses. *MSCs seeded on PAA gels functionalised with FN for 24 hours. A) Images of YAP translocation from MSCs seeded on PAA hydrogels of different stiffnesses. B) No significant differences in YAP translocation were found on stiffer surfaces. There is a lower nuclear location on 3 kPa surfaces (***P=0.001). C) MSCs presented similar areas in all the surfaces. Graphs shown mean ±SD of n≥10 from one experiment, differences were analysed via non-parametric ANOVA.*

YAP translocation was also studied in 3T3-L1 cells seeded on PAA gels of 3, 9 and 35 kPa. 3T3-L1 seeded on glass functionalised with fibronectin was used as a control. In all the surfaces YAP signal was mainly found in the nucleus (Figure 3-15).

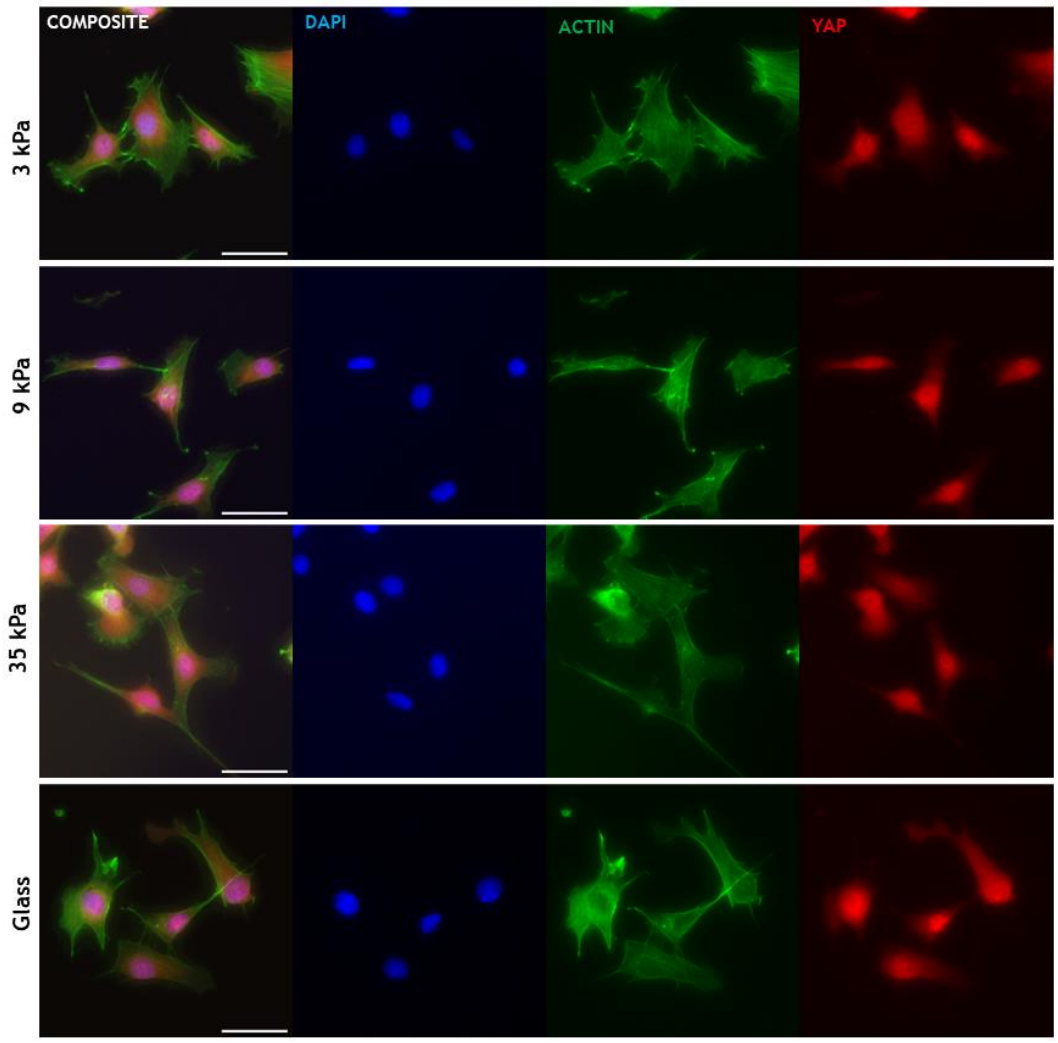

Figure 3-15. YAP translocation in 3T3-L1 cells seeded on PAA gels for 24 hours. *From left to right each column corresponds to composite of all the channels, nuclei (blue, DAPI), actin cytoskeleton (green) and YAP localisation (red). Each row corresponds to a different stiffness 3 kPa (first row), 9 kPa (second row), 35 kPa (third row and glass (last row). Scale bar 50 µm. In all the cases YAP nuclear localisation in visible (last column, red signal).*

When cell contractility was inhibited using blebbistatin 3T3-L1 cells presented a more branched aspect. YAP signal was detected either in the nucleus and in the cytoplasm (Figure 3-16).

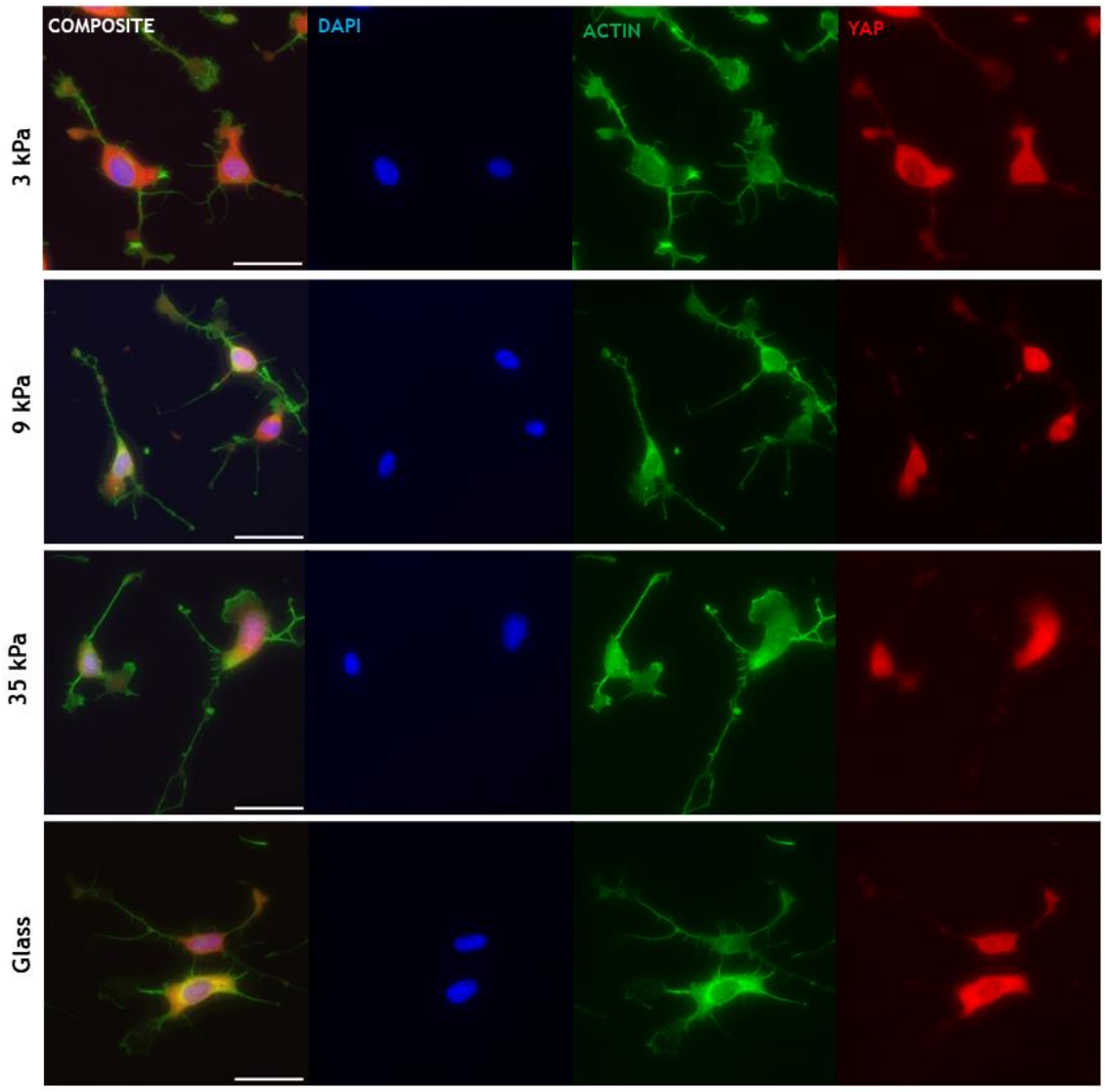

Figure 3-16. YAP translocation in 3T3-L1 cells on PAA gels when cell contractility is inhibited using blebbistatin for 1 hour before imaging*. From left to right each column corresponds to composite of all the channels, nuclei (blue, DAPI), actin cytoskeleton (green) and YAP localisation (red). Each row corresponds to a different stiffness 3 kPa (first row), 9 kPa (second row), 35 kPa (third row and glass (last row). Scale bar 50 μm.*

No significant differences were found among hydrogel's stiffnesses. YAP nuclear translocation ratio was the highest on glass. After inhibiting the contractility using blebbistatin there was still YAP nuclear signal. It did only decrease significantly on the softest surfaces (3 kPa). However, on 35 kPa gels n/c ratio increased after adding blebbistatin to the media (Figure 3-17A).

Looking at cell area, 3T3-L1 cells spread more on glass where they went thought a decrease after adding blebbistatin. On the gels no significant differences were found, not even when cell contractility was inhibited (Figure 3-17B).

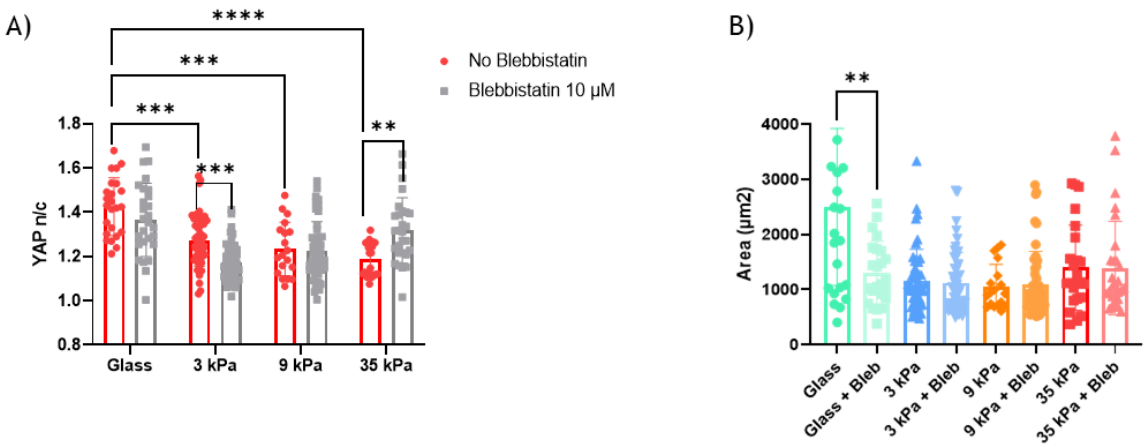

Figure 3-17. In 3T3-L1 cells, YAP kept translocating into the nucleus regardless the surface stiffness and the contractility inhibition with blebbistatin*. 3T3-L1 cells seeded on PAA gels functionalised with FN for 24 hours. Blebbistatin treatment was done for 1 hour before imaging. A) YAP n/c ratio is on glass. No significant differences were found among the different gel stiffnesses. When cell contractility is inhibited using blebbistatin, YAP kept translocating into the nucleus. (*P=0.03, ***P=0.004,****P<0.0001) B) 3T3-L1 cells spread similarly among the different surfaces. (**P=0.003). Graphs shown mean ±SD of n≥10 from one experiment, differences were analysed via non-parametric ANOVA and t-test.*

3.5. TRACTION FORCE MICROSCOPY

3.5.1. Influence of substrate degradability

To study the influence of matrix degradability on 2D models, murine fibroblast cells (L929) were seeded on biodegradable (VPM) and non-degradable (SH-PEG-SH) 5%PEG-(4)-Ac (8 kPa) hydrogels (Figure 3-18A). After 24 hours the traction stress was analysed by Fourier Transform Traction Cytometry (FTTC) method (Figure 3-18B) using an in-house software developed by Pompe T (148). L929 fibroblast were used at the beginning of the project to optimise the traction force

microscopy model. These cells are easy to work with as they proliferate fast and responded quite well to the surfaces used. Firstly, a unique stiffness was selected (8 kPa), leaving the surface degradability as the only variable. The idea was to have a quick overview of how cells respond to the surface degradability to use later only one type of matrix and change the stiffness.

L929 cells exerted higher forces on degradable gels compare with non-degradable (Figure 3-18B). In both surfaces, traction stress decrease after blebbistatin treatment.

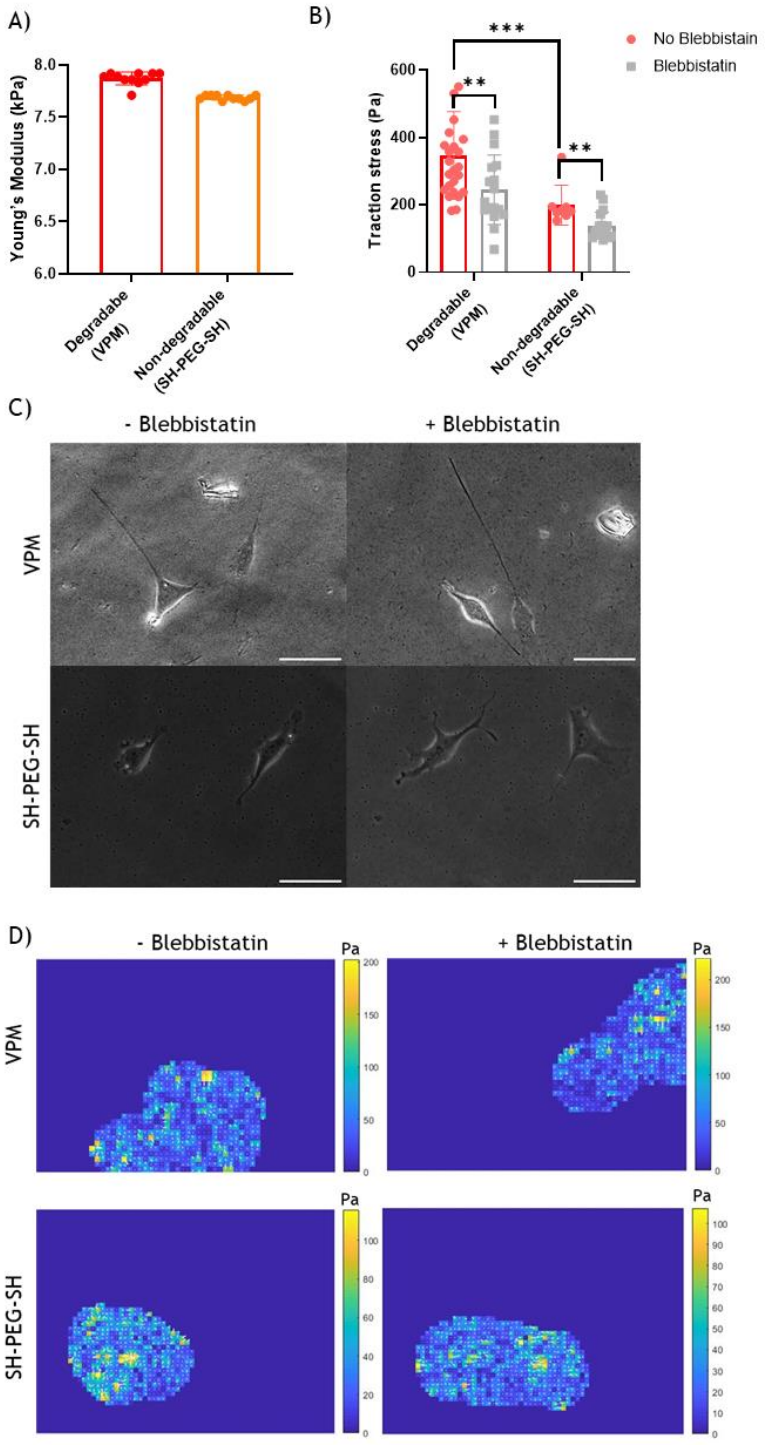

Figure 3-18. L929 traction force microscopy seeded on 8 kPa degradable (VPM) and non-degradable (SH-PEG-SH) full-length FN-PEG hydrogels for 24 hours. *A) Hydrogels with a degradable (VPM) and a non-degradable (SH-PEG-SH) crosslinker showed similar stiffness. In both cases a Young's Modulus of 8 kPa was obtained (no significant differences were observed). B) L929 cells on degradable (VPM) surfaces exerted higher traction stress, compare with non-degradable (SH-*

*PEG-SH). However, when cell contractility was inhibited using blebbistatin, a myosin II inhibitor, the traction stress in both surfaces dropped down. (***P<0.0001, **P=0.01). Graphs shown mean ±SD of n≥10 from one experiment, differences were analysed via non-parametric ANOVA and t-test. C) Bright field of cells seeded on degradable (VPM) and non-degradable (SH-PEG-SH) hydrogels (scale bar 50 µm). The images on the left are without blebbistatin treatment. The images on the right are with 10 µM blebbistatin treatment for 1h before imaging. D) Traction stress maps of L929 cells seeded on degradable (VPM, first row) and non-degradable (SH-PEG-SH, second row) full-length-FN-PEG hydrogels of 8 kPa. TFM analysed with MATLAB. On the left are the maps without blebbistatin treatment. The maps on the right represents the traction stress of L929 cells treated with 10 µM blebbistatin for 1h. Yellow pixels are the areas where cells are exerting higher traction stress.*

3.5.2. Influence of stiffness

To have a first sight of the traction stress in the first stages of cell attachment, human MSCs were seeded on biodegradable full-length FN-PEG hydrogels of different stiffnesses. Cell contractility was inhibited using 10 µM blebbistatin 1 hour before imaging.

On soft surfaces, MSCs exerted lower traction forces what leaded to a decrease in the traction stress transmitted to the ECM (Figure 3-19A). It was confirmed that contractility is important in force generation as traction stress drop to minimum values when blebbistatin was added to the media either on soft or stiffer surfaces (Figure 3-19A).

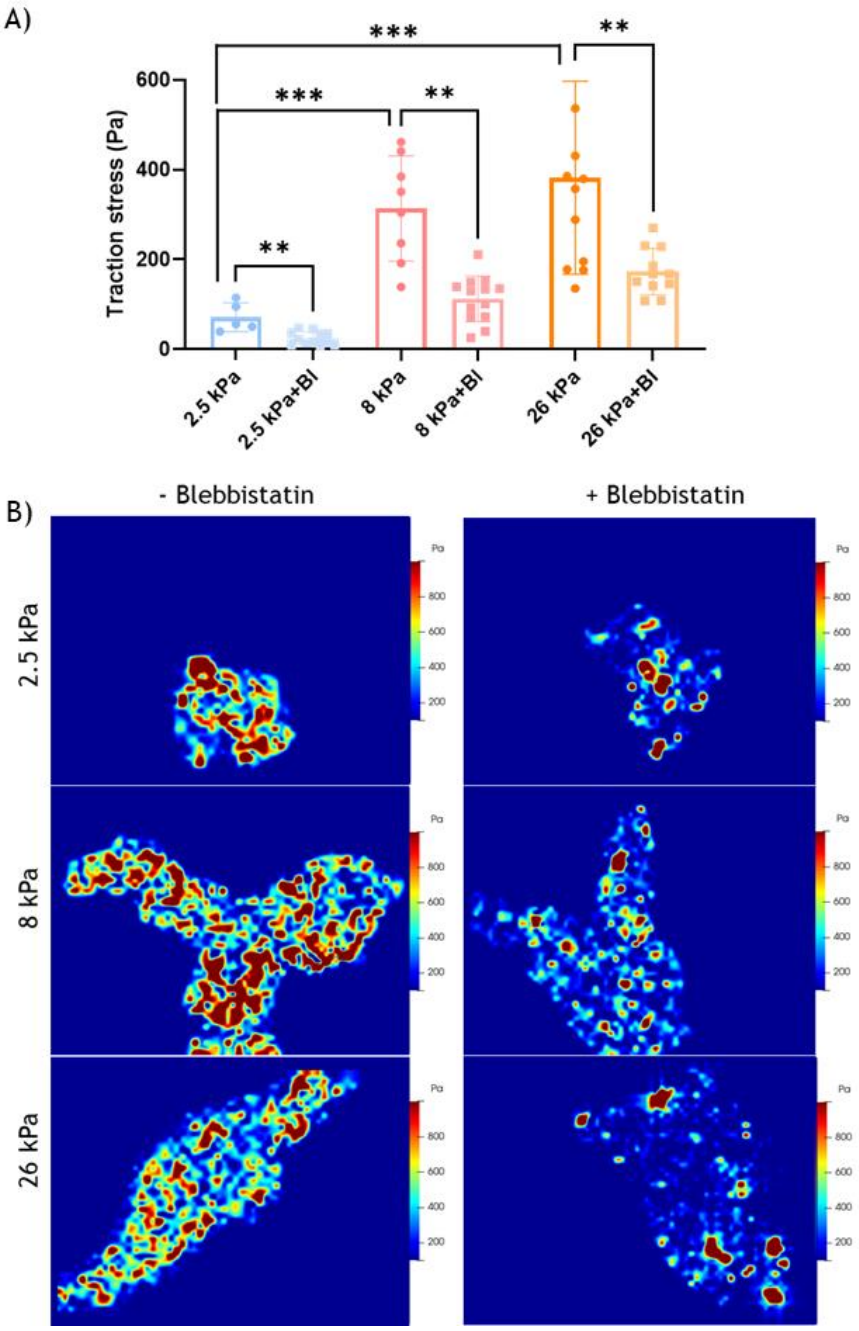

Figure 3-19. MSCs exert higher traction stress on stiffer surfaces. *MSCs seeded on full-length FN-PEG gels for 24 hours. A) MSCs seeded for 24 hours exerted higher traction stress on stiffer surfaces. In all cases, when cell contractility was inhibited with 10 μM blebbistatin, the traction stress registered was lower. (**P=0.001, ***P<0.0001) Graph shown mean ±SD of n≥10 from one experiment, differences were analysed via non-parametric ANOVA and t-test B) Traction stress maps of MSCs seeded on 2.5 kPa (fist row), 8 kPa (second row) and 26 kPa (third row) full-length FN-PEG degradable hydrogels, treated with blebbistatin (right column) and without blebbistatin (left column).*

During this project, two types of EVOS microscopes were used. For the first experiments, the imaging for the TFM was done in an EVOS™ FL Auto (ThermoFisher). After one year, the group acquired the new model EVOS™ M7000 (ThermoFisher). To make sure that the results we obtained from the images taken in this new microscope were comparable with the old one, we carried out an experiment with MSCs seeded again on full-length FN-PEG degradable hydrogels of 2.5 kPa, 8 kPa and 26 kPa (Figure 3-20). As it was observed before (Figure 3-20A), MSCs exerted higher forces on stiffer surfaces (Figure 3-20B). Therefore, it is possible to conclude that as the trend and the force magnitude were similar, the experiments run out in the different microscopes were comparable.

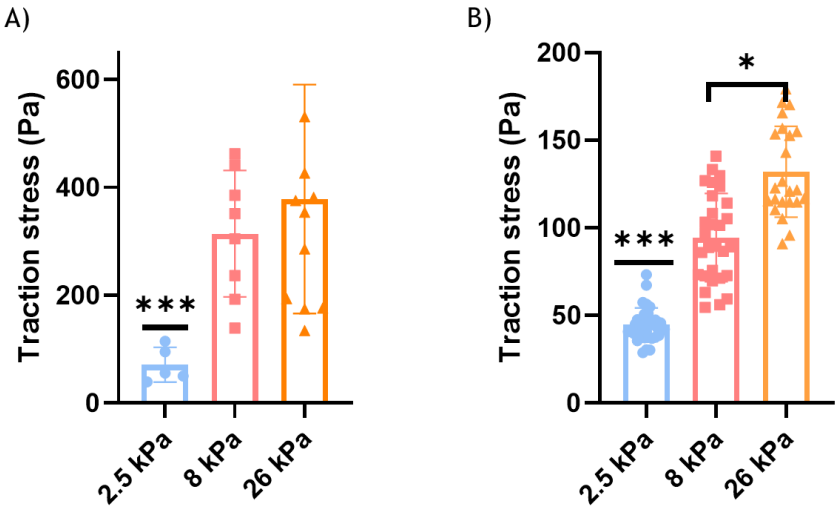

Figure 3-20. TFM carried out in MSCs seeded on degradable full-length FN-PEG gels for 24 hours in the different EVOS microscopes. *A) Traction stress exerted by MSCs imaged with EVOS™ FL Auto. MSCs seeded on soft surfaces (2.5 kPa) exerted lower forces than MSCs on stiffer surfaces (8 and 26 kPa). (***P<0.003). B) Traction stress exerted by MSCs imaged with EVOS™ M7000. As observed in the previous graph, MSCs seeded on soft surfaces (2.5 kPa) exert lower traction stress than MSCs seeded on stiffer surfaces (8 kPa or 26 kPa). Observing the highest traction stress on the stiffest surface (26 kPa). (*P=0.02, ***P<0.0001). Graphs shown mean ±SD of n≥10 each of them from one experiment performed in the different microscopes, differences were analysed via non-parametric ANOVA.*

For the last couple of years of the project, MSCs traction forces were measured on PAA gels, due to a series of problems with FN-PEG hydrogels synthesis.

The problems of using full-length FN-PEG gels for TFM were: i) we have to work with really thin hydrogels to be able to image the beads in the different planes and the cells seeded on top. ii) In other to obtain them we followed a *sandwich* model, polymerising the hydrogels between a hydrophobic and a silanised coverslip (Figure 2-4). On several occasions, it was difficult to separate both coverslips without breaking the hydrogel. iii) As described before, on top of these main problems, the polymerisation of the hydrogels started to fail. They were not forming properly, and cells were not able to survive on them (Figure 3-13).

Hereby, MSCs were seeded on PAA hydrogels with three different stiffnesses (3, 9,35 kPa). Looking at the traction stress maps (Figure 3-21A), the parts where the MSCs are exerting higher traction stress appear in red. On stiffer surfaces, there is an increase of these red areas, focalised on the edges, especially on the stiffest surface. When the analysis was done, the highest traction stress was on the stiffest surfaces (35 kPa). The values obtained were similar to the full-length FN-PEG hydrogels, on average 400 Pa (Figure 3-21B). However, there were no significant differences on the traction stress on 3 and 9 kPa surfaces (Figure 3-21B).

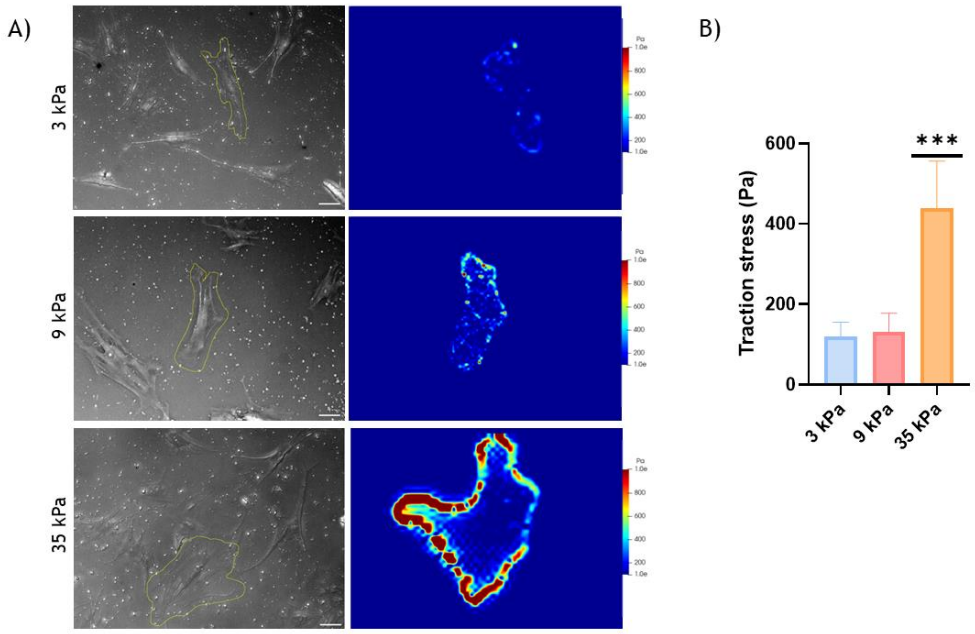

Figure 3-21. TFM of MSCs seeded on PAA hydrogels for 24 hours*. A) Bright field of MSCs seeded on PAA hydrogels for 24hours are shown on the left column (scale bar 50 µm). The cells selected with a yellow line were analysed for TFM. Their traction stress maps are represented in the right column. B) The highest traction stress was registered on the stiffest surfaces. However, there were no significant differences found between 3 kPa and 9 kPa surfaces. (***P<0.0001). Graph shown mean ±SD of n≥10 from one experiment, differences were analysed via non-parametric ANOVA.*

3.6. DISCUSSION

Focal adhesions (FAs) are the direct contact of the cells with the ECM.

FAs are the physical connection of the cells with the ECM, and they are dynamically engaging and disengaging, as has been described in the molecular clutch model (38). Vinculin is one of the main proteins in the FAs and is involved in the molecular clutch (38,65). When FAs formation was studied, accumulation of vinculin was observed on MSCs seeded on degradable FN-PEG hydrogels of 8 and 26 kPa (Figure 3-2). However, the statistical analysis did not show significant differences between these two stiffnesses. This might indicate that MSCs have reached a threshold in FAs formation above which the reinforcement of the FAs

starts to decrease. It has been demonstrated that FAs assembly is dependent on surface stiffness and the loading force exerted by the cells to the ECM (38,156). How rigidly the cells perceive the surface determines the rate at which forces are applied to the FAs. Upon a loading rate threshold (~10 pN), cells cannot face that much force generation, and FAs end up breaking (38,156,157). This same process also happens when cell contractility is inhibited. The actin filaments depolymerise and, hence, vinculin unbinds from the FAs complex. This leads to FAs turnover and dissipation (158). After treating MSCs and 3T3-L1 cells with blebbistatin, FAs dissipated, and vinculin appeared dispersed in the cytoplasm. The same pattern appeared on soft surfaces, actin cytoskeleton was not formed, and vinculin remained in the cytoplasm (Figure 3-3). Therefore, cells need to contract and generate enough internal tension to activate vinculin. On soft surfaces, or when cell contractility is inhibited, cells attachment to the surface is very poor and they cannot generate enough force to establish actin filaments and produce vinculin translocation to the FAs (38,159).

More FAs are formed on stiffer surfaces to exert higher forces.

The higher formation of FAs on stiffer surfaces coincides with a higher traction stress recorded (Figure 3-4B,D and Figure 3-19). These forces decreased when cell contractility was inhibited (Figure 3-19). Hence cell contractility is essential to create enough tension within the cell and transmit the forces to the ECM through the FAs (160,161). On stiffer surfaces cells create more FAs through which they can exert the required forces to compensate the resistance from the ECM and remained attached (156,160). However, if the cells are not able to contract there is not enough tension within the cell to generate the appropriate forces. In this situation cells attachment starts to get weaker and FAs disappear (38). Similar pattern is observed on soft surfaces, where no FAs are formed and there is a significant reduction of traction stress compared with the other substrates (37). These results suggest that MSCs on degradable full-length FN-PEG gels are mechanosensitive to matrix stiffness. However, FAs assembly and traction force exertion appeared to have little effect on YAP nuclear translocation. Although, higher nuclear translocation appeared on stiffer surfaces, YAP remained in the nucleus when cell contractility was suppressed. These results suggest that YAP

nuclear translocation is triggered by surface stiffness, but it is independent of myosin II inhibition (162). Hence, YAP would be able to escape blebbistatin inhibition. Furthermore, MSCs and 3T3-L1 cells kept similar areas with and without blebbistatin treatment on the different surfaces. This might be an indication that cells have memory of their state just before the treatment with blebbistatin. Therefore, they keep the same area after recognising the same substrate as before the treatment.

YAP nuclear translocation and traction forces exertion change depending on the mechanical properties of the surface.

On full-length FN-PEG hydrogels of different degradability YAP tended to translocate more into the nucleus as surface stiffness increases. Regardless matrix degradability, there was still nuclear translocation when MSCs contractility was inhibited using blebbistatin (Figure 3-12). On PAA gels functionalised with FN, MSCs showed YAP nuclear translocation in all the surfaces. There was only a small decrease on the softest surface (Figure 3-14). Similar values of YAP n/c ratio were obtained on PAA hydrogels and non-degradable full-length FN hydrogels. Moreover, both non-degradable systems presented higher YAP nuclear translocation than on degradable FN-PEG gels. This confirms that surface degradability and composition play an important role even in 2D.

As a matter of fact, a difference in force exertion was also observed in L929 fibroblasts. These cells exerted higher forces on degradable gels compare with non-degradable gels, confirming once again that the mechanical properties of the surface are going to affect the cellular response.

Cellular behaviour changes with matrix degradability even in 2D.

However, matrix degradation by the cells over time should be considered, as it might create inaccuracies in the analysis method. To analyse the TFM, the displacement of the fluorescent beads from a relaxed (no cellular influence) to a stressed (cellular influence) state is calculated to be transformed later in stress unit by FTTC. When the images of the hydrogel are taken, cells have started to manipulate the surface. Therefore, once cells are removed the fluorescent beads

embedded in the gel are not going to return to their original position, creating an extra displacement. On degradable surfaces, cells could be able to indent more in the hydrogel, establishing FAs also within the hydrogel (58). This phenomenon would allow the cells to pull more and exert higher forces, what is translated into a higher traction stress (Figure 3-18B). However, it is important to bear in mind that cells are also manipulating the surface and hence the data obtained might be a result, not only of the cellular effect itself, but also of the surface modification. When cells migrate within the degradable hydrogels the network breaks (34,53). The total displacement registered is going to be higher than it should be in theory. Not only because the cells are able to pull more, but also because of this extra movement of the beads.

On the other hand, on non-degradable surfaces, cells cannot indent within the hydrogel, establishing the FAs mainly on the surface (Figure 3-22A). In this case when the cells are removed, the hydrogel network is mainly intact, and the fluorescent beads go back to their original position (Figure 3-22A).

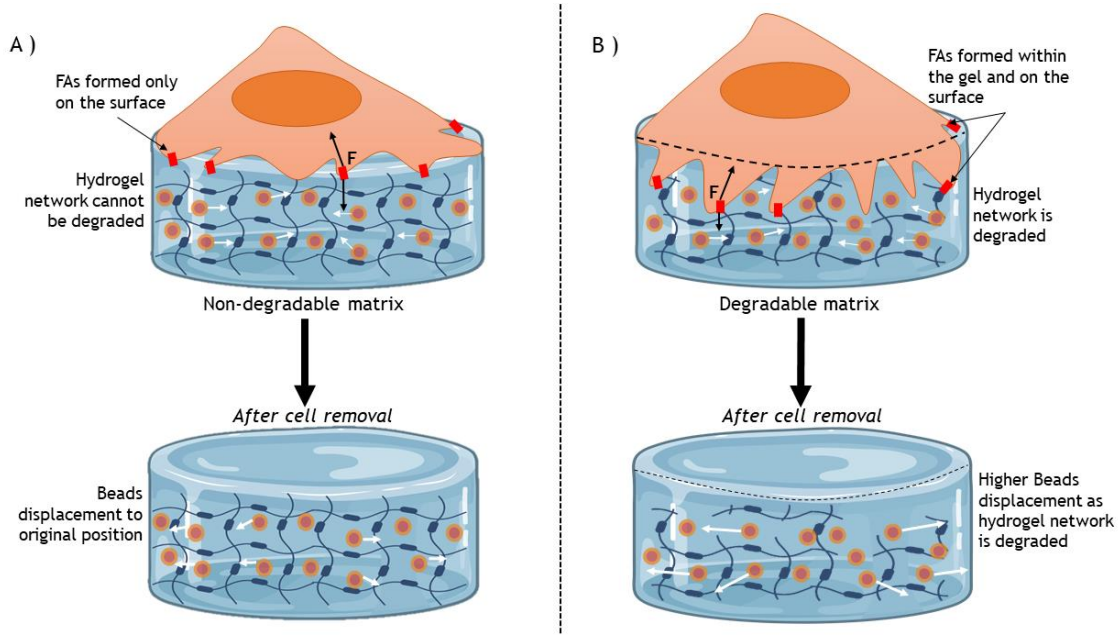

Figure 3-22. Cellular behaviour on non-degradable and degradable matrices in 2D models. *A) Cells seeded on non-degradable matrices are not able to break the hydrogel network. Most of the FAs are formed on top of the hydrogel (red squares). It is from these FAs that cells pull and exert forces, dragging the fluorescent beads embedded in the hydrogel towards them. When cells are*

removed the hydrogel network relaxes and the embedded fluorescent beads recover their original position. B) On the other hand, cells seeded on degradable surfaces can indent more in the hydrogel, breaking the hydrogel network. FAs are created within the hydrogel (pointed line delimitates the hydrogel edges), as well as on the surface. The force that they can apply from within the hydrogel network and on the surface is higher than on non-degradable surfaces. Also, when cells are removed the hydrogel network is broken, hence the fluorescent beads do not go back to the original position but move a bigger distance when the gel relaxes. Thereby, the displacement calculated is going to be higher, translated in a higher stress calculates in FTTC.

Surprisingly, the TFM results of MSCs on PAA gels did not demonstrate a gradual increase in traction stress with surface stiffness. MSCs exerted similar forces on 3 kPa and 9 kPa. It is not until they were seeded on 35 kPa surfaces that there was a significant increase in force exertion. It has been demonstrated that a difference in stiffness of 5-6 kPa, is enough to see an increase in traction forces (163). Therefore, the results seen here might be due to a poor attachment of cells on 9 kPa gels. If cells fail to attach and form enough FAs to anchor the surface, they will not be capable of generating enough forces (164–166).

3T3-L1 cells are less mechanoresponsive than MSCs.

When the mechanical response of 3T3-L1 cells was studied, they seemed to be less mechanoresponsive to matrix stiffness on PAA gels. There were no significant differences in FAs formation among the different stiffness evaluated. However, these values decreased when 3T3-L1 cells were treated with blebbistatin, what confirms that cells were responsive to external stimuli. The only parameter that did not change with blebbistatin was cell area. Either 3T3-L1 and MSCs cells on non-degradable surfaces presented similar areas when blebbistatin was added into the media. This could be because of the exposure time of cell to blebbistatin was not long enough to detach cells completely. Nonetheless, there may have been a cell area reorganisation to re-distribute forces and the characteristic branched aspect after treatment with blebbistatin was observed.

The FAs assembly in 3T3-L1 did not show significant differences were found. These results could be due to the method of analysis: analysis particles in ImageJ. Unfortunately, this method does not discriminate between the vinculin gathered in the FAs and the one dispersed in the cytoplasm. If there was a big accumulation of the protein in the cytoplasm, the method of analysis tended to cluster multiple points of the staining that were in proximity together, counting them as a unique FAs.

Another, observation that drives to think that 3T3-L1 cells might be less mechanosensitive than the MSCs is YAP nuclear translocation. 3T3-L1 showed lower values of YAP n/c ratios than MSCs and the average translocation was similar in all the stiffnesses. Nonetheless, even in this cell type, YAP was not sensitive to blebbistatin. After treating the MSCs and 3T3-L1 cells with the drug, similar translocation ratios than on non-treated cells were observed.

It is also important to have into consideration the difference in the integrins expression. MSCs express high amount of integrin α5β1 which bind to FN. They also express integrins that can bind to collagen such as α1β1 (167,168). On the other hand, 3T3-L1 express mainly the FN-binding integrin α5β1 only when they are in the phase of pre-adipocytes. During their differentiation into adipocytes α5β1 expression decreases in favour of the laminin-binding integrin α6β1 (169). The low response of 3T3-L1 cells to FN-coated surfaces in comparison to MSCs indicate their expression of α5β1 integrin might be lower. Also, they might have started to differentiate into adipocytes increases the integrin expression of α6β1.

These findings suggest that not all cells are equally mechanoresponsive and their response change depending on the matrix nature. However, all of them need to attach to the surface to generate forces and exert them through FAs (Figure 3-23). To assemble these FAs and exert forces, cells need to contract and generate intracellular tension. This exchange of forces triggers the nuclear translocation of YAP, which remains nuclear even when cell contractility is inhibited.

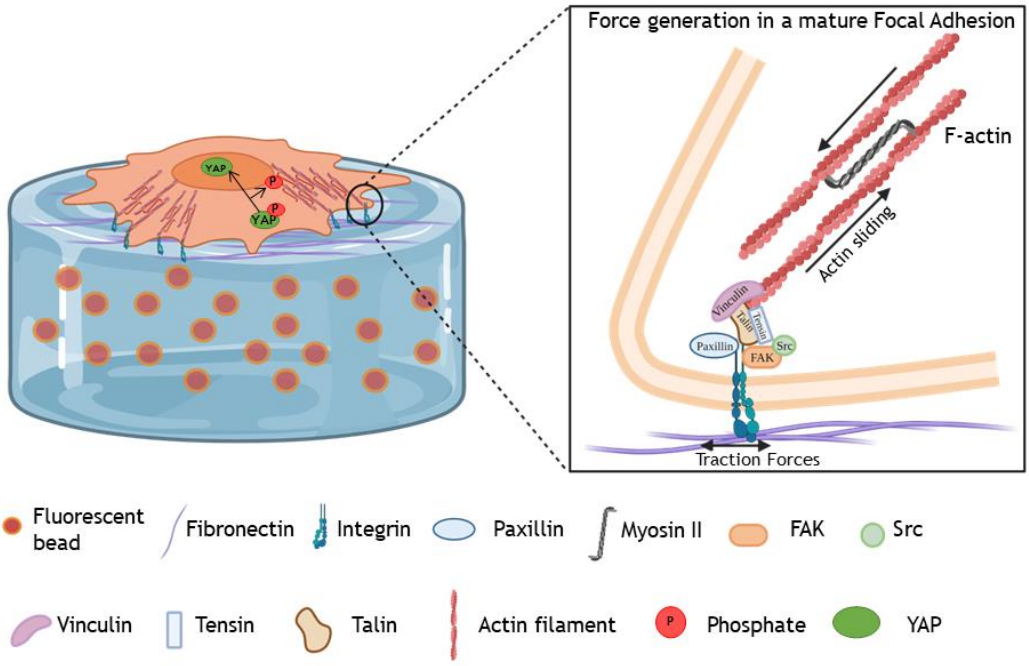

***Figure 3-23. Force generation in focal adhesions**. Hydrogels used in TFM are functionalised with a protein from the natural ECM to which cells can attach e.g.FN. Cells attach to the convenient domain in the protein through integrins. Once the cell detects the FNand attach to it, focal adhesions are formed. These multiprotein complexes are the physical connection of the cell with the ECM and, hence, through which forces are going to be exerted. When integrins binds to theFN, intracellular proteins, e.g. paxillin, tension, talin, vinculin; are gathered and they connect the integrins with the actin cytoskeleton. This complex triggers the molecular pathway to actin filaments contraction and force exertion. When cells exert these forces, they pull leading to substrate deformation and traction of the fluorescent beads embedded in the hydrogel.*

The table 3-3 summarises the experiments and the main results observed in chapter 3.

Table 3-3. Summary of experiments and results in chapter 3

EXPERIMENT	CELL TYPE	SURFACE	RESULT
Vinculin immunostaining	MSCs	Degradable full-length	MSCs spread more on stiffer surfaces where bigger FAs were found. When

		FN-PEG hydrogels	cell contractility is inhibited MSCs did not form mature FAs.
	3T3-L1	PAA hydrogels functionalised with FN	No significant differences in cell area and FAs formation were found among the different stiffnesses. When cell contractility was inhibited, FAs formation decreased.
YAP immunostaining	MSCs	Degradable full-length FN-PEG hydrogels	YAP tended to translocate to the nucleus on stiffer surfaces. When cell contractility was inhibited, YAP kept translocating into the nucleus.
		Non-degradable full-length FN-PEG hydrogels	There was a peak in YAP nuclear translocation on 8 kPa surfaces. YAP kept translocation into the nucleus when cell contractility was inhibited. There was only a decrease on 8 kPa surfaces.
		PAA hydrogels functionalised with FN	No significant differences in YAP nuclear translocation were found among the different stiffnesses.
	3T3-L1	PAA hydrogels functionalised with FN	No significant differences in YAP nuclear translocation were found among the different stiffnesses. When cell contractility is inhibited, YAP kept translocating into the nucleus.
TFM	L929	Degradable full-length FN-PEG hydrogels	L929 cells exerted higher forces on 8kPa degradable surfaces compared with non-degradable surfaces. In both cases. In both cases when cell contractility was inhibited the traction stress decreased.
		Non-degradable full-length	

		FN-PEG hydrogels	
	MSCs	Degradable full-length FN-PEG hydrogels	MSCs exerted higher forces on stiffer surfaces. When cell contractility was inhibited, the traction stress registered decreased on all the surfaces.

CHAPTER 4 : UNDERSTANDING CELL METABOLISM IN RELATION TO SURFACE STIFFNESS

4.1. INTRODUCTION

Metabolomics is the study of small biological molecules, known as metabolites, that form part of a biological system. Measuring the levels of metabolites provides information about what biochemical pathways might be triggered and how the cells are responding to their surroundings (170).

To trigger the mechanical cues and generate forces during ECM-cell interactions cells require energy obtained by the metabolism of nutrients. This energy is also necessary for the biosynthesis of macromolecules (e.g. proteins, lipids, nucleic acids, carbohydrates) that can be stored and works as an energy reservoir. In situations of nutrients deprivation, these macromolecules can be catabolised to supply energy to cellular functions (171). For instance, fatty acids are accumulated in lipid droplets when cells have access to nutrients (e.g. amino acids). In a situation of cell starvation, these lipid droplets go to the mitochondria where the ß-oxidation of the fatty acids takes place. The resultant acetyl-CoA is metabolised through OXPHOS to produce ATP. This change in metabolism during starvation is regulated by mechanistic target rapamycin complex 1 (mTORC1), a sensor of nutrient levels, and AMPK, an energy sensor. When mTOR is activated in presence of nutrients, AMPK is inactive which means that there are high levels of ATP. On the other hand, AMPK activates when there is a lack of nutrients and low levels of ATP, inhibiting mTORC1. Autophagy is upregulated liberating the lipid droplets to the cytoplasm and enhancing their migration to the mitochondria membrane. The lipid droplets go undergo lipolysis yielding fatty acids which enter the mitochondria to be oxidated (172,173). Interestingly, in another study made on mammary epithelial cells, it was observed that under nutrient limitations these cells upregulate and internalize ß4-integrin together with the ECM protein laminin. Once inside the cell, laminin is hydrolysed into amino acids which can be used to obtain energy. Restored the nutrient levels, mTOR is activated again and autophagy is inhibited (174). These studies suggest a link between integrin activity

and nutrients metabolism, being able to regulate one another to maintain cell homeostasis.

Even though cellular mechanics and metabolism are not independent of one another, the connection between them remains unknown. In the previous chapter, different aspects of cellular mechanics were covered. Following up on this, cellular metabolic activity was studied in MSCs and 3T3-L1 cells seeded on full-length FN-PEG, PAA hydrogels and Matrigel. Firstly, it was performed a general analysis of the metabolites profile of MSCs seeded on full-length FN-PEG hydrogels. Later the cellular respiration rate of MSCs and 3T3-L1 cells on PAA hydrogels was investigated using Seahorse. ATP accumulation of 3T3-L1 cells on PAA hydrogels and Matrigel were quantified using ATP assays. Ratiometric sensors were introduced to study the metabolism of different molecules in real time in living cells. These biosensors emit a fluorescence signal when a target molecule expressed within the cells binds to them. This work has shown that cells are sensitive to every stimulus in their environment. They adapt creating a mechanical and metabolic response.

To extend the study to more than one cell type, the metabolic response of MSCs and 3T3-L1 was compared. Furthermore, cells need to be transfected to incorporate the ratiometric sensors. Due to the difficulty to transfect primary cells (e.g. MSCs), 3T3-L1 cells were selected as they are easy to transfect and can differentiate into adipocytes, following a MSCs-like behaviour. The respiration rate and ATP levels were analysed in both types of cells to see if similar responses are generated and hence, the response observed in one type can be extrapolated to the other.

3T3-L1 cells are a murine line generated to study adipogenesis. They are fibroblasts that can acquire an adipocyte phenotype under suitable conditions (175,176). Their adipogenesis differentiation has been compared with the MSCs. For instance, it has been demonstrated that the expression of the receptor leukocyte common antigen related (LAR) decreases adipogenesis in both cell types. LAR decrease the tyrosine phosphorylation in the insulin receptor which leads to a downregulation of the Akt pathway and hence the transcriptional factor PPARγ, one of the main markers in adipogenesis (177). In another study, it was

observed the effect of surface charge on the cellular uptake and cytotoxicity of mesoporous silica nanoparticles. MSCs presented a higher uptake of charged particles. However, the viability, proliferation and differentiation of both cell types were not affected by the nanoparticles. Furthermore, they demonstrated that both cell types require of actin polymerisation for the endocytosis of the nanoparticles (178). Based on these experiments, 3T3-L1 cells seemed a proper cell line to compare with MSCs.

4.2. GENERAL METABOLOMICS

To understand the metabolic activity of MSCs, the level of metabolites was measured after 24 hours and 7 days of culture. These time points were selected to cover the metabolome profile in early stages of proliferation and differentiation. Both time points were compared with the basal level of metabolites before seeding (time 0), this provided a baseline measurement to compare the effects of the different culture conditions on the metabolic pathways. MSCs at time 0 were collected from the cell suspension which were kept at 37°C upon metabolites extraction. Between harvesting the cells from the flask to extracting the metabolites, MSCs were in suspension no more than 1 h. From all the metabolites obtained, six main metabolic pathways were selected to study the cellular metabolic activity: TCA cycle, glycolysis, glutathione metabolism, urea cycle, nucleotides and fatty acids biosynthesis. MSCs were seeded on glass and on FN-PEG hydrogels of different stiffnesses. The media was changed every two days to maintain the levels of nutrients.

Firstly, the level of metabolites after 24 hours, 7 days and time 0 were compared (Figure 4-1A). Generally, in all the surface stiffnesses, MSCs accumulated more metabolites after 24 hours of seeding than after 7 days. On both occasions, MSCs had similar levels of metabolites on glass and time 0.

Comparing 24 hours versus time 0, MSCs presented higher levels of metabolites on stiffer hydrogels compared with their basal activity at time 0. On glass, the highest activity was in the biosynthesis of fatty acids (Figure 4-1B).

After 7 days (Figure 4-1C), the activity registered was the opposite. On gels, MSCs had higher levels of metabolites on soft surfaces compared with 8 or 26 kPa stiffness. MSCs seeded on glass had a similar level of metabolites to time 0. It was especially apparent in the levels of glutathione observed.

At time 0, MSCs presented the highest levels of 2-oxoglutarate in comparison with the other time points.

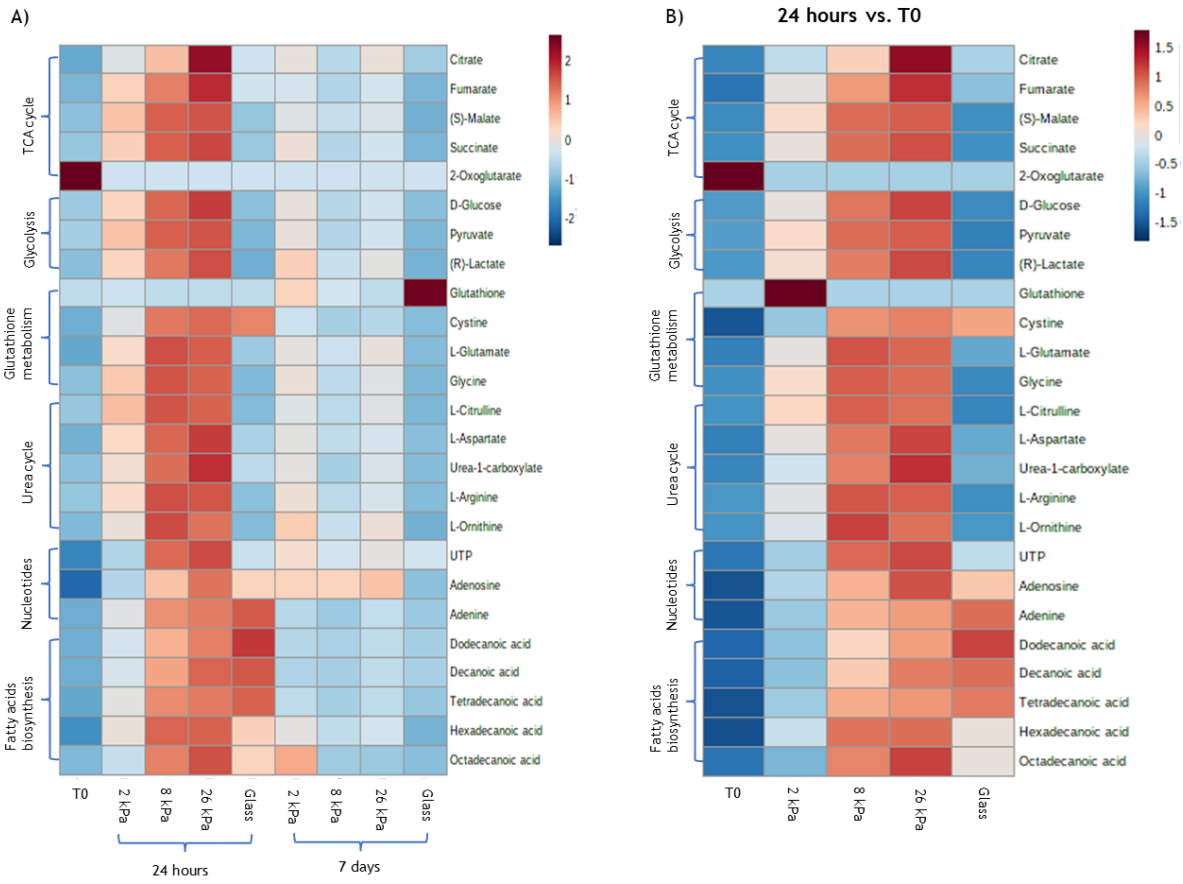

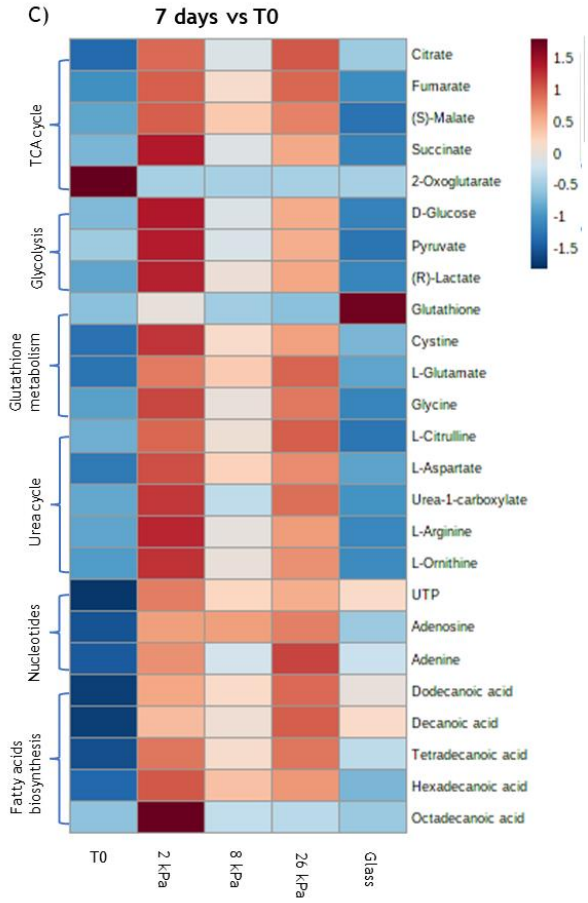

Figure 4-1. The metabolites profile of MSCs metabolites profile changes depending on surface stiffness*. The levels of metabolites were normalised by protein values measured with nanodrop. The absolute abundance of metabolites was detected by liquid chromatography mass spectrometry (LC-MS) using a ZIC-pHILIC column. Metabolites were extracted from n≥300000. Results come from one experiment. All the comparisons were done taking as a reference the metabolites levels at time 0. This will indicate the starting point and any value above these ones appears in red and below appears in blue. A) Level of metabolites of MSCs at time 0, 24h and 7 days. Compared with the levels of metabolites MSCs had just before seeding them (time 0, T0), MSCs produced and accumulate more metabolites after 24 hours than 7 days. B) Level of metabolites of MSCs seeded on different surfaces after 24 hours, compared with time 0. The level of metabolites increased with hydrogel stiffness. On glass, MSCs accumulated more fatty acids than at time 0. C) Level of metabolites after 7 days compared with time 0. The highest level of metabolites was on soft hydrogels. On glass, there was similar levels of metabolites to time 0.*

4.3. CELLS RESPIRATION RATE INCREASES WITH SURFACE STIFFNESS

Seahorse assay was used to study oxygen consumption rate in MSCs and 3T3-L1 cells. This test is used to assess the mitochondrial functionality by the manipulation of the electron transport chain (ETC) at different levels. It provides information about the basal respiration, ATP-link respiration, energy-accumulation capacity, and non-mitochondrial respiration, being possible to find any mitochondrial dysfunction (179,180). Different drugs were injected at different times (Table 4-1), disrupting a specific part of the ETC enabling reading to be taken at different stages of the ETC (Figure 4-2A,B).

Table 4-1. Drugs used during Seahorse assay and their mechanism of action

Drug	**Action**	**ETC's part affected**
Oligomycin	ATP synthesis inhibition by blocking the proton channel	Complex V
FCCP	Transports protons across the mitochondrial inner membrane	Membrane's proton gradient disrupted
Rotenone	Inhibition of electron transfer from iron-sulfur centres in complex I to ubiquinone	Complex I
Antimycin A	Inhibition of electron transport at complex III and reactive oxygen species (ROS) induction	Complex III

After normalising the data with the basal respiration, the oxygen consumption rate of cells seeded directly on tissue culture plates showed that MSCs had a higher respiration rate than 3T3-L1 (Figure 4-2D,F).

This technique uses specific plates with probes at the bottom of the well. The complexity of the plates made the polymerisation of FN-PEG or PAA gels challenging. For this reason, to understand how cells respond to surface stiffness, Matrigel was used. A higher respiration rate on stiff surfaces (E ≈ 1GPa) was observed compared with soft (E ≈ 250 Pa) for both cell types (Figure 4-2G). In this occasion 3T3-L1 cells showed a higher respiration rate than MSCs even after the normalisation with the basal respiration rate (Figure 4-2H).

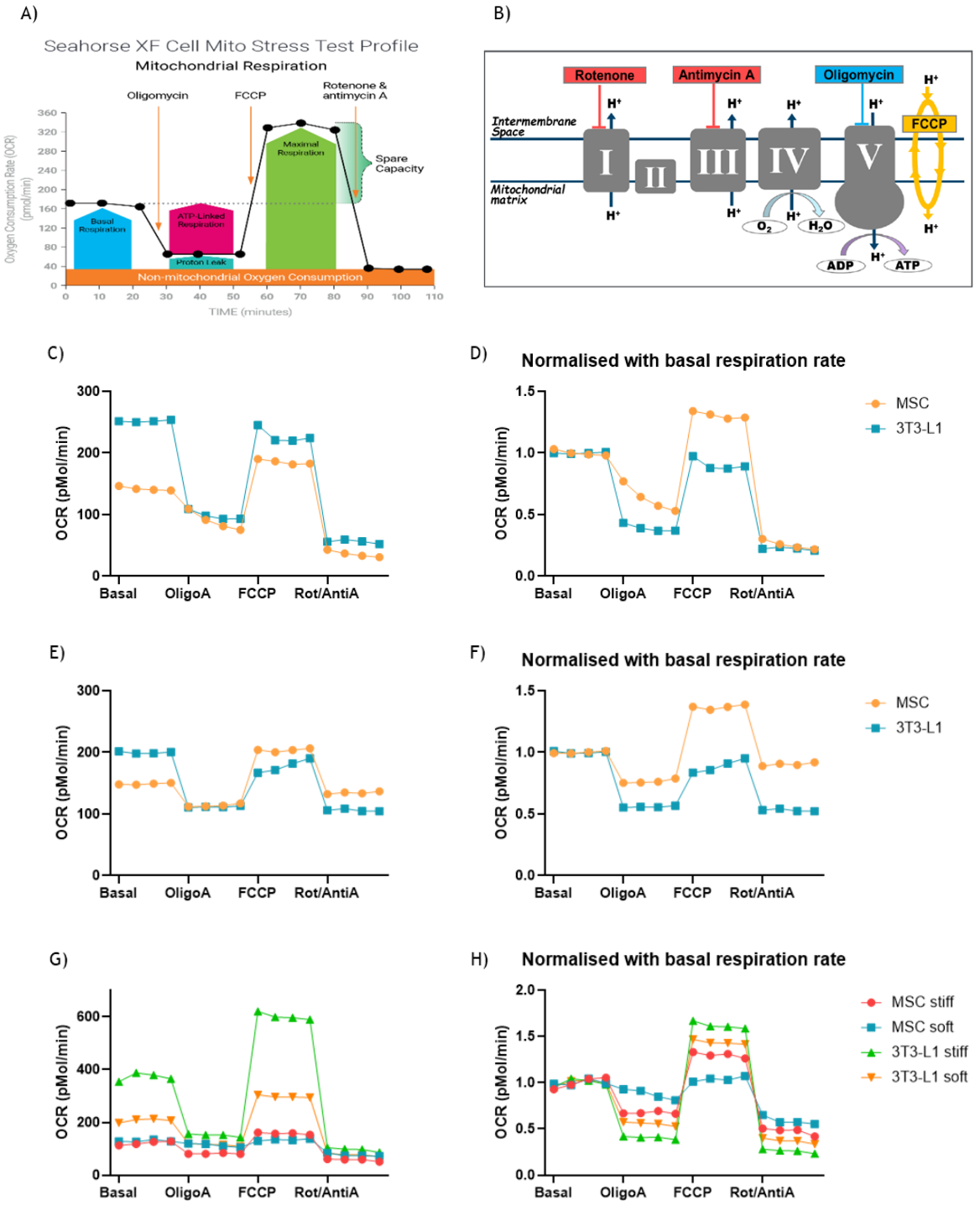

Figure 4-2. MSCs and 3T3-L1 cells oxygen consumption rate changes depending on surface stiffness and composition. *A) Agilent Seahorse XF Cell Mito Stress Test profile, showing the key parameters of mitochondrial function. B) Agilent Seahorse XF Cell Mito Stress Test modulators of the ETC. These images have been taken from the Agilent Seahorse XF Cell Mito Stress Test kit's user guide. C) and (E) show the oxygen consumption rate profile of MSCs (yellow line) and 3T3-L1 (blue line). In both cases 3T3-L1 cells showed higher basal respiration*

rate than MSCs. Each figure corresponds to two different experiments. In these two experiments MSCs and 3T3-L1 cells were seeded directly on TCP. D) and (F) show the oxygen consumption rate profile of MSCs (yellow line) and 3T3-L1 (blue line) normalised by cell basal respiratory rate obtained in (C) and (E) respectively. G) Oxygen consumption rate profile of MSCs and 3T3-L1 cells seeded on soft (E≈250 Pa) (MSCs in blue, 3T3-L1 in yellow) and stiff (E≈1GPa) (MSC in pink, 3T3-L1 in green) Matrigel coatings. H) Oxygen consumption rate profile normalised by basal respiration rate showed in (G) of MSCs and 3T3-L1 cells seeded on soft (MSCs in blue, 3T3-L1 in yellow) and stiff (MSC in pink, 3T3-L1 in green) Matrigel coatings. The raw results were normalised to basal respiration to be able to see differences in further stages considering that the cells start from the same respiration rate.

4.4. FIBROBLASTS 3T3-L1 ACCUMULATE MORE ATP ON SOFT SURFACES RICH IN COLLAGEN

For 3T3-L1, the level of ATP on hydrogels of different nature and stiffness were measured (Figure 4-3). Firstly, we performed a fluorometric ATP assay on 3T3-L1 cells seeded on soft (E ≈ 250 Pa) and stiff (E ≈ 1 GPa) Matrigel surfaces (Figure 4-3A,B). A trend in the amount of ATP was visible, showing higher levels on soft surfaces (Figure 4-3B).

Secondly, using a luminescence ATP kit, the concentration of ATP in 3T3-L1 cells on glass and on 3, 9 and 35 kPa PAA hydrogels functionalised with FN was analysed (Figure 4-3C,D). The lowest ATP concentration was found on 3 kPa surfaces and the highest on 9 kPa (Figure 4-3D). 3T3-L1 cells were treated with 10 μM blebbistatin, a myosin inhibitor, for one hour. The levels of ATP found were similar to non-treated cells (Figure 4-3D).

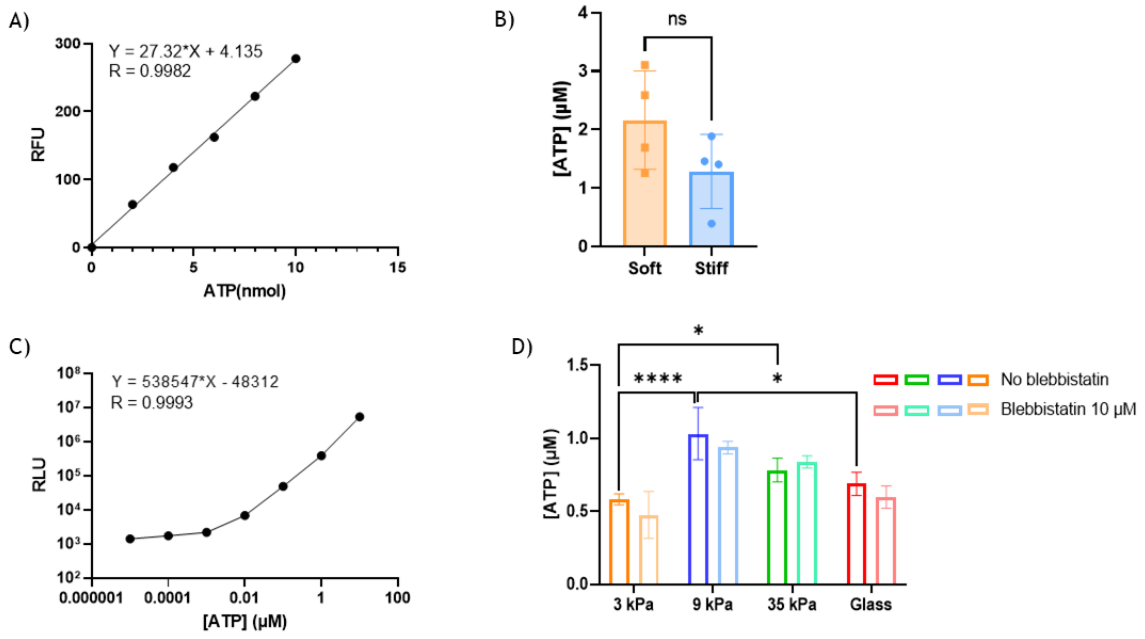

Figure 4-3. 3T3-L1 cells ATP accumulation is related with surface stiffness and composition. *A) Fluorometric ATP assay standard curve and trendline equation. B) ATP concentration of 3T3-L1 cells on soft and stiff Matrigel surfaces. 3T3-L1 cells accumulate more ATP on soft surfaces when their composition in collagen based as it is the case of Matrigel. C) Luminescence ATP assay standard curve and trendline equation. D) ATP concentration of 3T3-L1 cells seeded on 3, 9 and 36 kPa PAA hydrogels coated with FN. 3T3-L1 accumulate less ATP on soft surfaces FN-based compare with stiffer ones. Graphs shown mean ±SD of n≤10, differences were analysed via non-parametric ANOVA and Mann-Whitney test. NS p>0.9999, * p<0.03, **** p<0.0001.*

4.5. RATIOMETRIC SENSORS

Ratiometric sensors were incorporated in 3T3-L1 cells to study cellular metabolomic activity in real time. These biosensors are a useful tool to visualise how a protein of interest moves in the cell under different environments. Cells are required to be transfected with plasmids carrying the specific biosensor. Due to the difficulty of transfecting primary cells, these experiments were performed using 3T3-L1 cells. The signal of the biosensors was followed using different media conditions on 3T3-L1 cells culture on tissue culture plates (TCP) or Matrigel hydrogels (0.2 kPa).

4.5.1. PercevalHR and pHRed

PercevalHR is a biosensor used to monitor the intracellular ATP:ADP ratio in living cells. It provides important information about the energy status of the cells. The sensor has two excitation peaks: ~420 and ~500 nm. When ATP binds to the sensor there is more fluorescence signal at ~500 nm, and when it is bound to ADP, there is more signal at ~420 nm (181). The fluorescence emission was collected at 482 nm (for ATP) and 445 nm (for ADP).

The problem with this biosensor is that it is sensitive to the pH. Variations in the pH can modify PercevalHR signal yielding a false result. Therefore, it is necessary to correct the pH influence on the biosensor. 3T3-L1 cells were transfected simultaneously with PercevalHR and pHRed, a biosensor that gives information about the intracellular pH. It has dual excitation peaks at 440 and 585 nm (182). The fluorescence emission was collected at 578 nm and 445 nm.

The ATP:ADP ratio is interpreted by F_{482}/F_{445}. To analyse the influence of the pH, the signal of pHRed biosensor is represented as F_{578}/F_{445}. The signal of Perceval did not show any marked changes when it was stimulated with the addition of different molecules to the media. Three experiments were carried out at three different days. In the first experiment, different media conditions were used to compare with the other two.

The conditions used in each experiment are described in Table 4-2.

Table 4-2. Media conditions in PercevalHR and pHRed biosensors

Common conditions in the three experiments		
Condition	***Description***	***Objective***
Ctrl	3T3-L1 cells on TCP with regular culture media (High glucose DMEM + 1% sodium pyruvate + 2mM glutamine + 20% FBS + 1%Penicillin/Streptomycin)	Observe cellular response on stiff surfaces
0.2 kPa	3T3-L1 cells on Matrigel 0.2 kPa with regular media	Observe cellular response on soft surfaces

Glucose	DMEM + high glucose	Upregulate OXPHOS and ATP production
Conditions in experiment 1		
2-DG	2-Deoxyglucose is a modified glucose molecule: the 2-hydroxyl group has been replaced by hydrogen. It cannot be metabolised and blocks glycolysis (183)	ATP depletion
Sodium Pyruvate	DMEM + Sodium pyruvate	Maintain OXPHOS and ATP production
Conditions in experiment 2 and 3		
0.2 kPa + Glucose	3T3-L1 cells on soft Matrigel surfaces treated with DMEM + high glucose	Lower ATP/ADP ratio ATP levels with cells on TCP supplement with glucose
L-Glu	DMEM + L-Glu	Compare ATP production with glucose
DMEM	No supplements	Decrease of the ratio ATP/ADP

No consistency was observed in the experiments performed. In experiment 1 (Figure 4-4A,D), no change in PercevalHR signal was observed among conditions (Figure 4-4A). However, there was a change in intracellular pH (Figure 4-4D). In the next two experiments, the intracellular pH varied differently with the same condition (Figure 4-4E,F). PercevalHR signal did not show any marked changes. In experiment 2 (Figure 4-4B) there appears to be a slight decrease in ATP:ADP ratio when 3T3-L1 cells have been supplemented with glucose, either on soft or on tissue culture plate (TCP), and L-Glu. In experiment 3 (Figure 4-4C), PercevalHR signal remain constant, except for the presence of L-Glu where a lower concentration of ATP was observed.

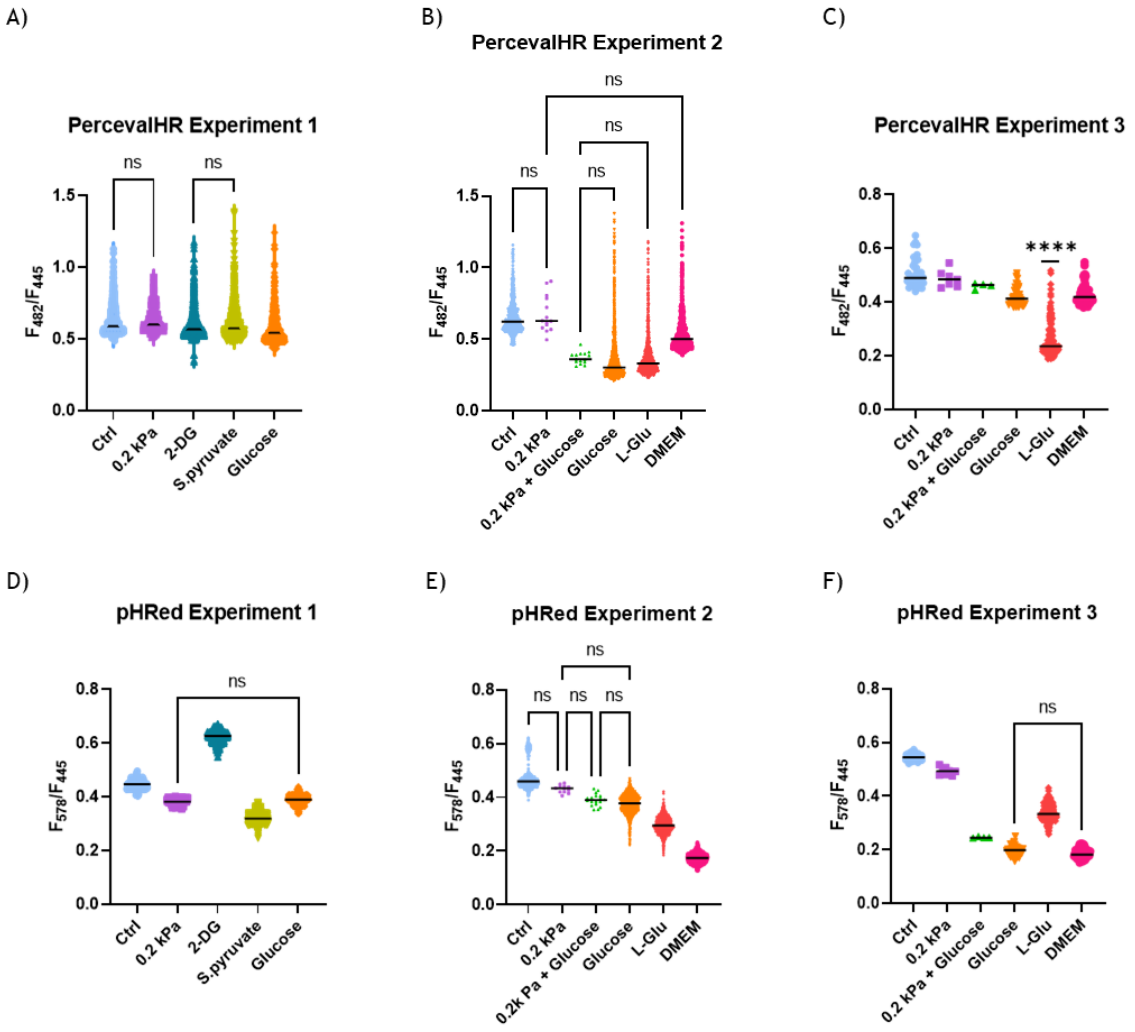

Figure 4-4. Perceval signal does not show any marked changes among conditions. Intracellular pH varies with media supplements. *3T3-L1 cells were seeded directly on TCP or on Matrigel gels which had a stiffness around 0.2 kPa (indicated in the graphs with stiffness value). A) PercevalHR signal ratio for experiment 1. Biosensor signal was similar in all the conditions. B) PercevalHR in experiment 2 shows a trend. There was a decrease in the signal when glucose (orange) was incorporated. The signal was recovered with DMEM (pink). C) PercevalHR signal ratio in experiment 3. There was a decrease in the signal when L-Glu (red) was incorporated. D) pHRed signal ratio in experiment 1. There was an increase in pHRed signal when 2-DG (dark blue) was incorporated. This indicated an acidification of the media. E) pHRed signal ratio in experiment 2. There is an opposite trend to Perceval. As control (light blue) and soft surfaces (purple) remain similar, there was an increase in the signal when glucose (green and orange) was incorporated and a decrease in the presence of L-Glu (red) and*

*DMEM (pink). F) pHRed signal ratio in experiment 3. There was an increase in media pH with glucose, either on soft (green) and stiff surfaces (orange), and DMEM, as biosensor signal decrease. L-Glu (red) increase media acidity. Graphs shown mean ±SD of n≥10, differences were analysed via non-parametric ANOVA. NS p>0.9999, * p<0.02, **** p<0.0001.*

To understand if these results were a consequence of PercevalHR sensitivity to pH, the signal at 482 nm due to ATP binding to PercevalHR was normalised with the signal of pHRed at 578 nm (Figure 4-5). In this case it was possible to see the fluctuation of ATP cellular accumulation in the different media conditions. In the first experiment there was a decrease in ATP when 2-DG is incorporated into the media. However, the ATP production increases with sodium pyruvate and glucose (Figure 4-5A).

In experiment 2, 3T3-L1 cells showed higher amount of ATP when the media was supplemented with glucose on soft surfaces and with L-Glu (Figure 4-5B). On the contrary, under the same conditions, in experiment 3 the ATP signal increased when the media was supplemented with glucose on TCP and when 3T3-L1 cells were in DMEM without extra supplements (Figure 4-5C)

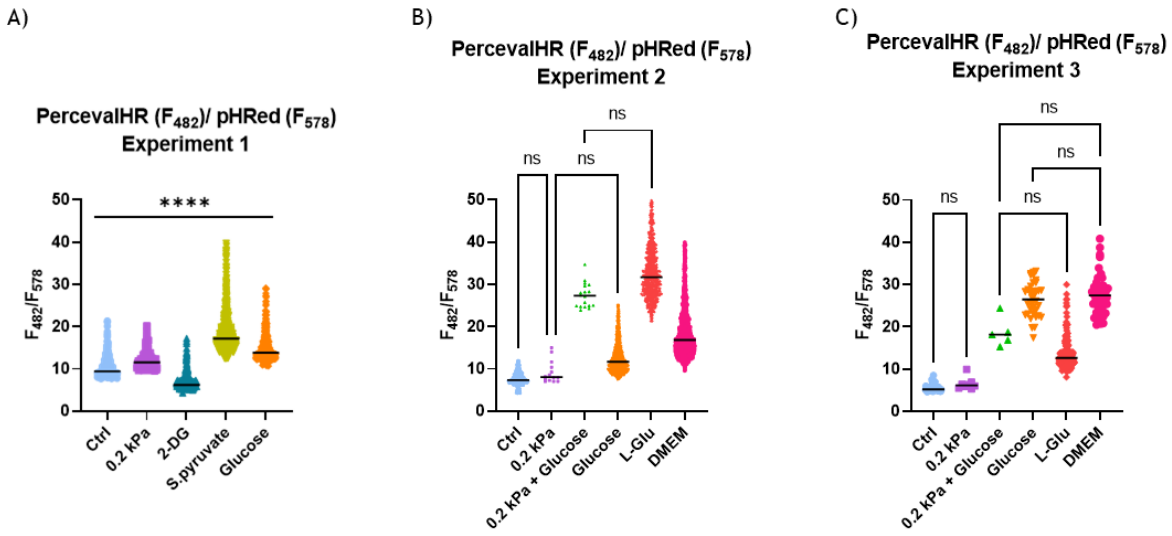

Figure 4-5. Depending on media composition, cellular ATP/ADP ratio change. *A) Experiment 1. Adding 2-DG minutes (dark blue) decreased biosensor signal. Sodium pyruvate (light brown) and glucose (orange) increase ATP/ADP ratio. B) Experiment 2. No significant differences were found in 3T3-L1 cells seeded on*

*soft surfaces (purple) or directly on the TCP (light blue). Higher values of ATP/ADP were found in cells seeded on soft surfaces with glucose addition (green) and cells on TCP with a L-Glu (red) supplement. 3) Experiment 3. The highest signal of the biosensors was found in 3T3-L1 cells supplemented with glucose (orange) and in DMEM (pink) without any other supplement. Graph shown mean ±SD of n≥10, differences were analysed via non-parametric ANOVA. NS p>0.9999, **** p<0.0001.*

4.5.2. ExRai AMPKAR

ExRai AMPKAR has been shown to be an advanced tool to study AMPK activation. This biosensor is a single-fluorophore ratiometric reporter with high affinity for AMPK. It integrates a circularly permuted enhanced green fluorescent protein (cpEGFP) between an AMPK substrate domain and the phosphoamino acid-binding forkhead associated domain 1 (FHA1), both domains are essential for AMPK activity (184). AMPK activated under stress situations when the ratio AMP:ATP increases (184,185). When AMPK is active, it can bind to ExRai AMPKAR by sensing the FHA1 domain and phosphorylate the substrate sequence in the reporter. This leads to an increase in the fluorescence emission at 480 nm excitation and a decrease in the 400 nm one (184). As a negative control it was used the biosensor with the phosphorylation site mutated from a threonine to an alanine (ExRai AMPKAR T/A), this result in a biosensor with minimal response (184).

Two experiments with different media conditions were performed in 3T3-L1 cells to study AMPK activation under cellular stress environments (Figure 4-6). In the first experiment 3T3-L1 cells were treated with 4 different drugs: 2-DG, a modified glucose molecule that cannot go through glycolysis; compound C, an AMPK inhibitor, with 2-DG; AICAR, an analogue of adenosine monophosphate (AMP) which stimulates AMPK activity; and YM, a combination of the two cellular contractility inhibitor Y27632 and ML7 (Figure 4-6A,B). AMPK activity was increased when 3T3-L1 cells were treated with 2-DG and AICAR. However, when compound C was incorporated into the media, the enzyme activity decreased. Inhibition of cellular contractility with YM, also increased AMPK activity (Figure 4-6A). Mutant signal did not have big fluctuations (Figure 4-6B).

For the second experiment (Figure 4-6C,D), 3T3-L1 cells were not treated with YM. Instead, a new condition was incorporated to understand cellular response to surface stiffness: cells seeded on soft surfaces and treated with 2-DG. An increase in AMPK activity was observed with 2-DG regardless surface stiffness. As it was observed in the first experiment, when compound C is incorporated into the media AMPK activity decreased even though 2-DG was in the media. Enzyme activity increased with AICAR (Figure 4-6C). Mutant fluorescence also showed significant differences (Figure 4-6D).

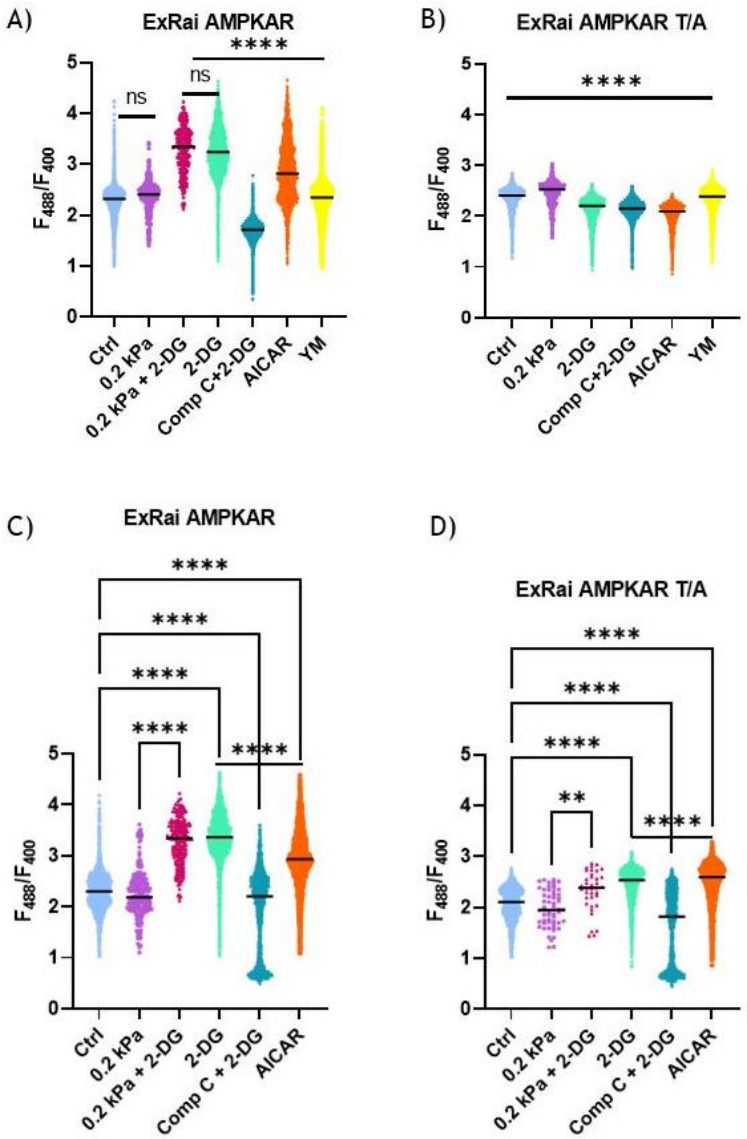

Figure 4-6. ExRai AMPKAR signal changed depending on AMPKAR activation. *A) ExRai AMPKAR signal ratio in the first experiment. There were no significant differences in AMPK activation in 3T3-L1 cells on control (light blue) and on soft*

*surfaces (purple). Compound C in combination with 2-DG (dark blue) leaded to a minimum activation of AMPKAR. AICAR (orange) and 2-DG alone (green) increased AMPKAR activity. Cell contractility inhibition with YM (yellow) showed similar activation than on control. B) ExRai AMPKAR T/A signal ratio in first experiment. Significant differences were obtained among conditions. C) ExRai AMPKAR signal ratio in the second experiment. There are no significant differences on soft (purple) or in control (light blue). AMPK activated with 2-DG (red and green). Compound C in combination with 2-DG (dark blue) decreased AMPK activity, while AICAR (orange) stimulated it. D) ExRai AMPKAR T/A signal ratio in the second experiment. No significant differences of AMPK activity were found among conditions. Graph shown mean ±SD of n≥10, differences were analysed via non-parametric ANOVA. NS p>0.07, ** p<0.002, **** p<0.0001. These results come from two different experiments.*

4.5.3. Peredox-mCherry

Peredox-mCherry biosensor was used to study the metabolism of NADH. The biosensor emits constantly red fluorescence. However, when NADH bind to the biosensor, green fluorescence increases. NAD+ union to the biosensor does not change the fluorescence emission (186).

Three different experiments were conducted to test NADH metabolism (Figure 4-7). The three experiments were performed after 24 hours of culture. For the first experiment (Figure 4-7A) 3T3-L1 cells were treated with 2-DG at different time points: few minutes before imaging and immediately before imaging. In both cases, 2-DG decreased intracellular NADH. However, the decrease was higher after few minutes of exposure to the drug. Supplementing the media with glucose and L-Glu increased NADH levels, as it did lactic acid. Surfaces stiffness did not seem to have an effect in NADH levels.

Next two experiments were done at different time points, but with the same conditions, to see the reproducibility of the experiment. In the second experiment (Figure 4-7B), significant differences were found on 3T3-L1 cells seeded directly on TCP and on soft surfaces, where 3T3-L1 cells showed higher levels of NADH.

Lactic acid increased NADH amount, although, this increasement was again higher on soft surfaces compare with 3T3-L1 cells on TCP (control). Glucose produced similar NADH levels as in lactic acid. Supplementing the media with sodium pyruvate decreased NADH.

In the third experiment (Figure 4-7C) no significant differences were found on different stiffnesses. Similarly, to what we observed previously, glucose and lactic acid increased NADH, while sodium pyruvate decreased it. This time, the increase with lactic acid was higher in 3T3-L1 cells on TCP rather than on soft surfaces.

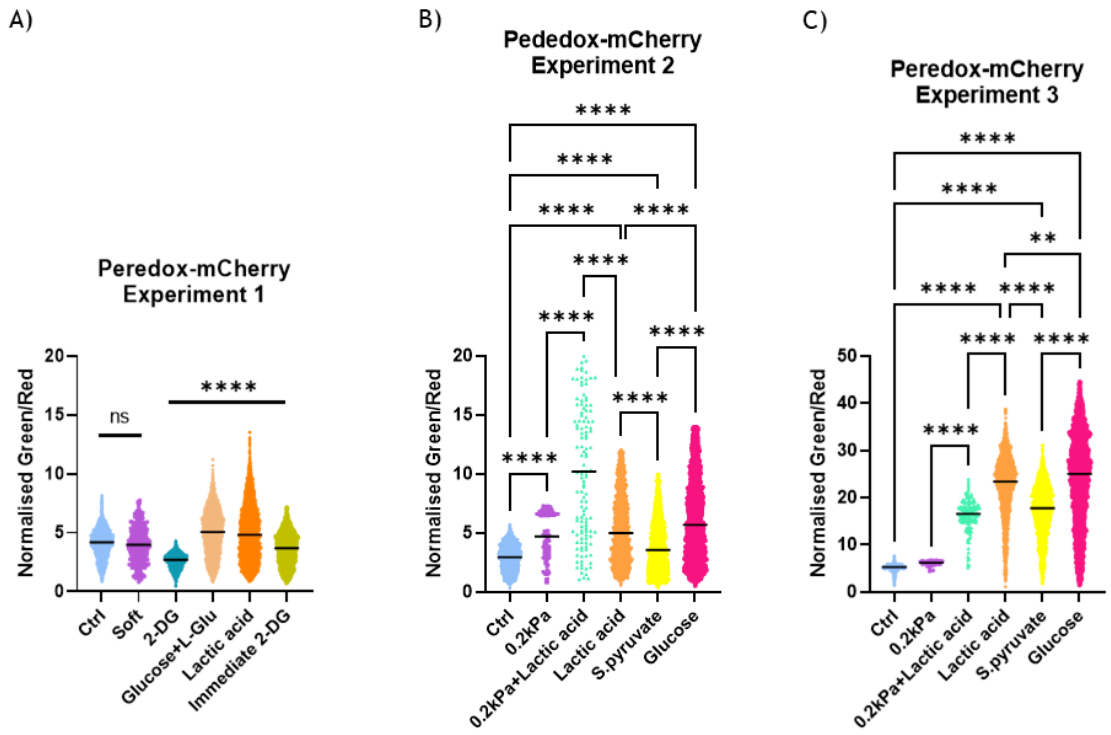

Figure 4-7. 3T3-L1 cells' NADH metabolism change depending what nutrients are in the media. *NADH bind to the biosensor increase green fluorescence, it does not influence in the red signal of mCherry. The data obtained from the protein expression (green signal) were normalised by the red fluorescence. The graphs show the ratio green/red florescence. A) Experiment 1. There are no differences in NADH levels on TCP (light blue) and on soft surfaces (purple). Treatment with 2-DG for a couple of minutes (dark blue) decrease the green signal of the sensor. Combination of glucose and L-Glu (light brown) and lactic acid (orange) increases NADH production (increase in green signal of the biosensor). B) Experiment 2. Lactic acid increases NADH levels more on soft*

*(green) than on TCP (orange). Sodium pyruvate (yellow) decrease the green signal (less NADH). Glucose (pink) increases the green signal (more NADH). C) Experiment 3. Higher values of the ratio green/red indicate a higher activation of Peredox compare with the other two experiments. The higher biosensor signal was found in media enriched with glucose (pink) and lactic acid (orange). In this occasion the increase with lactic acid on soft surfaces (green) was not as pronounce as in experiment 2. Sodium pyruvate (yellow) creates a decrease in green signal. Graph shown mean ±SD of n≥10, differences were analysed via non-parametric ANOVA. NS p>0.9999, **p<0.002, **** p<0.0001.*

4.5.4. iNap

iNap has been developed to study NADPH metabolism (187). It has two excitation peaks around 420 nm and 500 nm, and one emission peak 515 nm. Transfected cells are constantly emitting green fluorescence. When NADPH binds to the biosensor the fluorescence at 420 nm increases and the one around 500 nm (green) decreases. A mutant iNap form (iNapC) which cannot bind to the ligand was used as a control (187).

3T3-L1 Cells were cultured in different media conditions and on different stiffnesses. 3T3-L1 cells showed similar NADPH levels regardless of the surface stiffness (Figure 4-8). Lactic acid did not seem to cause any effect in NADPH metabolism, either on soft surfaces or on TCP (control). On the other hand, sodium pyruvate prompted NADPH generation, while treating 3T3-L1 cells with the combination of dehydroepiandrosterone and dimamide (DD) showed minimum values (Figure 4-8A). Dehydroepiandrosterone is a steroid hormone known for inhibiting G6PD activity and subsequently NADPH release in the reaction catalysed by this enzyme. Diamide is an oxidizing agent leading to the oxidation of NADPH. The combination of both creates a total depletion of NADPH, as it is consumed to reduce the oxidative effect of the diamide, and its synthesis is inhibited by dehydroepiandrosterone (188).

The signal of the biosensor might be influenced by the pH, to correct this fluctuation it is possible to normalise the results of iNapI by iNapC, which responds

similarly to pH, but NADPH cannot bind to it. In this case, the effect of the pH is eliminated.

After the correction, 3T3-L1 cells presented higher levels of NADPH when they were in regular culture media (high glucose DMEM, supplemented with sodium pyruvate, L-Glu, P/S and FBS) (Figure 4-8C). NADPH levels decreased when 3T3-L1 cells were seeded on soft surfaces. Treatment with DD showed minimum levels of NADPH. There are significant differences in 3T3-L1 cells seeded on different stiffnesses. Either in control media or in DMEM with lactic acid, 3T3-L1 cells showed lower levels of NADH on soft surfaces.

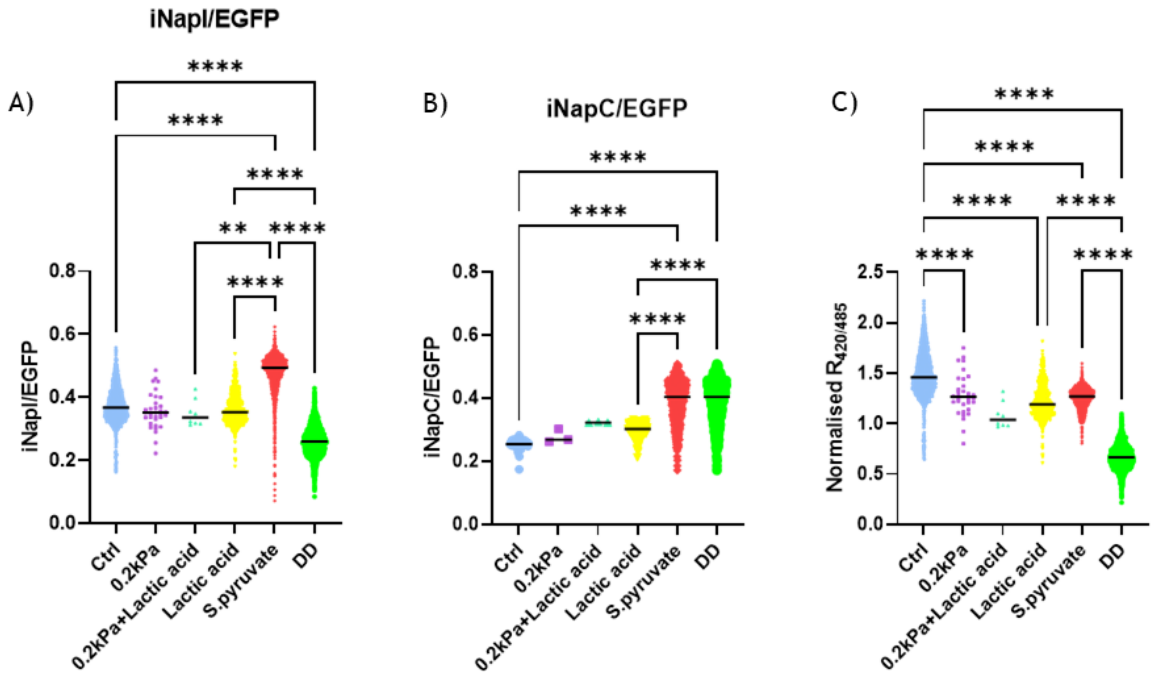

Figure 4-8. iNap is a good indicator for NADPH metabolism. *A) iNapI results. Lower signal of the biosensor was found when DD (green) was added into the media. Sodium pyruvate (red) increases biosensor signal. B) iNapC results. Increase of signal with sodium pyruvate (red) and DD (green). C) iNapI corrected by normalising to iNapC. The highest levels of NAPDH are in 3T3-L1 cells seeded on TCP (blue). The lowest levels were found in 3T3-L1 cells treated with DD (green). Lactic acid (yellow) and sodium pyruvate (red) increase slightly the amount of NADPH. Graph shown mean ±SD of n≥10, differences were analysed via non-parametric ANOVA. **** p<0.0001. these results come from two different experiments.*

4.6. DISCUSSION

MSCs accumulate higher levels of metabolites on stiff surfaces compare with soft. These metabolites will be used in later stages.

MSCs seeded on FN-PEG hydrogels of different stiffnesses showed higher accumulation of metabolites after 24 hours than 7 days compared with the basal levels at time 0. These results suggest that in early stages of culture MSCs are mainly interacting with the ECM and proliferating. Their metabolic activity is not particularly high; hence they are accumulating metabolites. After 7 days, the metabolic activity increases and MSCs start using these metabolites. In later stages there might be a balance between metabolites production and usage, a metabolite may be used or discarded before it can be accumulated.

After 24 hours of seeding there is a trend in relation with surface stiffness: MSCs accumulated more metabolites on stiffer surfaces than on soft. Following previous observations in this study, as MSCs are more mechanically and metabolically active on stiff surfaces, they generate metabolites at much higher speed than on soft surfaces. As in these early stages, MSCs are not using these metabolites, they accumulate higher levels on stiff surfaces. Nonetheless, previous studies have demonstrated that cells seeded on soft surfaces tend to accumulate more fatty acids and express more adipogenesis markers, compare with cells seeded on stiff matrices (106,189). However, in this occasion, the levels of fatty acids after 24 hours were higher on stiff surfaces compare with the softest ones. The difference in the results obtained in this study might be for the supplements used in the media, the different composition in the matrix (here FN-PEG hydrogels were used, while the other studies were performed on PAA hydrogels functionalised with FN), the different stiffness use for soft matrices (~0.5 kPa in previous studies, 2.5 kPa in this study) or, in this case, the donor from who the MSCs were obtained, was low responsive for adipogenesis.

The trend observed after 24 hours is lost after 7 days of culture. At this time point the highest levels of metabolites were found on soft surfaces. This observation supports the hypothesis that cells are less active on soft surfaces. As their

metabolic activity is lower, the metabolites produced are not consumed at the same rate than on stiffer surfaces, thereby they can accumulate over time. Furthermore, after 7 days it is important to have into consideration the proliferation rate. Cells proliferate faster on stiff surfaces compare with soft. When cells are confluent they start to enter in oxidative stress and they nutrients available in the media are much lower. Therefore, they need to use these metabolites to supply energy. On soft surfaces, the proliferation rate is lower, hence more nutrients are available in the media, and they do not need to use the metabolites generated. An indication of high proliferation on stiff surfaces could be the high levels of glutathione on glass. Glutathione is the main antioxidant factor towards reactive oxygen species (ROS) generated under oxidative stress in the cells (190). When cells are confluent, they compete for the available nutrients initiating oxidative stress. Consequentially, glutathione becomes upregulated to maintain cell homeostasis. In a study carried out in cancer cells from Waldenstrom Macroglobulinemia, it was observed that when glutathione synthesis was inhibiting using buthionine sulphoximine there was a significant reduction in cell proliferation and growth, as well as a downregulation in proinflammatory pathways (e.g. NFkB and MAPK-p38) (191). Therefore, glutathione also regulates cell proliferation and growth. Furthermore, the metabolites levels in glass were similar to T0. This could be another indication of high proliferation. MSCs need to use the metabolites generated to survive and their synthesis rate is not enough to accumulate them. Also, after 24hours the higher accumulation of nucleotides and fatty acids on glass than at T0, could be to get nutrients to survive. When MSCs are overconfluent the nutrients in the media start to be limited and cells need to use their own resources to supply this nutrients deprivation.

Compared with the other time points. The metabolite that was highly produced at time 0 was 2-oxoglutarato, an intermediate metabolite in TCA cycle. These cells were coming from the MSC suspension pool prior to cell seeding. When cells detach and lose the contact with the ECM there is a decrease in nutrients uptake (e.g. glucose) which leads to a downregulation of the subsequent pathways (e.g. glycolysis and TCA cycle). This leads to a reduce in NADPH levels and increase of ROS in mitochondria (192). In these circumstances, glutamine translocate to the cytoplasm where is converted into 2-oxoglutarate which enter the mitochondria

to produce NADPH to neutralise ROS (192–194). Also, it has been also observed an implication of 2-oxoglutarate in hypoxia. The 2-oxoglutarate dependent dioxygenases depend on oxygen, reduced iron and 2-oxogluratate to act. They act as an oxygen sensor and when the levels drop, they initiate the expression of hypoxia inducible factor 1 (HIF1) (195,196). Based on these observations, the high levels of 2-oxoglutarate at time 0 might indicate a situation of cellular stress and hypoxia.

MSCs and 3T3-L1 respiration rate increases with surface stiffness. The increase in the cellular activity requires ATP.

MSCs respiration rate was higher on stiffer surfaces compare with soft surfaces after 24 hours of culture. This observation correlates with the results obtained in the metabolomics analysis after 24 hours, where MSCs produced more metabolites on stiff surfaces. These results indicate that MSCs were more metabolically active on stiffer surfaces, as reflected by their increased respiration rate. Furthermore, MSCs seeded on soft matrices after 24 hours showed increasing levels of adenosine with surface stiffness (Figure 4-1), which is required for ATP synthesis. 3T3-L1 cells followed a similar pattern when they were seeded on different stiffness of Matrigel. Their respiration rate was higher on stiff surfaces compare with soft. Plus, the ATP concentration obtained in the ATP assay was higher on soft surfaces compare with stiff. The lower levels of ATP on stiff surfaces indicates that 3T3-L1 required this energy in the form of ATP to supply their metabolic activity. A previous study done by MA et al. demonstrated the implication of surface stiffness in mitochondria morphology and function. The mitochondria of human periodontal ligament stem cells (PDLSCs) on soft surfaces appeared short and round, followed by a mitochondrial dysfunction. Consequently, osteogenesis differentiation was disrupted. However, mitochondria were capable to recover their regular activity and osteogenesis was upregulated, when cells were transfer to a stiff surface (197).

The nature of the surface has a influence in cell response.

Cellular respiration rate is related with the nature of the ECM (197). 3T3-L1 cells seeded directly on the TCP had lower respiration rate than MSCs. However, when

the cells were seeded on stiff and soft surfaces of Matrigel we observed the opposite: 3T3-L1 shown higher respiration rates than MSCs. Matrigel is made of collagen, therefore the proteins presented in the ECM may have an influence in cellular respiration. Furthermore, in the case of 3T3-L1 cells ATP production was also influenced by the nature of the hydrogel. Higher concentration of ATP on soft surfaces was found when the surface was collagen based. However, on PAA hydrogels functionalised with FN, higher concentration of ATP was found on stiffer surfaces, especially on medium rigidity (9 kPa). Moreover, the ATP concentration measured on the FN based surfaces was lower than on collagen, what might indicate that 3T3-L1 cells are more receptive to collagen and their metabolic activity is promoted on these surfaces. Indeed, 3T3-L1 are collagen dependent for their differentiation into adipocytes. It has been studied that the inhibition of the receptor GPR56 which bind to collagen type III reduces adipogenesis in 3T3-L1, as well as cell attachment and proliferation (198). Also, 3T3-L1 remodel ECM secreting and exerting collagen (199). Therefore, culturing 3T3-L1 on Matrigel is likely to impact on cell behaviour. Hereby, these results have shown that cellular response seems to be influenced by matrix stiffness and composition. However, if cells are more sensitive to one or another is difficult to tell. In a study made in mammary epithelium, it was observed that keeping the ECM composition constant and increasing the stiffness induced malignant phenotypes. Conversely, changing the matrix composition by decreasing the density of cell-adhesion ligands available decreased malignancy development (200). Also, melanoma cells have shown to be responsive to an increase in matrix stiffness only when fibronectin was present, whereas in a collagen-based matrix they did not respond to surface stiffness (201). Nonetheless, the cellular response to matrix stiffness and composition also depends on the matrix receptors expressed (e.g. integrins, filamin A, talin) (49,200,201). Filamin A is an actin-binding protein implicated in cell adhesion and migration. The melanoma cells response described above was in the absence of filamin A expression. On the other hand, when a melanoma cell line overexpressing filamin A was seeded in the same surfaces, they change their adherent area either on collagen and fibronectin coated surface with an increasing stiffness (201).

ATP levels in 3T3-L1 cells are kept constant after contractility inhibition.

It was interesting to observe that ATP production is not dependent of cell contractility inhibition with blebbistatin. Blebbistatin inhibits myosin II-ATPase, ATP hydrolysis slows down and as a consequence, cells cannot contract. As explained in previous chapters, cell contractility plays an important role in cellular behaviour. When cell contractility is inhibited, cells cannot exert enough forces and the FAs decrease. Therefore, ATP is not going to be consumed to form the actin cytoskeleton and generate forces. The ATP synthesized might be consume at a lower rate, being accumulated for longer time. These results correlate with a study carried out by Xie et al. where they measured the ATP levels in MSCs seeded on 20 kPa PAA gels functionalised with collagen I. After 3 hours of culture, cell contractility was inhibited with blebbistatin and they observed that ATP levels were not affected, showing similar levels than cells without the treatment. Interestingly, inhibiting cell contractility with blebbistatin after 10 and 20 hours of culture, the levels of ATP started to increase. This indicates that ATP is mainly consume at early stages of cell spreading to create an organised actin cytoskeleton and generate tension that can be maintain in later time points (202). A Seahorse assay should be done to confirm if cellular respiration rate decreases with blebbistatin treatment and what the respiration patten of 3T3-L1 cells on fibronectin-based surfaces is following treatment.

3T3-L1 need nutrients to carry out their metabolic activities.

The results obtained with the ratiometric sensors had high variability. Cell responded differently on different experiments. The main advantage of these type of biosensors is that it is possible to have a real-time sight of cellular response and if they are going through a stress situation. However, they have the inconvenience that their signal is highly influenced by the intracellular conditions. For instance, acid pH interferes in PercevalHR signal (181). Furthermore, these experiments relay on the number of cells transfected. Nonetheless, these results demonstrate that cells respond to small changes in the media. Cells need from their main fuel sources to survive when these are not provided, or are blocked, cellular metabolic activity decrease. When the glucose analogue, 2-DG, was present in the media the biosynthesis pathways were disrupted (e.g. ATP and NADH synthesis) (Figure 4-4,

Figure 4-7, Figure 4-8) and stress protection mechanisms are activated (e.g. AMPK activity increases) (Figure 4-6). However, when the media was supplemented with glucose, L-Glu, sodium pyruvate or lactic acid, cellular metabolic activity increased. Generally, when significant differences were found with cells seeded on soft surfaces, the signal of the biosensor was lower, what confirms that in these circumstances cells are less metabolically active.

It is necessary to investigate more with these biosensors to fully understand their dynamics, what can affect their signal and how they can be activated. Nonetheless, these first experiments have demonstrated that cells are responsive but sensitive to any change in the environment. Also, the changes in biosensor signal might be due to a poor cell transfection. If cells have been damaged during the process or if they have not been fully transfected, the response seen might be affected. It would be interesting to study longer time points, where changes in the biosensor signal can be immediately observed and tracked when the molecule of interest is incorporated into the system. In the future, transfection efficacy could be confirm using fluorescence-activated cell sorting (FACS).

Overview of the metabolic activity.

MSCs after 24 hours accumulate higher levels of metabolites on stiff surfaces compare with soft ones. In particular, there was a high accumulation of metabolites implicated in glycolysis and OXPPHOS. This pattern was also observed on the Seahorse where the respiration rate was higher on stiffer surfaces. These findings might also indicate that on stiff surfaces MSCs have an OXPHOS-based metabolites compare with soft where it is glycolysis-based. Moreover, after 7 days the metabolites accumulated on soft surfaces are more for glycolysis than for TCA, that might be an indication that this pathway is more active.

Similar behaviour was found on 3T3-L1 cells seeded on Matrigel. A higher respiration rate was observed on stiff surfaces compare with soft. This finding was confirmed with ATP assay and ratiometric sensors. On collagen-based surfaces, 3T3-L1 cells accumulated more ATP on soft surfaces, this ATP might come from a glycolysis-based metabolism. Also, as cells are less active than on stiff surfaces, they can accumulate this ATP. When nutrients such as glucose or L-Glu was

presented in the media when 3T3-L1 cells were seeded on stiff surfaces, they were able to generate more ATP and NADH, what indicates that not glycolysis might be activated but also OXPHOS.

CHAPTER 5 : GENERAL DISCUSSION AND CONCLUSIONS

5.1. GENERAL DISCUSSION

How cells sense their microenvironment is going to determine their fate.

The results encountered in this project suggest that any change in the cellular microenvironment is going to have an implication in cellular mechanical and metabolic activity. However, how these two cellular activities are connected remained unknown (171). Here it has been demonstrated that as matrix stiffness increases cells are able to form mature focal adhesions and exert higher forces, for what they need to assemble the actin-cytoskeleton and initiate the myosin-contractility. That said, all these actions are not possible without ATP, which is mainly generated during mitochondrial respiration (181). Indeed, after 24 hours of culture cells have shown a high activity profile, which increased with surface stiffness (Figure 4-1B). More adenosine and metabolites implicated in the TCA cycle and glycolysis were accumulated on stiffer surfaces. This increment in these metabolites also correlated with a higher respiration rate (Figure 4-2D,F,H). Therefore, at early time points, when cell activity is mainly focused on ECM sensing and interaction (e.g. FAs assembly, cell contractility and spreading), cells must have a higher demand for ATP on stiffer surfaces (92).

Cellular response change depending on the composition of the matrix. To generate this response, it is essential the presence of nutrients.

The cellular response will be influenced by factors other than surface stiffness, such as the matrix composition and the soluble molecules present in the media (22,203). For instance, ATP accumulation in 3T3-L1 cells was higher on collagen-based surfaces compared with fibronectin-based surfaces (Figure 4-3). Plus, their respiration rate was enhanced on collagen-based surfaces compared with the OCR obtained in cells seeded on TCP without coating (Figure 4-2D,F,H). On the other hand, when nutrients were limited in the media (e.g. adding 2-DG), ATP levels decreased as glucose metabolism is blocked (Figure 4-5A). This also leads to a decrease in NADH levels (Figure 4-7A) and an increase in AMPK activity (Figure 4-6 A,C), which will trigger compensation pathways to regulate the ATP levels (171).

When the media was enriched with nutrients (e.g. glucose, sodium pyruvate), ATP levels were upregulated (Figure 4-5), while AMPK decreased (Figure 4-6). In relation to surface composition, Kechagia et.al. have recently demonstrated that breast epithelial cells seeded on surfaces functionalised with laminin reduce cell response to substrate stiffness and YAP nuclear localization. Contrary to what has previously been shown on surfaces coated with fibronectin or collagen I (11). When cell-laminin interactions were interrupted by inhibiting integrin β4, YAP nuclear translocation was recovered in response to surface rigidity, without affection cell forces or FAs (204). This study has demonstrated that apart from matrix composition, cellular integrins expression also regulates cellular response.

Different cell types (MSC and 3T3-L1) generate different response during ECM-cell interaction. For that, cells need to contract.

How cells interact with the proteins in the ECM, also depends on the cell type (171). These findings show that 3T3-L1 cells seeded on PAA hydrogels functionalised with FN presented similar spreading and focal adhesions maturation in the three stiffnesses investigated (3, 9 and 35 kPa) (Figure 3-7). On the other hand, MSCs seeded on degradable full-length FN-PEG hydrogels of 2.5, 8 and 26 kPa, showed a higher spread area and focal adhesion maturation on stiffer surfaces (Figure 3-4). Nonetheless, when cell contractility was inhibited, in both cases cell spreading was not affected, whereas FA maturation decreased. These findings suggest that cell contractility is essential for vinculin recruitment in the FAs and spreading. When cell contractility is suppressed, FAs cannot be assembled and cell spreading is halted (114). In line with the relation between vinculin and myosin contractility, MSCs showed an increase in traction forces exertion with surface stiffness (Figure 3-19), which is consistent with an upregulation of vinculin reinforcement. However, when cell contractility is inhibited and FAs are not formed, MSCs were not capable to exert forces. These findings imply that vinculin is a critical mechanosensor of surface stiffness and that it may play a role in cell contractility and traction force transmission via FAs (114).

YAP nuclear translocation changes with the mechanical properties of the surface and it is independent of cell contractility inhibition with blebbistatin.

When cell mechanotransduction was studied, different responses were observed depending on the matrix characteristics. In MSCs seeded on degradable hydrogels, YAP tended to translocate to the nucleus on stiffer surfaces, where cell area also increased (Figure 3-12A,C). On the other hand, when MSCs were seeded on nondegradable hydrogels cell area did not change and YAP n/c was similar in all the surfaces (Figure 3-13B,C). The same pattern was observed in 3T3-L1 (Figure 3-7) seeded on PAA hydrogels functionalised with FN. In this case, there was a similar behaviour of the different cell types on matrices with similar properties: non-degradable hydrogels functionalised with fibronectin. Hence, cellular response does not only depend on the proteins available, but also on the material degradability (34). Furthermore, L929 fibroblast exerted higher forces on degradable hydrogels compared with non-degradable (Figure 3-18).

It has been widely studied the regulation of YAP nuclear translocation in relation with surface stiffness and cell contractility (6,11,61). However, none of the cases studies in this project showed an upregulation of YAP nuclear translocation in relation to surface stiffness. As a matter of fact, 3T3-L1 cells present a similar translocation in all the rigidities. Moreover, when myosin contractility was inhibited with blebbistatin YAP kept translocated into the nucleus regardless of matrix characteristics or cell type (Figure 3-12, Figure 3-17). Das et. al. have demonstrated that when cell-ECM interactions prime over cell-cell contact, YAP nuclear translocation is favoured and contractility inhibition is not sufficient to exclude YAP from the nucleus (162). These observations might indicate that in the experiments performed in this project, cell-cell contact was reduced and these findings are the result of the interactions between cells and the ECM.

Cellular mechanical and metabolic activity are linked.

To sum up, cellular mechanical and metabolic activity are connected (Figure 5-1). These findings have demonstrated that any small change in how cells interact with the microenvironment, either physically with the ECM or through soluble molecules in the media, is going to have a direct effect on cellular response. In

the last few years, there have been arising multiple studies that have tried to link these two cellular activities (108,171,203). Nonetheless, how they are connected and how it can be regulated have not been elucidated yet.

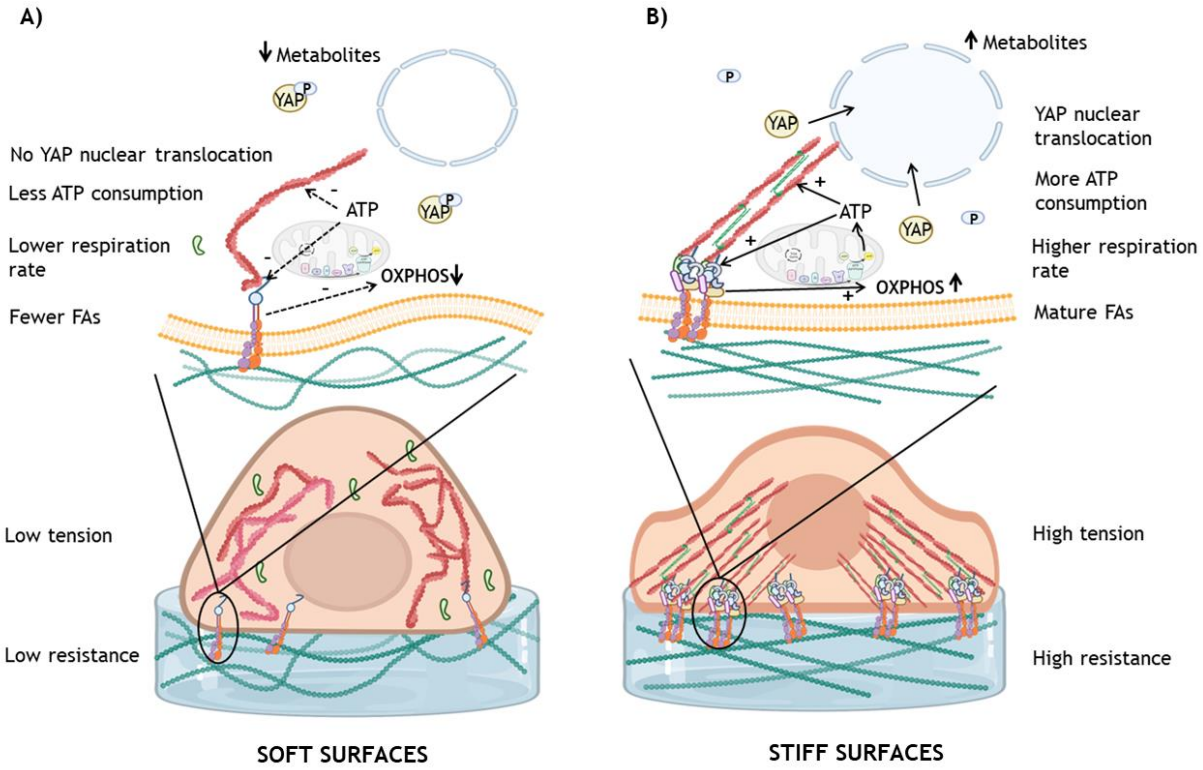

Figure 5-1. Cells are more active on stiff surfaces. *The three cell types used in this project (MSCs, 3T-L1 and L929 cells) have demonstrated higher activity on stiffer surfaces. A) In general, it has been possible to observed that on soft surfaces there is a low resistance from the surfaces, this is going to lead to a poor FAs generation and low tension in the cells. As a consequence, cellular respiration rate decrease and less ATP in generated to contract and trigger YAP nuclear translocation. In this situation less metabolites are generated. B) On the other hand, when cells are seeded on stiff surfaces, they sense high resistance from the surface. To compensate it, they generate higher number of FAs and intracellular tension. Cells are able to form their actin-cytoskeleton and their respiration rate is enhanced generating the required ATP to reinforce the FAs and contract. YAP nuclear translocation increases and more levels of metabolites are synthesised.*

5.2. CONCLUSIONS

Based on the results obtained in this project in the last years it is possible to conclude:

- Full-length FN-PEG hydrogels were well characterised and functionalised. However, there might be other factors that affect their polymerisation.
- PAA hydrogels and Matrigel are well-known hydrogels that can be easily used *in vitro* to study cellular response. However, they have the disadvantages that cannot be used *in vivo* or in 3D in the case of PAA hydrogels.
- Cellular response change depending on matrix mechanical properties and how cells interact with it.
- Surface degradability affects cellular response even in 2D models: L929 fibroblasts exerted higher forces on degradable hydrogels compare with non-degradable.
- MSCs exerted higher forces on stiffer surfaces. This force increasement is correlated with an upregulation of FAs formation and YAP nuclear translocation on degradable surfaces.
- YAP nuclear translocation in MSCs seeded on non-degradable cells in not dependent on surface stiffness.
- Surface stiffness does not affect the production of FAs or the nuclear translocation of YAP in 3T3-L1 cells.
- Myosin contractility is essential for force generation and FAs maturation. However, it does not affect YAP nuclear translocation and ATP accumulation.
- MSCs accumulate more metabolites in early stages of cell-ECM interactions. At this point, MSCs are creating enough biomass that will be used in later stages where metabolites accumulation is not possible due to an increase in cellular mechanical and metabolic activity.
- Metabolites accumulation increase with surface stiffness in early stages. This pattern is lost after 7 days when MSCs appear to be more active on stiffer surfaces, reducing the amount of metabolites available.

- Cellular respiration rate increases with surface stiffness to generate more energy in form of ATP to supply cellular activity (e.g. force generation, myosin contractility, FAs maturation).
- 3T3-L1 are more responsive to collagen-based matrices.
- Cell starvation triggers cell defences pathways (e.g. NADPH and AMPK) to restore the nutrient and energy levels.
- Ratiometric sensors are a promising technique to study real time cellular metabolic activity. However, their signal is highly sensible to the atmosphere conditions.

CHAPTER 6 : FUTURE WORK

This project has been able to cover different aspect of cellular mechanical and metabolic activity, providing a good insight of cellular response to early cell-ECM interactions. Nonetheless, more future work is necessary to finish elucidating the connection between these two cellular activities. The potential experiments proposed are:

- TFM in MSCs and 3T3-L1 cells seeded on the same surface with similar properties, and study cell contractility inhibition in force exertion.
- To Inhibit other protein implicated in FAs formation (e.g. integrins).
- To understand YAP nuclear translocation and its relation with cell-contractility by triggering other pathways (e.g. RhoA/ROCK).
- To study cellular contractility inhibition in the metabolites profile and cellular respiration in MSCs and 3T3-L1.
- To incorporate qPCR to study cell phenotype.
- To study cell proliferation in different stiffnesses to understand the implication of cell density in force generation, FAs assembly and cell metabolism.
- To look at mitochondria mass on different stiffness using MitoTracker.

REFERENCES

1. Engler AJ, Sen S, Sweeney HL, Discher DE. Matrix Elasticity Directs Stem Cell Lineage Specification. Cell [Internet]. 2006 Aug 25 [cited 2019 Apr 7];126(4):677–89. Available from: https://www.sciencedirect.com/science/article/pii/S0092867406009615

2. Frantz C, Stewart KM, Weaver VM. The extracellular matrix at a glance. J Cell Sci [Internet]. 2010 Dec 15 [cited 2019 Apr 7];123(Pt 24):4195–200. Available from: http://www.ncbi.nlm.nih.gov/pubmed/21123617

3. Uccelli A, Moretta L, Pistoia V. Mesenchymal stem cells in health and disease. Nat Rev Immunol [Internet]. 2008 Sep 1 [cited 2019 Apr 8];8(9):726–36. Available from: http://www.nature.com/articles/nri2395

4. Fitzsimmons REB, Mazurek MS, Soos A, Simmons CA. Mesenchymal Stromal/Stem Cells in Regenerative Medicine and Tissue Engineering. Stem Cells Int [Internet]. 2018 Aug 19 [cited 2019 Apr 30];2018:1–16. Available from: https://www.hindawi.com/journals/sci/2018/8031718/

5. Lv H, Li L, Sun M, Zhang Y, Chen L, Rong Y, et al. Mechanism of regulation of stem cell differentiation by matrix stiffness. Stem Cell Res Ther [Internet]. 2015 May 27 [cited 2023 Apr 2];6(1):1–11. Available from: https://stemcellres.biomedcentral.com/articles/10.1186/s13287-015-0083-4

6. Brusatin G, Panciera T, Gandin A, Citron A, Piccolo S. Biomaterials and engineered microenvironments to control YAP/TAZ-dependent cell behaviour. Nat Mater [Internet]. 2018;17(12):1063–75. Available from: http://dx.doi.org/10.1038/s41563-018-0180-8

7. Ge H, Tian M, Pei Q, Tan F, Pei H. Extracellular Matrix Stiffness: New Areas Affecting Cell Metabolism. Front Oncol. 2021 Feb 24;11:8.

8. Smith LR, Cho S, Discher DE. Stem Cell Differentiation is Regulated by Extracellular Matrix Mechanics. Physiology [Internet]. 2018 Jan [cited 2019 Apr 18];33(1):16–25. Available from: http://www.physiology.org/doi/10.1152/physiol.00026.2017

9. Style RW, Boltyanskiy R, German GK, Hyland C, MacMinn CW, Mertz AF, et al. Traction force microscopy in physics and biology. Soft Matter [Internet]. 2014 May 21 [cited 2019 Apr 14];10(23):4047. Available from: http://xlink.rsc.org/?DOI=c4sm00264d

10. Hoffman LM, Smith MA, Jensen CC, Yoshigi M, Blankman E, Ullman KS, et al. Mechanical stress triggers nuclear remodeling and the formation of transmembrane actin nuclear lines with associated nuclear pore complexes. Mol Biol Cell [Internet]. 2020 Jul 21 [cited 2023 Apr 13];31(16):1774–87. Available from: https://www.molbiolcell.org/doi/10.1091/mbc.E19-01-0027

11. Elosegui-Artola A, Andreu I, Beedle AEM, Lezamiz A, Uroz M, Kosmalska AJ, et al. Force Triggers YAP Nuclear Entry by Regulating Transport across Nuclear Pores. Cell [Internet]. 2017 Nov 30 [cited 2019 Mar 5];171(6):1–14. Available from: https://www.sciencedirect.com/science/article/pii/S0092867417311923

12. Andreu I, Granero-Moya I, Chahare NR, Clein K, Molina-Jordán M, Beedle AEM, et al. Mechanical force application to the nucleus regulates nucleocytoplasmic transport. Nature Cell Biology 2022 24:6 [Internet]. 2022 Jun 9 [cited 2023 Apr 13];24(6):896–905. Available from: https://www.nature.com/articles/s41556-022-00927-7

13. Wei Q, Holle A, Li J, Posa F, Biagioni F, Croci O, et al. BMP-2 Signaling and Mechanotransduction Synergize to Drive Osteogenic Differentiation via YAP/TAZ. Advanced Science [Internet]. 2020 Jun 16 [cited 2020 Jun 26];1902931. Available from: https://onlinelibrary.wiley.com/doi/abs/10.1002/advs.201902931

14. Bonnans C, Chou J, Werb Z. Remodelling the extracellular matrix in development and disease. Nat Rev Mol Cell Biol [Internet]. 2014 Dec [cited 2019 Apr 6];15(12):786–801. Available from: http://www.ncbi.nlm.nih.gov/pubmed/25415508

15. Daley WP, Peters SB, Larsen M. Extracellular matrix dynamics in development and regenerative medicine. J Cell Sci [Internet]. 2008 Feb 1 [cited 2019 Apr 7];121(Pt 3):255–64. Available from: http://www.ncbi.nlm.nih.gov/pubmed/18216330

16. Humphrey JD, Dufresne ER, Schwartz MA. Mechanotransduction and extracellular matrix homeostasis. Nat Rev Mol Cell Biol [Internet]. 2014;15(12):802–12. Available from: http://dx.doi.org/10.1038/nrm3896

17. Pankov R, Yamada KM. Fibronectin at a glance. J Cell Sci [Internet]. 2002 Oct 15 [cited 2019 Apr 7];115(Pt 20):3861–3. Available from: http://www.ncbi.nlm.nih.gov/pubmed/12244123

18. Bella J, Hulmes DJS. Fibrillar collagens. Subcell Biochem [Internet]. 2017 Jan 1 [cited 2023 Apr 1];82:457–90. Available from: https://link.springer.com/chapter/10.1007/978-3-319-49674-0_14

19. Xue M, Jackson CJ. Extracellular Matrix Reorganization During Wound Healing and Its Impact on Abnormal Scarring. Adv Wound Care (New Rochelle) [Internet]. 2015 Mar [cited 2019 Apr 7];4(3):119–36. Available from: http://www.liebertpub.com/doi/10.1089/wound.2013.0485

20. Mouw JK, Ou G, Weaver VM. Extracellular matrix assembly: a multiscale deconstruction. Nature Reviews Molecular Cell Biology 2014 15:12 [Internet]. 2014 Nov 5 [cited 2023 Apr 1];15(12):771–85. Available from: https://www.nature.com/articles/nrm3902

21. Heino J. The collagen family members as cell adhesion proteins. BioEssays. 2007 Oct;29(10):1001–10.

22. Kubow KE, Vukmirovic R, Zhe L, Klotzsch E, Smith ML, Gourdon D, et al. Mechanical forces regulate the interactions of fibronectin and collagen I in extracellular matrix. Nat Commun [Internet]. 2015 Nov 14 [cited 2019 May 20];6(1):8026. Available from: http://www.nature.com/articles/ncomms9026

23. Knight CG, Morton LF, Peachey AR, Tuckwell DS, Farndale RW, Barnes MJ. The Collagen-binding A-domains of Integrins α1ß1 and α2ß1Recognize the Same Specific Amino Acid Sequence, GFOGER, in Native (Triple-helical) Collagens. Journal of Biological Chemistry. 2000 Jan 7;275(1):35–40.

24. Borza DB, Bondar O, Ninomiya Y, Sado Y, Naito I, Todd P, et al. The NC1 Domain of Collagen IV Encodes a Novel Network Composed of the α1, α2, α5, and α6 Chains in Smooth Muscle Basement Membranes. Journal of Biological Chemistry. 2001 Jul 27;276(30):28532–40.

25. Woltersdorf C, Bonk M, Leitinger B, Huhtala M, Käpylä J, Heino J, et al. The binding capacity of α1ß1-, α2ß1- and α10ß1-integrins depends on non-collagenous surface macromolecules rather than the collagens in cartilage fibrils. Matrix Biology. 2017 Nov 1;63:91–105.

26. To WS, Midwood KS. Plasma and cellular fibronectin: distinct and independent functions during tissue repair. Fibrogenesis & Tissue Repair 2011 4:1 [Internet]. 2011 Sep 16 [cited 2023 Apr 26];4(1):1–17. Available from: https://fibrogenesis.biomedcentral.com/articles/10.1186/1755-1536-4-21

27. Kapp TG, Rechenmacher F, Neubauer S, Maltsev O V., Cavalcanti-Adam EA, Zarka R, et al. A comprehensive evaluation of the activity and selectivity profile of ligands for RGD-binding integrins. Sci Rep. 2017 Jan 11;7(1):1–13.

28. B Geiger JSAB. Environmental sensing through focal adhesions. Nat Rev Mol Cell Biol. 2008;10:21–33.

29. Pytela R, Pierschbacher M, Ginsberg M, Plow E, Ruoslahti E. Platelet membrane glycoprotein IIb/IIIa: member of a family of Arg-Gly-Asp--specific adhesion receptors. Science (1979) [Internet]. 1986 Mar 28 [cited 2019 Apr 7];231(4745):1559–62. Available from: http://www.ncbi.nlm.nih.gov/pubmed/2420006

30. Kolf CM, Cho E, Tuan RS. Mesenchymal stromal cells. Biology of adult mesenchymal stem cells: Regulation of niche, self-renewal and differentiation. Vol. 9, Arthritis Research and Therapy. BioMed Central; 2007. p. 204.

31. Prabhakaran MP, Venugopal JR, Ramakrishna S. Mesenchymal stem cell differentiation to neuronal cells on electrospun nanofibrous substrates for nerve tissue engineering. Biomaterials [Internet]. 2009 Oct 1 [cited 2019 Apr 8];30(28):4996–5003. Available from: https://www.sciencedirect.com/science/article/pii/S0142961209005705

32. Teng M, Huang Y, Zhang H. Application of stems cells in wound healing-An update. Wound Repair and Regeneration [Internet]. 2014 Mar 1 [cited 2020 Apr 21];22(2):151–60. Available from: http://doi.wiley.com/10.1111/wrr.12152

33. Pittenger MF, Discher DE, Péault BM, Phinney DG, Hare JM, Caplan AI. Mesenchymal stem cell perspective: cell biology to clinical progress. npj Regenerative Medicine 2019 4:1 [Internet]. 2019 Dec 2 [cited 2023 Apr 1];4(1):1–15. Available from: https://www.nature.com/articles/s41536-019-0083-6

34. Vining KH, Mooney DJ. Mechanical forces direct stem cell behaviour in development and regeneration. Nat Rev Mol Cell Biol [Internet]. 2017 Nov 8 [cited 2019 Apr 9];18(12):728–42. Available from: http://www.nature.com/doifinder/10.1038/nrm.2017.108

35. Lv H, Li L, Sun M, Zhang Y, Chen L, Rong Y, et al. Mechanism of regulation of stem cell differentiation by matrix stiffness [Internet]. Vol. 6, Stem Cell

Research and Therapy. BioMed Central Ltd.; 2015 [cited 2020 Apr 21]. p. 103. Available from: http://stemcellres.com/content/6/1/103

36. Gauthier NC, Roca-Cusachs P. Mechanosensing at integrin-mediated cell–matrix adhesions: from molecular to integrated mechanisms. Curr Opin Cell Biol [Internet]. 2018 Feb 1 [cited 2019 Apr 13];50:20–6. Available from: https://www.sciencedirect.com/science/article/pii/S0955067417301266

37. Sun Z, Guo SS, Fässler R. Integrin-mediated mechanotransduction. J Cell Biol [Internet]. 2016 Nov 21 [cited 2019 Apr 13];215(4):445–56. Available from: http://www.ncbi.nlm.nih.gov/pubmed/27872252

38. Elosegui-Artola A, Trepat X, Roca-Cusachs P. Control of Mechanotransduction by Molecular Clutch Dynamics. Trends Cell Biol [Internet]. 2018;28(5):356–67. Available from: http://dx.doi.org/10.1016/j.tcb.2018.01.008

39. Bennett M, Cantini M, Reboud J, Cooper JM, Roca-Cusachs P, Salmeron-Sanchez M. Molecular clutch drives cell response to surface viscosity. Proc Natl Acad Sci U S A. 2018;115(6):1192–7.

40. Ghosh D, McGrail DJ, Dawson MR. TGF-β1 pretreatment improves the function of mesenchymal stem cells in the wound bed. Front Cell Dev Biol. 2017;5(APR).

41. Uhler C, Shivashankar G V. Regulation of genome organization and gene expression by nuclear mechanotransduction [Internet]. Vol. 18, Nature Reviews Molecular Cell Biology. Nature Publishing Group; 2017 [cited 2020 Aug 28]. p. 717–27. Available from: https://www.nature.com/articles/nrm.2017.101

42. Elosegui-Artola A, Oria R, Chen Y, Kosmalska A, Pérez-González C, Castro N, et al. Mechanical regulation of a molecular clutch defines force transmission and transduction in response to matrix rigidity. Nat Cell Biol. 2016;18(5):540–8.

43. Chaudhuri O, Gu L, Darnell M, Klumpers D, Bencherif SA, Weaver JC, et al. Substrate stress relaxation regulates cell spreading. Nat Commun [Internet]. 2015 Feb 19 [cited 2020 Apr 15];6(1):1–7. Available from: http://dx.doi.org/10.1038/ncomms7365

44. Gerardo H, Lima A, Carvalho J, Ramos JRD, Couceiro S, Travasso RDM, et al. Soft culture substrates favor stem-like cellular phenotype and facilitate reprogramming of human mesenchymal stem/stromal cells (hMSCs) through mechanotransduction. Sci Rep [Internet]. 2019 Dec 1 [cited 2020 Aug 27];9(1):1–18. Available from: https://doi.org/10.1038/s41598-019-45352-3

45. Marrella A, Lee TY, Lee DH, Karuthedom S, Syla D, Chawla A, et al. Engineering vascularized and innervated bone biomaterials for improved skeletal tissue regeneration. Materials Today [Internet]. 2018 May 1 [cited 2019 Apr 30];21(4):362–76. Available from: https://www.sciencedirect.com/science/article/pii/S1369702117304121

46. Cai M, Shen R, Song L, Lu M, Wang J, Zhao S, et al. Bone Marrow Mesenchymal Stem Cells (BM-MSCs) Improve Heart Function in Swine Myocardial Infarction Model through Paracrine Effects. Sci Rep [Internet]. 2016 Sep 20 [cited 2019 Apr 30];6(1):28250. Available from: http://www.nature.com/articles/srep28250

47. Vogel V, Sheetz M. Local force and geometry sensing regulate cell functions. Nat Rev Mol Cell Biol [Internet]. 2006 Apr 22 [cited 2019 Jan 25];7(4):265–75. Available from: http://www.nature.com/articles/nrm1890

48. Dufort CC, Paszek MJ, Weaver VM. Balancing forces: Architectural control of mechanotransduction. Vol. 12, Nature Reviews Molecular Cell Biology. 2011. p. 308–19.

49. Elosegui-Artola A, Bazellières E, Allen MD, Andreu I, Oria R, Sunyer R, et al. Rigidity sensing and adaptation through regulation of integrin types. Nat Mater [Internet]. 2014 Jun 4 [cited 2019 Apr 9];13(6):631–7. Available from: http://www.nature.com/articles/nmat3960

50. Cabral-Pacheco GA, Garza-Veloz I, Rosa CCD La, Ramirez-Acuña JM, Perez-Romero BA, Guerrero-Rodriguez JF, et al. The roles of matrix metalloproteinases and their inhibitors in human diseases. Int J Mol Sci. 2020 Dec 2;21(24):1–53.

51. Peng Y, Liu QJ, He T, Ye K, Yao X, Ding J. Degradation rate affords a dynamic cue to regulate stem cells beyond varied matrix stiffness. Biomaterials. 2018 Sep 1;178:467–80.

52. Adelöw C, Segura T, Hubbell JA, Frey P. The effect of enzymatically degradable poly(ethylene glycol) hydrogels on smooth muscle cell phenotype. Biomaterials. 2008 Jan 1;29(3):314–26.

53. Madl CM, LeSavage BL, Dewi RE, Lampe KJ, Heilshorn SC, Madl CM, et al. Matrix Remodeling Enhances the Differentiation Capacity of Neural Progenitor Cells in 3D Hydrogels. Advanced Science [Internet]. 2019 Feb 1 [cited 2023 Apr 25];6(4):1801716. Available from: https://onlinelibrary.wiley.com/doi/full/10.1002/advs.201801716

54. Chaudhuri O, Gu L, Klumpers D, Darnell M, Bencherif SA, Weaver JC, et al. Hydrogels with tunable stress relaxation regulate stem cell fate and activity. Nat Mater [Internet]. 2016 Mar 30 [cited 2019 Apr 14];15(3):326–34. Available from: http://www.nature.com/articles/nmat4489

55. Walters NJ, Gentleman E. Evolving insights in cell-matrix interactions: Elucidating how non-soluble properties of the extracellular niche direct stem cell fate. Vol. 11, Acta Biomaterialia. Elsevier Ltd; 2015. p. 3–16.

56. Khetan S, Guvendiren M, Legant WR, Cohen DM, Chen CS, Burdick JA. Degradation-mediated cellular traction directs stem cell fate in covalently crosslinked three-dimensional hydrogels. Nat Mater. 2013 Mar 24;12(5):458–65.

57. Pemberton GD, Childs P, Reid S, Nikukar H, Monica Tsimbouri P, Gadegaard N, et al. Nanoscale stimulation of osteoblastogenesis from mesenchymal

stem cells: Nanotopography and nanokicking. Nanomedicine. 2015;10(4):547–60.

58. Kristal-Muscal R, Dvir L, Weihs D. Metastatic cancer cells tenaciously indent impenetrable, soft substrates. New J Phys [Internet]. 2013 Mar 21 [cited 2023 Apr 25];15(3):035022. Available from: https://iopscience.iop.org/article/10.1088/1367-2630/15/3/035022

59. Kostic A, Lynch CD, Sheetz MP. Differential Matrix Rigidity Response in Breast Cancer Cell Lines Correlates with the Tissue Tropism. Aziz SA, editor. PLoS One [Internet]. 2009 Jul 23 [cited 2020 Apr 16];4(7):e6361. Available from: http://dx.plos.org/10.1371/journal.pone.0006361

60. Cora-Cruz JJ, Diffoot-Carlo N, Sundaram PA. Vinculin expression in MC3T3-E1 cells in response to mechanical stimulus. Data Brief [Internet]. 2016 Mar 1 [cited 2019 Feb 21];6:94–100. Available from: https://www.sciencedirect.com/science/article/pii/S2352340915003479?via%3Dihub

61. Dupont S, Morsut L, Aragona M, Enzo E, Giulitti S, Cordenonsi M, et al. Role of YAP/TAZ in mechanotransduction. Nature [Internet]. 2011 Jun 9 [cited 2019 Apr 11];474(7350):179–84. Available from: http://dx.doi.org/10.1038/nature10137

62. Kovács M, Tóth J, Hetényi C, Málnási-Csizmadia A, Seller JR. Mechanism of blebbistatin inhibition of myosin II. Journal of Biological Chemistry. 2004 Aug 20;279(34):35557–63.

63. Roman BI, Verhasselt S, Stevens C V. Medicinal Chemistry and Use of Myosin II Inhibitor (S)-Blebbistatin and Its Derivatives. Vol. 61, Journal of Medicinal Chemistry. American Chemical Society; 2018. p. 9410–28.

64. Vicente-Manzanares M, Ma X, Adelstein RS, Horwitz AR. Non-muscle myosin II takes centre stage in cell adhesion and migration. Vol. 10, Nature Reviews Molecular Cell Biology. Nature Publishing Group; 2009. p. 778–90.

65. Ziegler WH, Liddington RC, Critchley DR. The structure and regulation of vinculin. Trends Cell Biol [Internet]. 2006 Sep 1 [cited 2019 Apr 11];16(9):453–60. Available from: https://www.sciencedirect.com/science/article/pii/S0962892406001930

66. Kuroda M, Wada H, Kimura Y, Ueda K, Kioka N. Vinculin promotes nuclear localization of TAZ to inhibit ECM stiffness-dependent differentiation into adipocytes. 2017 [cited 2019 Apr 11]; Available from: http://jcs.biologists.org/content/joces/130/5/989.full.pdf

67. Burridge K, Wennerberg K. Rho and Rac Take Center Stage. Vol. 116, Cell. Cell Press; 2004. p. 167–79.

68. McBeath R, Pirone DM, Nelson CM, Bhadriraju K, Chen CS. Cell shape, cytoskeletal tension, and RhoA regulate stem cell lineage commitment. Dev Cell. 2004 Apr 1;6(4):483–95.

69. Sonam S, Sathe SR, Yim EKF, Sheetz MP, Lim CT. Cell contractility arising from topography and shear flow determines human mesenchymal stem cell fate. Sci Rep [Internet]. 2016 Apr 16 [cited 2019 Apr 12];6(1):20415. Available from: http://www.nature.com/articles/srep20415

70. Sharanek A, Burban A, Burbank M, Le Guevel R, Li R, Guillouzo A, et al. Rho-kinase/myosin light chain kinase pathway plays a key role in the impairment of bile canaliculi dynamics induced by cholestatic drugs. Scientific Reports 2016 6:1 [Internet]. 2016 May 12 [cited 2023 Apr 3];6(1):1–18. Available from: https://www.nature.com/articles/srep24709

71. Srinivasan S, Das S, Surve V, Srivastava A, Kumar S, Jain N, et al. Blockade of ROCK inhibits migration of human primary keratinocytes and malignant epithelial skin cells by regulating actomyosin contractility. Scientific Reports 2019 9:1 [Internet]. 2019 Dec 27 [cited 2023 Apr 3];9(1):1–13. Available from: https://www.nature.com/articles/s41598-019-56447-2

72. Lomakin A, Nader G, Piel M. Forcing Entry into the Nucleus. Dev Cell [Internet]. 2017;43(5):547–8. Available from: https://doi.org/10.1016/j.devcel.2017.11.015

73. Totaro A, Panciera T, Piccolo S. YAP/TAZ upstream signals and downstream responses. Nat Cell Biol [Internet]. 2018;20(8):888–99. Available from: http://dx.doi.org/10.1038/s41556-018-0142-z

74. Nardone G, Oliver-De La Cruz J, Vrbsky J, Martini C, Pribyl J, Skládal P, et al. YAP regulates cell mechanics by controlling focal adhesion assembly. Nat Commun. 2017;8(May).

75. Oliver-De La Cruz J, Nardone G, Vrbsky J, Pompeiano A, Perestrelo AR, Capradossi F, et al. Substrate mechanics controls adipogenesis through YAP phosphorylation by dictating cell spreading. Biomaterials. 2019 Jun 1;205:64–80.

76. Dupont S. Role of YAP/TAZ in cell-matrix adhesion-mediated signalling and mechanotransduction. Exp Cell Res [Internet]. 2016;343(1):42–53. Available from: http://dx.doi.org/10.1016/j.yexcr.2015.10.034

77. Lee JY, Dominguez AA, Nam S, Stowers RS, Qi LS, Chaudhuri O. Identification of cell context-dependent YAP-associated proteins reveals β1 and β4 integrin mediate YAP translocation independently of cell spreading. Sci Rep [Internet]. 2019;9(1):1–11. Available from: http://dx.doi.org/10.1038/s41598-019-53659-4

78. Caliari SR, Vega SL, Kwon M, Soulas EM, Burdick JA. Dimensionality and spreading influence MSC YAP/TAZ signaling in hydrogel environments. Biomaterials. 2016 Oct 1;103:314–23.

79. Lee JY, Chang JK, Dominguez AA, Lee H pyo, Nam S, Chang J, et al. YAP-independent mechanotransduction drives breast cancer progression. Nat Commun [Internet]. 2019 Dec 1 [cited 2020 Sep 1];10(1):1–9. Available from: https://doi.org/10.1038/s41467-019-09755-0

80. Stanton AE, Tong X, Lee S, Yang F. Biochemical Ligand Density Regulates Yes-Associated Protein Translocation in Stem Cells through Cytoskeletal Tension and Integrins. ACS Appl Mater Interfaces [Internet]. 2019 Mar 6 [cited 2023 Apr 4];11(9):8849–57. Available from: https://pubs.acs.org/doi/full/10.1021/acsami.8b21270

81. Furukawa KT, Yamashita K, Sakurai N, Ohno S. The Epithelial Circumferential Actin Belt Regulates YAP/TAZ through Nucleocytoplasmic Shuttling of Merlin. Cell Rep. 2017 Aug 8;20(6):1435–47.

82. Evans RD, Heather LC. Human metabolism: pathways and clinical aspects. Surgery (Oxford) [Internet]. 2022 Apr 1 [cited 2023 Apr 26];40(4):219–26. Available from: https://linkinghub.elsevier.com/retrieve/pii/S0263931922000163

83. Hu C, Fan L, Cen P, Chen E, Jiang Z, Li L. Energy metabolism plays a critical role in stem cell maintenance and differentiation. Int J Mol Sci. 2016;17(2).

84. Alfarouk KO, Verduzco D, Rauch C, Muddathir AK, Bashir AHH, Elhassan GO, et al. Glycolysis, tumor metabolism, cancer growth and dissemination. A new pH-based etiopathogenic perspective and therapeutic approach to an old cancer question. Oncoscience [Internet]. 2014 [cited 2020 Aug 31];1(12):777–802. Available from: /pmc/articles/PMC4303887/?report=abstract

85. Wanet A, Arnould T, Najimi M, Renard P. Connecting Mitochondria, Metabolism, and Stem Cell Fate. Stem Cells Dev. 2015 Sep 1;24(17):1957–71.

86. Folmes CDL, Terzic A. Energy metabolism in the acquisition and maintenance of stemness. Semin Cell Dev Biol [Internet]. 2016 Apr 1 [cited 2020 Jun 24];52:68–75. Available from: https://linkinghub.elsevier.com/retrieve/pii/S1084952116300520

87. Meleshina A V., Dudenkova V V., Bystrova AS, Kuznetsova DS, Shirmanova M V., Zagaynova E V. Two-photon FLIM of NAD(P)H and FAD in mesenchymal stem cells undergoing either osteogenic or chondrogenic differentiation. Stem Cell Res Ther [Internet]. 2017 Jan 28 [cited 2021 Feb 24];8(1):15. Available from: http://stemcellres.biomedcentral.com/articles/10.1186/s13287-017-0484-7

88. Guo Y, Chi X, Wang Y, Heng BC, Wei Y, Zhang X, et al. Mitochondria transfer enhances proliferation, migration, and osteogenic differentiation of bone marrow mesenchymal stem cell and promotes bone defect healing. Stem Cell Res Ther [Internet]. 2020 Jun 25 [cited 2020 Aug 25];11(1):245. Available from: https://stemcellres.biomedcentral.com/articles/10.1186/s13287-020-01704-9

89. Xiao Y, McGuinness CAS, Doherty-Boyd WS, Salmeron-Sanchez M, Donnelly H, Dalby MJ. Current insights into the bone marrow niche: From biology in vivo to bioengineering ex vivo. Biomaterials. 2022 Jul 1;286:121568.

90. Zhang CC, Sadek HA. Hypoxia and metabolic properties of hematopoietic stem cells. Antioxid Redox Signal [Internet]. 2014 Apr 20 [cited 2023 Apr 26];20(12):1891–901. Available from: https://www.liebertpub.com/doi/10.1089/ars.2012.5019

91. Xie J, Bao M, Hu X, Koopman WJH, Huck WTS. Energy expenditure during cell spreading influences the cellular response to matrix stiffness. Biomaterials. 2021 Jan 1;267:120494.

92. Isogai T, Park JS, Danuser G. Cell forces meet cell metabolism. Vol. 19, Nature Cell Biology. Nature Publishing Group; 2017. p. 591–3.

93. Mousawi F, Peng H, Li J, Ponnambalam S, Roger S, Zhao H, et al. Chemical activation of the Piezo1 channel drives mesenchymal stem cell migration via inducing ATP release and activation of P2 receptor purinergic signaling.

Stem Cells [Internet]. 2020 Mar 1 [cited 2023 Apr 10];38(3):410–21. Available from: https://academic.oup.com/stmcls/article/38/3/410/6409387

94. Milanese C, Bombardieri CR, Sepe S, Barnhoorn S, Payán-Goméz C, Caruso D, et al. DNA damage and transcription stress cause ATP-mediated redesign of metabolism and potentiation of anti-oxidant buffering. Nature Communications 2019 10:1 [Internet]. 2019 Oct 25 [cited 2023 Apr 10];10(1):1–16. Available from: https://www.nature.com/articles/s41467-019-12640-5

95. Moon SJ, Dong W, Stephanopoulos GN, Sikes HD. Oxidative pentose phosphate pathway and glucose anaplerosis support maintenance of mitochondrial NADPH pool under mitochondrial oxidative stress. Bioeng Transl Med [Internet]. 2020 Sep 1 [cited 2023 Apr 10];5(3):e10184. Available from: https://onlinelibrary.wiley.com/doi/full/10.1002/btm2.10184

96. Rodrigues RJ, Tomé AR, Cunha RA. ATP as a multi-target danger signal in the brain. Front Neurosci [Internet]. 2015 [cited 2023 Apr 11];9(APR):148. Available from: /pmc/articles/PMC4412015/

97. Bertrand PP. ATP and Sensory Transduction in the Enteric Nervous System. http://dx.doi.org/101177/1073858403253768 [Internet]. 2003 Aug 1 [cited 2023 Apr 11];9(4):243–60. Available from: https://journals.sagepub.com/doi/10.1177/1073858403253768?url_ver=Z39.88-2003&rfr_id=ori%3Arid%3Acrossref.org&rfr_dat=cr_pub++0pubmed

98. Villa-Bellosta R. Role of the extracellular ATP/pyrophosphate metabolism cycle in vascular calcification. Purinergic Signal [Internet]. 2022 May 5 [cited 2023 Apr 11];1:1–8. Available from: https://link.springer.com/article/10.1007/s11302-022-09867-1

99. Hatzivassiliou G, Zhao F, Bauer DE, Andreadis C, Shaw AN, Dhanak D, et al. ATP citrate lyase inhibition can suppress tumor cell growth. Cancer Cell. 2005 Oct 1;8(4):311–21.

100. Herzig S, Shaw RJ. AMPK: guardian of metabolism and mitochondrial homeostasis. Nature Reviews Molecular Cell Biology 2017 19:2 [Internet]. 2017 Oct 4 [cited 2023 Apr 12];19(2):121–35. Available from: https://www.nature.com/articles/nrm.2017.95

101. Li Y, Xu S, Mihaylova MM, Zheng B, Hou X, Jiang B, et al. AMPK phosphorylates and inhibits SREBP activity to attenuate hepatic steatosis and atherosclerosis in diet-induced insulin-resistant mice. Cell Metab [Internet]. 2011 Apr 6 [cited 2023 Apr 12];13(4):376–88. Available from: http://www.cell.com/article/S1550413111000969/fulltext

102. Liu GY, Sabatini DM. mTOR at the nexus of nutrition, growth, ageing and disease. Nature Reviews Molecular Cell Biology 2020 21:4 [Internet]. 2020 Jan 14 [cited 2023 Apr 12];21(4):183–203. Available from: https://www.nature.com/articles/s41580-019-0199-y

103. Andreu I, Falcones B, Hurst S, Chahare N, Quiroga X, Le Roux AL, et al. The force loading rate drives cell mechanosensing through both reinforcement and cytoskeletal softening. Nature Communications 2021 12:1 [Internet]. 2021 Jul 9 [cited 2023 Apr 13];12(1):1–12. Available from: https://www.nature.com/articles/s41467-021-24383-3

104. Bays JL, Campbell HK, Heidema C, Sebbagh M, Demali KA. Linking E-cadherin mechanotransduction to cell metabolism through force-mediated activation of AMPK. Nat Cell Biol. 2017 May 31;19(6):724–31.

105. Mani S, Katkar HH, Voth GA. Compressive and Tensile Deformations Alter ATP Hydrolysis and Phosphate Release Rates in Actin Filaments. J Chem Theory Comput [Internet]. 2021 Mar 9 [cited 2023 Apr 13];17(3):1900–13. Available from: https://pubs.acs.org/doi/full/10.1021/acs.jctc.0c01186

106. Romani P, Brian I, Santinon G, Pocaterra A, Audano M, Pedretti S, et al. Extracellular matrix mechanical cues regulate lipid metabolism through Lipin-1 and SREBP. Nature Cell Biology 2019 21:3 [Internet]. 2019 Feb 4

[cited 2023 Apr 22];21(3):338–47. Available from: https://www.nature.com/articles/s41556-018-0270-5

107. Romani P, Brian I, Santinon G, Pocaterra A, Audano M, Pedretti S, et al. Extracellular matrix mechanical cues regulate lipid metabolism through Lipin-1 and SREBP. Nat Cell Biol. 2019;21(3):338–47.

108. Bartolák-Suki E, Imsirovic J, Nishibori Y, Krishnan R, Suki B. Regulation of Mitochondrial Structure and Dynamics by the Cytoskeleton and Mechanical Factors. International Journal of Molecular Sciences 2017, Vol 18, Page 1812 [Internet]. 2017 Aug 21 [cited 2023 Apr 26];18(8):1812. Available from: https://www.mdpi.com/1422-0067/18/8/1812/htm

109. Papalazarou V, Zhang T, Paul NR, Juin A, Cantini M, Maddocks ODK, et al. The creatine–phosphagen system is mechanoresponsive in pancreatic adenocarcinoma and fuels invasion and metastasis. Nature Metabolism 2020 2:1 [Internet]. 2020 Jan 20 [cited 2023 Apr 26];2(1):62–80. Available from: https://www.nature.com/articles/s42255-019-0159-z

110. Sun J, Chen J, Mohagheghian E, Wang N. Force-induced gene up-regulation does not follow the weak power law but depends on H3K9 demethylation. Sci Adv [Internet]. 2020 Apr 1 [cited 2023 Apr 13];6(14). Available from: https://www.science.org/doi/10.1126/sciadv.aay9095

111. Park JS, Burckhardt CJ, Lazcano R, Solis LM, Isogai T, Li L, et al. Mechanical regulation of glycolysis via cytoskeleton architecture. Nature. 2020 Feb 27;578(7796):621–6.

112. Chai Q, Jiao Y, Yu X. Hydrogels for Biomedical Applications: Their Characteristics and the Mechanisms behind Them. Gels. 2017 Jan 24;3(1):6.

113. Zhu J. Bioactive modification of poly(ethylene glycol) hydrogels for tissue engineering. Biomaterials [Internet]. 2010 Jun 1 [cited 2019 Apr 17];31(17):4639–56. Available from:

https://www.sciencedirect.com/science/article/pii/S0142961210002899?via%3Dihub

114. Zhou DW, Lee TT, Weng S, Fu J, García AJ. Effects of substrate stiffness and actomyosin contractility on coupling between force transmission and vinculin–paxillin recruitment at single focal adhesions. Mol Biol Cell. 2017;

115. Gomillion CT, Burg KJL. 6.22 Adipose Tissue Engineering. Comprehensive Biomaterials II. 2017 Jan 1;403–15.

116. Chae MP, Hunter-Smith DJ, Murphy S V., Findlay MW. 3D bioprinting adipose tissue for breast reconstruction. 3D Bioprinting for Reconstructive Surgery: Techniques and Applications. 2018 Jan 1;305–53.

117. Chillà A, Margheri F, Biagioni A, Del Rosso M, Fibbi G, Laurenzana A. Mature and progenitor endothelial cells perform angiogenesis also under protease inhibition: The amoeboid angiogenesis. Journal of Experimental and Clinical Cancer Research [Internet]. 2018 Apr 3 [cited 2023 Apr 9];37(1):1–14. Available from: https://jeccr.biomedcentral.com/articles/10.1186/s13046-018-0742-2

118. Gangadaran P, Rajendran RL, Oh JM, Oh EJ, Hong CM, Chung HY, et al. Identification of Angiogenic Cargo in Extracellular Vesicles Secreted from Human Adipose Tissue-Derived Stem Cells and Induction of Angiogenesis In Vitro and In Vivo. Pharmaceutics 2021, Vol 13, Page 495 [Internet]. 2021 Apr 5 [cited 2023 Apr 9];13(4):495. Available from: https://www.mdpi.com/1999-4923/13/4/495/htm

119. Salimath AS, Phelps EA, Boopathy A V., Che P lin, Brown M, García AJ, et al. Dual Delivery of Hepatocyte and Vascular Endothelial Growth Factors via a Protease-Degradable Hydrogel Improves Cardiac Function in Rats. Hsieh PCH, editor. PLoS One [Internet]. 2012 Nov 30 [cited 2019 Apr 17];7(11):e50980. Available from: https://dx.plos.org/10.1371/journal.pone.0050980

120. Pelham RJ, Wang YL. Cell locomotion and focal adhesions are regulated by substrate flexibility. Proc Natl Acad Sci U S A [Internet]. 1997 Dec 9 [cited 2023 Apr 9];94(25):13661–5. Available from: https://www.pnas.org/doi/abs/10.1073/pnas.94.25.13661

121. Charrier EE, Pogoda K, Wells RG, Janmey PA. Control of cell morphology and differentiation by substrates with independently tunable elasticity and viscous dissipation. Nature Communications 2018 9:1 [Internet]. 2018 Jan 31 [cited 2023 Apr 9];9(1):1–13. Available from: https://www.nature.com/articles/s41467-018-02906-9

122. Charrier EE, Pogoda K, Li R, Park CY, Fredberg JJ, Janmey PA. A novel method to make viscoelastic polyacrylamide gels for cell culture and traction force microscopy. APL Bioeng [Internet]. 2020 Sep 1 [cited 2023 Apr 9];4(3):36104. Available from: /pmc/articles/PMC7334032/

123. Zhu J, Tang C, Kottke-Marchant K, Marchant RE. Design and synthesis of biomimetic hydrogel scaffolds with controlled organization of cyclic RGD peptides. Bioconjug Chem [Internet]. 2009 [cited 2023 Apr 26];20(2):333–9. Available from: https://pubs.acs.org/doi/full/10.1021/bc800441v

124. Fu Y, Kao WJ. In situ forming poly(ethylene glycol)-based hydrogels via thiol-maleimide Michael-type addition. J Biomed Mater Res A [Internet]. 2011 Aug 1 [cited 2019 Apr 23];98A(2):201–11. Available from: http://doi.wiley.com/10.1002/jbm.a.33106

125. Salinas CN, Anseth KS. Mixed Mode Thiol - Acrylate Photopolymerizations for the Synthesis of PEG - Peptide Hydrogels. Macromolecules [Internet]. 2008 Aug 26 [cited 2023 Apr 26];41(16):6019–26. Available from: https://pubs.acs.org/doi/full/10.1021/ma800621h

126. Brown TE, Carberry BJ, Worrell BT, Dudaryeva OY, McBride MK, Bowman CN, et al. Photopolymerized dynamic hydrogels with tunable viscoelastic properties through thioester exchange. Biomaterials [Internet].

2018;178:496–503. Available from: https://doi.org/10.1016/j.biomaterials.2018.03.060

127. Nguyen KT, West JL. Photopolymerizable hydrogels for tissue engineering applications. Biomaterials [Internet]. 2002 Nov 1 [cited 2019 Apr 17];23(22):4307–14. Available from: https://www.sciencedirect.com/science/article/pii/S0142961202001758

128. Zhu J, Marchant RE. Design properties of hydrogel tissue-engineering scaffolds. Expert Rev Med Devices [Internet]. 2011 Sep [cited 2019 Apr 6];8(5):607–26. Available from: http://www.ncbi.nlm.nih.gov/pubmed/22026626

129. Polio SR, Parameswaran H, Canović EP, Gaut CM, Aksyonova D, Stamenović D, et al. Topographical control of multiple cell adhesion molecules for traction force microscopy. Integrative Biology [Internet]. 2014 Mar 24 [cited 2019 Apr 14];6(3):357–65. Available from: https://academic.oup.com/ib/article/6/3/357/5199132

130. Schiller ZA, Schiele NR, Sims JK, Lee K, Kuo CK. Adipogenesis of adipose-derived stem cells may be regulated via the cytoskeleton at physiological oxygen levels in vitro. Stem Cell Res Ther [Internet]. 2013 Jul 9 [cited 2019 Apr 30];4(4):79. Available from: http://www.ncbi.nlm.nih.gov/pubmed/23838354

131. Zhang C, Hekmatfar S, Ramanathan A, Karuri NW. PEGylated human plasma fibronectin is proteolytically stable, supports cell adhesion, cell migration, focal adhesion assembly, and fibronectin fibrillogenesis. Biotechnol Prog [Internet]. 2013 Mar 1 [cited 2019 Apr 18];29(2):493–504. Available from: http://doi.wiley.com/10.1002/btpr.1689

132. Zhang C, Desai R, Perez-Luna V, Karuri N. PEGylation of lysine residues improves the proteolytic stability of fibronectin while retaining biological activity. Biotechnol J [Internet]. 2014 Aug 1 [cited 2019 Apr 18];9(8):1033–43. Available from: http://doi.wiley.com/10.1002/biot.201400115

133. Trujillo S, Gonzalez-Garcia C, Rico P, Reid A, Windmill J, Dalby MJ, et al. Engineered 3D hydrogels with full-length fibronectin that sequester and present growth factors. Biomaterials. 2020 Sep 1;252:120104.

134. Bednar RA. Reactivity and pH Dependence of Thiol Conjugation to iV-Ethylmaleimide: Detection of a Conformational Change in Chalcone Isomerase1" [Internet]. Vol. 29, Biochemistry. 1990 [cited 2019 Apr 18]. Available from: https://pubs.acs.org/sharingguidelines

135. Maruthamuthu V, Sabass B, Schwarz US, Gardel ML. Cell-ECM traction force modulates endogenous tension at cell-cell contacts. Proceedings of the National Academy of Sciences [Internet]. 2011 Mar 22 [cited 2019 Jan 25];108(12):4708–13. Available from: http://www.pnas.org/cgi/doi/10.1073/pnas.1011123108

136. Zancla A, Mozetic P, Orsini M, Forte G, Rainer A. A primer to traction force microscopy. Journal of Biological Chemistry. 2022 May 1;298(5):101867.

137. Roca-Cusachs P, Conte V, Trepat X. Quantifying forces in cell biology. Nat Cell Biol [Internet]. 2017 Jul 19 [cited 2019 Apr 13];19(7):742–51. Available from: http://www.nature.com/articles/ncb3564

138. Lin L, Marchant RE, Zhu J, Kottke-Marchant K. Extracellular matrix-mimetic poly(ethylene glycol) hydrogels engineered to regulate smooth muscle cell proliferation in 3-D. Acta Biomater [Internet]. 2014 Dec 1 [cited 2019 Apr 17];10(12):5106–15. Available from: https://www.sciencedirect.com/science/article/pii/S1742706114003705

139. Legant WR, Choi CK, Miller JS, Shao L, Gao L, Betzig E, et al. Multidimensional traction force microscopy reveals out-of-plane rotational moments about focal adhesions. [cited 2019 Apr 24]; Available from: https://www.pnas.org/content/pnas/110/3/881.full.pdf

140. Colin-York H, Fritzsche M. The future of traction force microscopy. Curr Opin Biomed Eng [Internet]. 2018 Mar 1 [cited 2019 Apr 14];5:1–5. Available from:

https://www.sciencedirect.com/science/article/pii/S2468451117300727#bib14

141. Ray A, Lee O, Win Z, Edwards RM, Alford PW, Kim DH, et al. Anisotropic forces from spatially constrained focal adhesions mediate contact guidance directed cell migration. Nat Commun [Internet]. 2017 Apr 12 [cited 2019 Jan 25];8:14923. Available from: http://www.nature.com/doifinder/10.1038/ncomms14923

142. Souza-Moreira L, Soares VC, Dias S da SG, Bozza PT. Adipose-derived Mesenchymal Stromal Cells Modulate Lipid Metabolism and Lipid Droplet Biogenesis via AKT/mTOR –PPARγ Signalling in Macrophages. Scientific Reports 2019 9:1 [Internet]. 2019 Dec 30 [cited 2023 Apr 17];9(1):1–11. Available from: https://www.nature.com/articles/s41598-019-56835-8

143. Zhang Y, Marsboom G, Toth PT, Rehman J. Mitochondrial Respiration Regulates Adipogenic Differentiation of Human Mesenchymal Stem Cells. PLoS One. 2013;8(10).

144. De Feng X, Guo Q, Yuan Qiu K. Study of the initiation mechanism of the vinyl polymerization with the system persulfate/ N,N,N ',N '-tetramethylethylenediamine. Vol. 189, Makromol. Chem. 1988.

145. Tse JR, Engler AJ. Preparation of Hydrogel Substrates with Tunable Mechanical Properties. Curr Protoc Cell Biol [Internet]. 2010 Jun 1 [cited 2022 Nov 3];47(1):10.16.1-10.16.16. Available from: https://onlinelibrary.wiley.com/doi/full/10.1002/0471143030.cb1016s47

146. Petrenko Y, Vackova I, Kekulova K, Chudickova M, Koci Z, Turnovcova K, et al. A Comparative Analysis of Multipotent Mesenchymal Stromal Cells derived from Different Sources, with a Focus on Neuroregenerative Potential. Sci Rep [Internet]. 2020 Dec 1 [cited 2022 Nov 7];10(1). Available from: /pmc/articles/PMC7062771/

147. Romani P, Nirchio N, Arboit M, Barbieri V, Tosi A, Michielin F, et al. Mitochondrial fission links ECM mechanotransduction to metabolic redox homeostasis and metastatic chemotherapy resistance. Nature Cell Biology 2022 24:2 [Internet]. 2022 Feb 14 [cited 2023 Apr 25];24(2):168–80. Available from: https://www.nature.com/articles/s41556-022-00843-w

148. Müller C, Pompe T. Distinct impacts of substrate elasticity and ligand affinity on traction force evolution. Soft Matter [Internet]. 2015 Dec 16 [cited 2023 Feb 25];12(1):272–80. Available from: https://pubs.rsc.org/en/content/articlehtml/2016/sm/c5sm01706h

149. Pompe T, Kaufmann M, Kasimir M, Johne S, Glorius S, Renner L, et al. Friction-Controlled Traction Force in Cell Adhesion. Biophys J [Internet]. 2011 Oct 10 [cited 2023 Jan 30];101(8):1863. Available from: /pmc/articles/PMC3192957/

150. Tseng Q, Duchemin-Pelletier E, Deshiere A, Balland M, Guilloud H, Filhol O, et al. Spatial organization of the extracellular matrix regulates cell-cell junction positioning. Proc Natl Acad Sci U S A. 2012 Jan 31;109(5):1506–11.

151. Piccolo S, Dupont S, Cordenonsi M. The biology of YAP/TAZ: Hippo signaling and beyond. Physiol Rev. 2014 Oct 1;94(4):1287–312.

152. Mason DE, Collins JM, Dawahare JH, Nguyen TD, Lin Y, Voytik-Harbin SL, et al. YAP and TAZ limit cytoskeletal and focal adhesion maturation to enable persistent cell motility. Journal of Cell Biology. 2019;218(4):1369–89.

153. Straight AF, Cheung A, Limouze J, Chen I, Westwood NJ, Sellers JR, et al. Dissecting temporal and spatial control of cytokinesis with a myosin II Inhibitor. Science [Internet]. 2003 Mar 14 [cited 2019 Apr 12];299(5613):1743–7. Available from: http://www.ncbi.nlm.nih.gov/pubmed/12637748

154. Lekka M, Gnanachandran K, Kubiak A, Zieliński T, Zemła J. Traction force microscopy – Measuring the forces exerted by cells. Micron. 2021 Nov 1;150.

155. Yeh YC, Ling JY, Chen WC, Lin HH, Tang MJ. Mechanotransduction of matrix stiffness in regulation of focal adhesion size and number: reciprocal regulation of caveolin-1 and β1 integrin. Scientific Reports 2017 7:1 [Internet]. 2017 Nov 8 [cited 2023 Apr 24];7(1):1–14. Available from: https://www.nature.com/articles/s41598-017-14932-6

156. Andreu I, Falcones B, Hurst S, Chahare N, Quiroga X, Le Roux AL, et al. The force loading rate drives cell mechanosensing through both reinforcement and cytoskeletal softening. Nature Communications 2021 12:1 [Internet]. 2021 Jul 9 [cited 2023 Apr 25];12(1):1–12. Available from: https://www.nature.com/articles/s41467-021-24383-3

157. Yu M, Le S, Ammon YC, Goult BT, Akhmanova A, Yan J. Force-Dependent Regulation of Talin-KANK1 Complex at Focal Adhesions. Nano Lett [Internet]. 2019 Sep 11 [cited 2023 Apr 25];19(9):5982–90. Available from: https://pubs.acs.org/doi/full/10.1021/acs.nanolett.9b01732

158. Peng X, Nelson ES, Maiers JL, DeMali KA. New Insights into Vinculin Function and Regulation. Int Rev Cell Mol Biol. 2011 Jan 1;287:191–231.

159. Jiang L, Sun Z, Chen X, Li J, Xu Y, Zu Y, et al. Cells sensing mechanical cues: Stiffness influences the lifetime of cell-extracellular matrix interactions by affecting the loading rate. ACS Nano [Internet]. 2016 Jan 26 [cited 2023 Apr 25];10(1):207–17. Available from: https://pubs.acs.org/doi/full/10.1021/acsnano.5b03157

160. Feld L, Kellerman L, Mukherjee A, Livne A, Bouchbinder E, Wolfenson H. Cellular contractile forces are nonmechanosensitive. Sci Adv [Internet]. 2020 Apr 1 [cited 2023 Apr 25];6(17). Available from: https://www.science.org/doi/10.1126/sciadv.aaz6997

161. Prager-Khoutorsky M, Lichtenstein A, Krishnan R, Rajendran K, Mayo A, Kam Z, et al. Fibroblast polarization is a matrix-rigidity-dependent process controlled by focal adhesion mechanosensing. Nature Cell Biology 2011

13:12 [Internet]. 2011 Nov 13 [cited 2023 Apr 25];13(12):1457–65. Available from: https://www.nature.com/articles/ncb2370

162. Das A, Fischer RS, Pan D, Waterman CM. YAP nuclear localization in the absence of cell-cell contact is mediated by a filamentous actin-dependent, Myosin IIand Phospho-YAP-independent pathway during extracellular matrix mechanosensing. Journal of Biological Chemistry. 2016 Mar 18;291(12):6096–110.

163. Wei Q, Huang C, Zhang Y, Zhao T, Zhao P, Butler P, et al. Mechanotargeting: Mechanics-Dependent Cellular Uptake of Nanoparticles. Advanced Materials [Internet]. 2018 Jul 1 [cited 2023 Jan 22];30(27):1707464. Available from: https://onlinelibrary.wiley.com/doi/full/10.1002/adma.201707464

164. Casanellas I, Lagunas A, Vida Y, Pérez-Inestrosa E, Andrades JA, Becerra J, et al. Matrix Nanopatterning Regulates Mesenchymal Differentiation through Focal Adhesion Size and Distribution According to Cell Fate. Biomimetics 2019, Vol 4, Page 43 [Internet]. 2019 Jun 25 [cited 2023 Feb 27];4(2):43. Available from: https://www.mdpi.com/2313-7673/4/2/43/htm

165. Holland EN, Lobaccaro D, Fu J, García AJ. Impact of adhesive area on cellular traction force and spread area. J Biomed Mater Res A [Internet]. 2023 [cited 2023 Feb 27]; Available from: https://onlinelibrary.wiley.com/doi/full/10.1002/jbm.a.37518

166. Rosowski KA, Boltyanskiy R, Xiang Y, Van Den Dries K, Schwartz MA, Dufresne ER. Vinculin and the mechanical response of adherent fibroblasts to matrix deformation. Sci Rep [Internet]. 2018 [cited 2019 Feb 21];8(1):2–4. Available from: www.nature.com/scientificreports

167. Cha BH, Kim JS, Bello A, Lee GH, Kim DH, Kim BJ, et al. Efficient Isolation and Enrichment of Mesenchymal Stem Cells from Human Embryonic Stem Cells by Utilizing the Interaction between Integrin α5ß1 and Fibronectin. Advanced Science. 2020 Sep 1;7(17).

168. Zwolanek D, Flicker M, Kirstätter E, Zaucke F, Van Osch GJVM, Erben RG. β1 integrins mediate attachment of mesenchymal stem cells to cartilage lesions. Biores Open Access. 2015 Jan 1;4(1):39–53.

169. Liu J, DeYoung SM, Zhang M, Zhang M, Cheng A, Saltiel AR. Changes in integrin expression during adipocyte differentiation. Cell Metab. 2005 Sep;2(3):165–77.

170. Clish CB. Metabolomics: an emerging but powerful tool for precision medicine. 2015 [cited 2022 Nov 4]; Available from: http://www.ebi.ac.uk/metabolights

171. Romani P, Valcarcel-Jimenez L, Frezza C, Dupont S. Crosstalk between mechanotransduction and metabolism. Nature Reviews Molecular Cell Biology 2020 22:1 [Internet]. 2020 Nov 13 [cited 2023 Apr 20];22(1):22–38. Available from: https://www.nature.com/articles/s41580-020-00306-w

172. Rambold AS, Cohen S, Lippincott-Schwartz J. Fatty Acid Trafficking in Starved Cells: Regulation by Lipid Droplet Lipolysis, Autophagy, and Mitochondrial Fusion Dynamics. Dev Cell. 2015 Mar 23;32(6):678–92.

173. Nguyen TB, Louie SM, Daniele JR, Tran Q, Dillin A, Zoncu R, et al. DGAT1-Dependent Lipid Droplet Biogenesis Protects Mitochondrial Function during Starvation-Induced Autophagy. Dev Cell. 2017 Jul 10;42(1):9-21.e5.

174. Muranen T, Iwanicki MP, Curry NL, Hwang J, DuBois CD, Coloff JL, et al. Starved epithelial cells uptake extracellular matrix for survival. Nature Communications 2017 8:1 [Internet]. 2017 Jan 10 [cited 2023 Apr 21];8(1):1–12. Available from: https://www.nature.com/articles/ncomms13989

175. Fan JY, Carpentier T louis, Van Obberghen E, Grunfeld C, Gorden P, Orci L. MORPHOLOGICAL CHANGES OF THE 3T3-L1 FIBROBLAST PLASMA MEMBRANE UPON DIFFERENTIATION TO THE ADIPOCYTE FORM. y Cell Sci. 1983;61:219–30.

176. Green H, Meuth M. An established pre-adipose cell line and its differentiation in culture. Cell. 1974 Oct 1;3(2):127–33.

177. Kim WK, Jung H, Kim DH, Kim EY, Chung JW, Cho YS, et al. Regulation of adipogenic differentiation by LAR tyrosine phosphatase in human mesenchymal stem cells and 3T3-L1 preadipocytes. J Cell Sci [Internet]. 2009 Nov 15 [cited 2023 Apr 18];122(22):4160–7. Available from: https://journals.biologists.com/jcs/article/122/22/4160/31009/Regulation-of-adipogenic-differentiation-by-LAR

178. Chung TH, Wu SH, Yao M, Lu CW, Lin YS, Hung Y, et al. The effect of surface charge on the uptake and biological function of mesoporous silica nanoparticles in 3T3-L1 cells and human mesenchymal stem cells. Biomaterials. 2007 Jul 1;28(19):2959–66.

179. Gu X, Ma Y, Liu Y, Wan Q. Measurement of mitochondrial respiration in adherent cells by Seahorse XF96 Cell Mito Stress Test. STAR Protoc. 2021 Mar 19;2(1):100245.

180. Little AC, Kovalenko I, Goo LE, Hong HS, Kerk SA, Yates JA, et al. High-content fluorescence imaging with the metabolic flux assay reveals insights into mitochondrial properties and functions. Communications Biology 2020 3:1 [Internet]. 2020 May 29 [cited 2023 Apr 27];3(1):1–10. Available from: https://www.nature.com/articles/s42003-020-0988-z

181. Tantama M, Martínez-François JR, Mongeon R, Yellen G. Imaging energy status in live cells with a fluorescent biosensor of the intracellular ATP-to-ADP ratio. Nature Communications 2013 4:1 [Internet]. 2013 Oct 7 [cited 2023 Apr 21];4(1):1–11. Available from: https://www.nature.com/articles/ncomms3550

182. Tantama M, Hung YP, Yellen G. Imaging intracellular pH in live cells with a genetically encoded red fluorescent protein sensor. J Am Chem Soc [Internet]. 2011 Jul 6 [cited 2023 Apr 21];133(26):10034–7. Available from: https://pubs.acs.org/doi/full/10.1021/ja202902d

183. Suginohara T, Wakabayashi K, Ato S, Ogasawara R. Effect of 2-deoxyglucose-mediated inhibition of glycolysis on the regulation of mTOR signaling and protein synthesis before and after high-intensity muscle contraction. Metabolism. 2021 Jan 1;114:154419.

184. Schmitt DL, Curtis SD, Lyons AC, Zhang J fan, Chen M, He CY, et al. Spatial regulation of AMPK signaling revealed by a sensitive kinase activity reporter. Nat Commun. 2022 Dec 1;13(1).

185. Tsou P, Zheng B, Hsu CH, Sasaki AT, Cantley LC. A Fluorescent Reporter of AMPK Activity and Cellular Energy Stress. Cell Metab. 2011 Apr 6;13(4):476–86.

186. Hung YP, Albeck JG, Tantama M, Yellen G. Imaging Cytosolic NADH-NAD+ Redox State with a Genetically Encoded Fluorescent Biosensor. Cell Metab. 2011 Oct 5;14(4):545–54.

187. Li T, Zou Y, Liu S, Yang Y, Zhang Z, Zhao Y. Monitoring NAD(H) and NADP(H) dynamics during organismal development with genetically encoded fluorescent biosensors. Cell Regeneration [Internet]. 2022 Dec 1 [cited 2023 Apr 21];11(1):1–11. Available from: https://cellregeneration.springeropen.com/articles/10.1186/s13619-021-00105-4

188. Roshanzadeh A, Kang H, You SH, Park J, Khoa ND, Lee DH, et al. Real-time monitoring of NADPH levels in living mammalian cells using fluorescence-enhancing protein bound to NADPHs. Biosens Bioelectron. 2019 Dec 15;146:111753.

189. Bertolio R, Napoletano F, Mano M, Maurer-Stroh S, Fantuz M, Zannini A, et al. Sterol regulatory element binding protein 1 couples mechanical cues and lipid metabolism. Nature Communications 2019 10:1 [Internet]. 2019 Mar 22 [cited 2023 Apr 22];10(1):1–11. Available from: https://www.nature.com/articles/s41467-019-09152-7

190. Kwon DH, Cha HJ, Lee H, Hong SH, Park C, Park SH, et al. Protective Effect of Glutathione against Oxidative Stress-induced Cytotoxicity in RAW 264.7 Macrophages through Activating the Nuclear Factor Erythroid 2-Related Factor-2/Heme Oxygenase-1 Pathway. Antioxidants [Internet]. 2019 Apr 1 [cited 2023 Apr 19];8(4):82. Available from: /pmc/articles/PMC6523540/

191. Jalali S, Shi J, Buko A, Ahsan N, Paludo J, Serres M, et al. Increased glutathione utilization augments tumor cell proliferation in Waldenstrom Macroglobulinemia. Redox Biol. 2020 Sep 1;36:101657.

192. Grassian AR, Metallo CM, Coloff JL, Stephanopoulos G, Brugge JS. Erk regulation of pyruvate dehydrogenase flux through PDK4 modulates cell proliferation. Genes Dev [Internet]. 2011 Aug 15 [cited 2023 Apr 23];25(16):1716–33. Available from: http://genesdev.cshlp.org/content/25/16/1716.full

193. Labuschagne CF, Cheung EC, Blagih J, Domart MC, Vousden KH. Cell Clustering Promotes a Metabolic Switch that Supports Metastatic Colonization. Cell Metab. 2019 Oct 1;30(4):720-734.e5.

194. Intlekofer AM, Wang B, Liu H, Shah H, Carmona-Fontaine C, Rustenburg AS, et al. L-2-Hydroxyglutarate production arises from noncanonical enzyme function at acidic pH. Nature Chemical Biology 2017 13:5 [Internet]. 2017 Mar 6 [cited 2023 Apr 23];13(5):494–500. Available from: https://www.nature.com/articles/nchembio.2307

195. Losman JA, Koivunen P, Kaelin WG. 2-Oxoglutarate-dependent dioxygenases in cancer. Nature Reviews Cancer 2020 20:12 [Internet]. 2020 Oct 21 [cited 2023 Apr 22];20(12):710–26. Available from: https://www.nature.com/articles/s41568-020-00303-3

196. Frost J, Frost M, Batie M, Jiang H, Rocha S. Roles of HIF and 2-Oxoglutarate-Dependent Dioxygenases in Controlling Gene Expression in Hypoxia. Cancers 2021, Vol 13, Page 350 [Internet]. 2021 Jan 19 [cited 2023 Apr 22];13(2):350. Available from: https://www.mdpi.com/2072-6694/13/2/350/htm

197. Ma S, Ding R, Cao J, Liu Z, Li A, Pei D. Mitochondria transfer reverses the inhibitory effects of low stiffness on osteogenic differentiation of human mesenchymal stem cells. Eur J Cell Biol. 2023 Jun 1;102(2):151297.

198. Al Hasan M, Roy P, Dolan S, Martin PE, Patterson S, Bartholomew C. Adhesion G-protein coupled receptor 56 is required for 3T3-L1 adipogenesis. J Cell Physiol [Internet]. 2020 Feb 1 [cited 2023 Mar 21];235(2):1601–14. Available from: https://onlinelibrary.wiley.com/doi/full/10.1002/jcp.29079

199. Al Hasan M, Martin PE, Shu X, Patterson S, Bartholomew C. Type III Collagen is Required for Adipogenesis and Actin Stress Fibre Formation in 3T3-L1 Preadipocytes. Biomolecules 2021, Vol 11, Page 156 [Internet]. 2021 Jan 25 [cited 2023 Mar 21];11(2):156. Available from: https://www.mdpi.com/2218-273X/11/2/156/htm

200. Chaudhuri O, Koshy ST, Branco Da Cunha C, Shin JW, Verbeke CS, Allison KH, et al. Extracellular matrix stiffness and composition jointly regulate the induction of malignant phenotypes in mammary epithelium. Nature Materials 2014 13:10 [Internet]. 2014 Jun 15 [cited 2023 Apr 27];13(10):970–8. Available from: https://www.nature.com/articles/nmat4009

201. Byfield FJ, Wen Q, Levental I, Nordstrom K, Arratia PE, Miller RT, et al. Absence of Filamin A Prevents Cells from Responding to Stiffness Gradients on Gels Coated with Collagen but not Fibronectin. Biophys J. 2009 Jun 17;96(12):5095–102.

202. Xie J, Bao M, Hu X, Koopman WJH, Huck WTS. Energy expenditure during cell spreading influences the cellular response to matrix stiffness. Biomaterials. 2021 Jan 1;267:120494.

203. Zhu J, Thompson CB. Metabolic regulation of cell growth and proliferation. Nat Rev Mol Cell Biol [Internet]. 2019;20(7):436–50. Available from: http://dx.doi.org/10.1038/s41580-019-0123-5

204. Kechagia Z, Sáez P, Gómez-González M, Zamarbide M, Andreu I, Koorman T, et al. The laminin-keratin link shields the nucleus from mechanical deformation and signalling. bioRxiv [Internet]. 2022 Mar 1 [cited 2023 Apr 27];2022.03.01.482474. Available from: https://www.biorxiv.org/content/10.1101/2022.03.01.482474v1